Engineering

Journal of Research

of the

National Bureau of Standards

U.S.

APRIL 1954

VOLUME 52 NUMBER 4

U.S. DEPARTMENT OF COMMERCE
Sinclair Weeks, Secretary
NATIONAL BUREAU OF STANDARDS
A. V. Astin, Director

APRIL 1954
VOLUME 52
NUMBER 4

JOURNAL OF RESEARCH

of the

NATIONAL BUREAU OF STANDARDS

PERIODICALS OF THE NATIONAL BUREAU OF STANDARDS

The National Bureau of Standards is engaged in fundamental and applied research in physics, chemistry, mathematics, and engineering. Projects are conducted in thirteen fields: electricity, optics and metrology, heat and power, atomic and radiation physics, chemistry, mechanics, organic and fibrous materials, metallurgy, mineral products, building technology, applied mathematics, electronics, and radio propagation. The Bureau has custody of the national standards of measurement and conducts research leading to the improvement of scientific and engineering standards and of techniques and methods of measurement. Testing methods and instruments are developed; physical constants and properties of materials are determined and technical processes are investigated.

JOURNAL OF RESEARCH

[illegible] as a leading scientific periodical, the Journal publishes research papers by authors [illegible] the specialized fields of physics, mathematics, chemistry, and engineering. Complete details of the work are presented, including laboratory data, experimental procedures, and theoretical and mathematical [illegible]. Annual subscription: domestic, $3.50; foreign, $4.75.

TECHNICAL NEWS BULLETIN

[illegible] research at the National Bureau of Standards are published each month in the Technical [illegible]. The articles are brief, with [illegible] the results of research, chosen on the basis of their [illegible] importance. Lists of [illegible] publications [illegible] preceding months are given. [illegible] Papers, Handbooks, [illegible] Materials and Structures Miscellaneous Publications, and [illegible] Each issue [illegible] or more [illegible] pages. Annual subscription: domestic, $1.25; foreign, $1.50.

BASIC RADIO [illegible] PUBLICATIONS

[illegible] provide the information [illegible] for communication [illegible] in the world at [illegible] These data are important to all [illegible] communications [illegible] ship, and [illegible] to investigate [illegible] Each [illegible] ering a [illegible] issued three [illegible] eminent [illegible]. Annual publication: $1.00.

[illegible] all publications [illegible] U. S. Government [illegible]

[illegible] has been [illegible]

Journal of Research of the National Bureau of Standards Vol. 52, No. 4, April 1954 Research Paper 2486

Use of Callendar's "Radio-Balance" for the Measurement of the Energy Emission from Radioactive Sources

W. B. Mann

In 1910 H. L. Callendar described a calorimeter for measurement of radiant energy in which the quantity of heat to be measured is balanced against the cooling from a Peltier couple. He called this thermal-balance device a "radio-balance." The operation of the radio-balance has been extensively investigated to see whether it could be used for the accurate determination of the energy emission from radioactive sources. In the present experiments, measurements have been confined solely to radium preparations. For an absorption equivalent to 0.126 cm of lead a heat emission of 128.9 cal g^{-1} hr^{-1} has been found for radium in equilibrium with its products down to radium D. The estimated accuracy of this result is ± 0.7 percent.

1. Introduction

In 1910, in a paper that seems to have caused little interest in the intervening years, H. L. Callendar [1],[1] described a calorimeter in which the quantity of heat to be measured was to be balanced by the cooling from a Peltier couple. With this calorimeter, which he called a radio-balance [2] because it gave a null reading, he made measurements of the solar radiation, and he also carried out a somewhat rudimentary measurement of the energy emitted in unit time from a sealed source of radon emanation lent to him for the purpose by Lord Rutherford. The results obtained with the emanation, although qualitatively interesting, were not of great value from a quantitative point of view.

Some 20 years later Hoare [2, 3] used a radio-balance to determine the Stefan-Boltzmann radiation constant. This appears to be the only other recorded application of the radio-balance, and no other reference to it in the scientific literature of the last 23 years has been found. It seems, however, that this method of determining the energy dissipation has much to commend itself, and experiments have recently been carried out to see whether or not it might be feasible to apply it to determine the rate of energy production by radioactive sources. For this purpose, several radio-balances were constructed. The outstanding merit of this form of microcalorimeter is its extreme compactness, the first simple version used in the experiments here described being contained in a cylindrical copper box only 2⅛ in. high and 2 in. in diameter, whereas the final version was contained in what was essentially a cylindrical copper block 2¼ in. in height and 4 in. in diameter. These are shown in figure 1.

[1] Figures in brackets indicate the literature references at the end of the paper.
[2] This instrument should perhaps be renamed the "Radiation Balance."

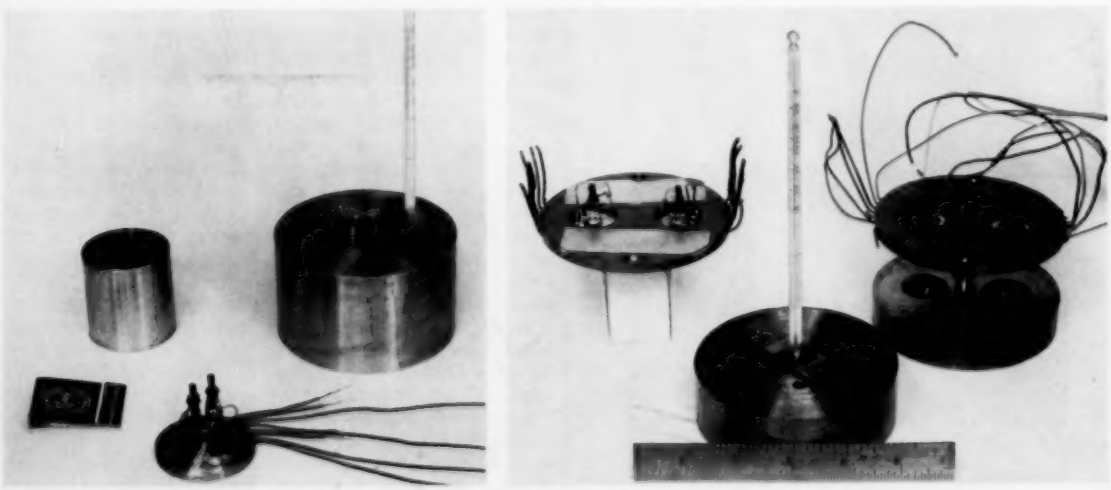

FIGURE 1. *Three radio-balances.*

The radio-balances are shown, from left to right, in chronological order. The second and third cup assemblies fit into the same copper block housing. The second radio-balance is that with four Peltier junctions.

2. Theory

In the radio-balance the energy incident upon, or transmitted to, a small disk or cup is balanced by the cooling effected by a Peltier junction attached to the same disk or cup. Callendar used both a disk and a cup radio-balance as a pyrheliometer, and Hoare used a cup balance to measure the Stefan-Boltzmann radiation constant.

In the present experiments a cup-type radio-balance was used, consisting, in its final version, of two copper cups $^{13}/_{16}$ in. long and having internal and external diameters of 0.099 and 0.130 in., respectively. Each cup was mounted on a six-junction constantan-chromel thermopile by means of an equatorial ring, as illustrated in figure 2. The lower junctions of each thermopile dip into silicone vacuum oil contained in two small cavities in the lower copper block constituting the container of the radio-balance. A constantan-chromel Peltier couple is soldered to the base of each cup.

The radio-balance may be used in two ways. Each cup may be used singly, or they may be used together in opposition. In the present experiments the interest has lain in the measurement of the energy emission from radioactive sources and not of energy flux from an external source of radiation. Such a radioactive source, as, for example, a radium needle, may be placed in either cup A or cup B of the radio-balance and a current passed through the Peltier junction in such a direction and of such magnitude that the cooling due to the Peltier junction shall exactly balance the heating due to the radioactive preparation. The criterion for such balance is obtained by reducing to zero the deflection of a sensitive galvanometer connected to the thermopile. For zero deflection, the temperature of the cup is restored to the same temperature as the base of the thermopile, and there should be an exact balance between the heat energy supplied to the cup by the radioactive source and the heat removed by the Peltier cooling. In this condition the energy, H, supplied by the radioactive source is given by

$$H=PC-C^2R, \tag{1}$$

where P is the Peltier coefficient, C is the current passing through the Peltier junction, and R is its resistance.

In order to determine the resistance of the Peltier junction, a subsidiary experiment may be carried out, in which a dummy source is substituted for the radioactive source, in order to simulate external heat-loss conditions and the thermal conductivity along the length of the cup, and the current is again adjusted to give zero deflection of the thermopile galvanometer. In this condition

$$0=PC-C^2R,$$

or

$$R=P/C. \tag{2}$$

By differentiation of eq (1) it is clear that the maximum cooling effect that can be obtained is

$$H=P^2/4R. \tag{3}$$

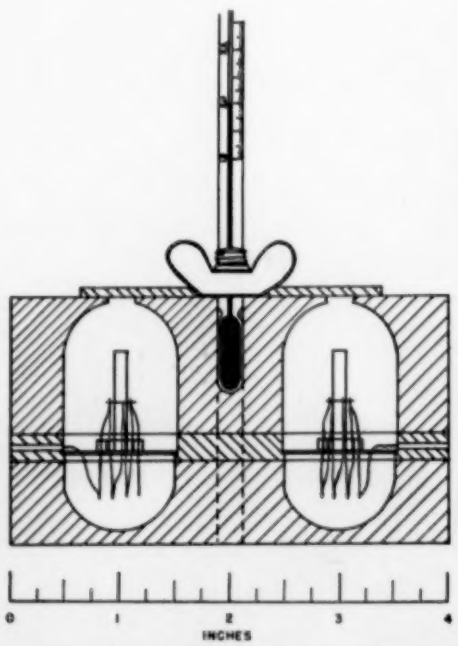

FIGURE 2. *Elevation drawing through the vertical axis of symmetry of the third and final radio-balance.*

In the second method of using the radio-balance the thermopiles of cup A and cup B are connected in series with one another and with the galvanometer so as to act in opposition to each other. Thus an equal rise in temperature of both cup A and cup B relative to the thermopile bases will give a zero galvanometer deflection. The Peltier junctions are also connected in opposition and in series, so that the same current flows through each but will cause a heating in the one cup and a cooling in the other.

In all the radio-balances that have been constructed in this investigation a small residual galvanometer deflection was almost invariably detected, indicating a slight temperature difference between cup A or cup B and the thermopile bases, with no source in either cup and no Peltier current flowing. This could be due to a very slight difference in temperature between the top and bottom of the copper block container. With the piles of cup A and cup B connected in opposition, however, the "zero deflection" was invariably negligible, any slight rise in temperature in cup A being compensated for by a similar rise in cup B.

In this second method of using the radio-balance, which was also proposed by Callendar, another advantage derives from the fact that the Joule heating of the Peltier junctions is also eliminated. To describe this method, assume that a radioactive

source dissipating energy W' watts is placed in cup A and that another dissipating W'' watts is placed in cup B. If a dummy is used in cup B, then W'' is zero, but this is not necessarily so, and the method can in fact be used to compare two nearly equal sources without involving the use of Peltier cooling or heating at all. This appears to be a new and very accurate application of the radio-balance, as will be demonstrated by the experimental results obtained. This application would certainly have been most apparent to Callendar from his derivation of the relevant equations; the need for such an application did not, however, exist to the same extent more than 40 years ago.

It will be assumed that W' is greater than W'' and that a current C is passed through the Peltier junctions in such a direction as to give a cooling of cup A and a heating of cup B. The value of C is then adjusted to give an approximately zero balance of the thermopile galvanometer. Suppose, however, that the residual galvanometer deflection is d_1. The sources W' and W'' are now interchanged between cup A and cup B and the current C is reversed so that cup A is now heated and cup B is cooled. As slight differences will exist between cup A and cup B, a new residual galvanometer deflection, d_2, will be observed. Under these conditions Callendar showed that

$$W'-W''=2PC+(d_1-d_2)/s, \qquad (4)$$

where s is the galvanometer-scale sensitivity in millimeters per microwatt transferred from cup A to cup B, and P is the average of the values of P_A and P_B for the individual cups. In the final version of the radio-balance used in these experiments, s was of the order of 0.7 mm/μw when the current through the galvanometer was reversed. That a reversal of the current does, in fact, correspond to a transfer of energy equal to $2PC$ from the one cup to the other is clear from the energy-dissipation-level diagram in figure 3, which refers to either cup A or cup B. If cup A gains $2PC$, then cup B correspondingly loses $2PC$. The value of R in figure 3 would be that appropriate to cup A or cup B.

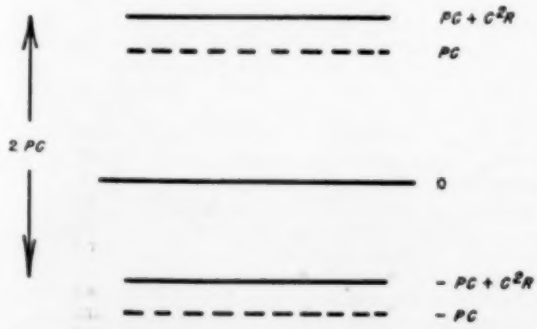

FIGURE 3. *Energy-dissipation-level diagram illustrating the elimination of Joule heating on reversal of the current through the Peltier junction of either cup.*

3. Experimental Procedure

The cups of the third, and final, radio-balance were constructed from copper and were 0.099-in. internal diameter, 0.130-in. external diameter, and $^{13}/_{16}$ in. long. The cups were supported on the upper end of a six-junction chromel-constantan thermopile by means of an equatorial annular ring with six small holes. The junctions of the thermopile were insulated from each of the cups by means of six disks of rubber hydrochloride, 0.0002 in. thick, which were cut out by means of a paper punch. The junctions were then sealed in position by means of a small amount of glyptal.

The Peltier junctions are secured to the lower ends of the radio-balance cups by means of soft solder. The Peltier-junction assembly consisted of a framework of four wires in the form of a Cleopatra needle silver-soldered at the apex. A constantan wire and a chromel wire, each 0.020 in. in diameter, along opposite corners of the needle formed the actual Peltier junction. The other two wires formed a thermocouple, by means of which the lowering in temperature of the Peltier junction could be measured. These consisted of constantan and chromel 0.010 in. and 0.012 in. in diameter, respectively. When assembled each cup stood upon the apex of the Cleopatra needle in the manner indicated in figure 4.

The thermopiles were constructed with the help of a number of lucite annuli of $^{3}/_{8}$-in. external diameter, $^{7}/_{32}$-in. internal diameter, and $^{3}/_{32}$ in. thick. Twelve small holes were drilled through each of these annuli

FIGURE 4. *"Cleopatra-needle" assembly of Peltier junction and thermocouple for measuring the temperature of the Peltier junction.*

parallel to the axis and at 30-deg intervals. Alternate 0.010-in. diameter constantan and 0.012-in diameter chromel wires, 6 lengths of each, were now threaded through the 12 holes of 6 of these annuli in series. The annuli were separated by some 2½ in. from each other along the wires and secured to the wires by painting with glyptal cement. When the glyptal hardened the wires were cut midway between each anulus, and the basic units for six thermopiles were obtained. A thermopile was then simply obtained by hard-soldering adjacent constantan and chromel wires at each end in such a manner as to give one continuous circuit.

The cup and thermopile assemblies were finally mounted on two lucite disks in a copper disk mount in the manner illustrated in figures 1 and 2.

An intermediate type of radio-balance, illustrated in figure 1, was also constructed, in which four Peltier junctions were bound with nylon thread to the cup, 2 above and 2 below the thermopile, to investigate the effect of distributing the cooling effect. However, apparently due to the fact that no part of the cup is ever very different in temperature from the surroundings at balance, this type had no advantages over that of simple construction and was, in fact, less satisfactory in use.

The Peltier current was derived from a 6-v battery in series with a 1,000-ohm variable resistance and a standard 1-ohm and standard 10-ohm coil. The value of the current flowing through the Peltier junctions was then determined by measuring the potential drop across either of the standard resistances by means of a potentiometer. The current from the thermopiles was measured by means of a high-sensitivity galvanometer of nominal sensitivity equal to 0.000029 μa/mm. The thermopiles were connected either individually to the galvanometer or in opposition to each other through the galvanometer by means of mercury switches. A reversing switch made from three-contact mercury switches enabled the current through the galvanometer to be reversed. To eliminate extraneous thermal effects copper wire was used throughout, and the connections to the mercury switches and the switches themselves were immersed in an oil bath. An 18° to 28° C thermometer was used to measure the temperature of the copper block containing the radio-balance. This enables the variation in P with temperature to be calculated, using the thermodynamical relation that

$$P = T dE/dT, \tag{5}$$

where T is the absolute temperature, and E is the thermoelectromotive force.

In the present series of experiments the performance of the radio-balance has been very extensively investigated by using ordinary commercial radium preparations contained in platinum-iridium needles having a wall thickness of 0.5 mm.

The value of P may be determined in a subsidiary experiment by measuring the variation of thermoelectromotive force with temperature of a thermocouple made from the same wire as that used to construct the Peltier junctions. This in fact was done, the thermoelectromotive force being measured at 25° and 50° C. In practice, however, a slight temperature gradient of a few hundredths of a degree will exist along the cup between its base, to which the Peltier junction is attached, and the equatorial ring of the thermocouple junctions. This means that the cooled cup will gain a small quantity of heat from the surroundings, and the heated cup will lose a corresponding amount. The net effect will be to decrease slightly the effective Peltier coefficient. It is better therefore to measure the Peltier coefficient under the conditions of the experiment in the radio-balance itself.

For the purpose of determining the Peltier coefficient in this way, two pairs of small resistance coils were wound on platinum wire to simulate the thermal conductivity of the platinum-iridium needles. Each pair of coils consisted of a main resistance (R) with a compensating resistance (r), consisting of only a few turns of wire, in series. One pair of coils was wound from 33 gage manganin and the other from 38 gage constantan wire. They were then impregnated with glyptal cement and baked. To determine the Peltier coefficient, a pair of coils was connected in series with the Peltier junctions, so that the same current flowed through the coils and the junctions. The coils were then inserted into the radio-balance, one into each cup. The current was then adjusted in magnitude and direction to give approximate balance of the thermopile galvanometer, and the value of the current and residual galvanometer deflection was determined. The coils were then interchanged between the two cups, the current reversed, and the new residual deflection measured. Knowing the value of the resistance of each coil, W' and W'' in eq (4) may be calculated, and d_1, d_2, and C have been measured directly. The value of s need only be known approximately as $d_1 - d_2$ is, in general, only a small correcting term. The value of P can thus be obtained directly with the help of eq (4). It should be noted that the energy dissipation of the coils appears in eq (4) as the difference between two wattages. The losses along the leads to the coils are, therefore, exactly compensated.

The approximate value of s is determined by reversing a suitably small current through the Peltier junctions connected in opposition, with no source or coil in either cup, and noting the change in galvanometer deflection. Ideally, dummy radium needles should be placed in the two cups. As W'' and W''' are now zero, s can be determined directly from eq (4), using the thermoelectric value of P determined from eq (5).

The values of R and r were determined in terms of the standard resistances, using the potentiometer. For this purpose, the lead wires were bared, and potential leads were attached at equal distances from the point of the coil, which had previously rested on the base of the radio-balance cup. As already pointed out, only $W' - W'''$, and therefore $R - r$, is needed with accuracy. To obtain this, each coil was mounted on millimeter graph paper, and the distance from the

point of the coil to the point where the potential leads were soldered was determined to less than one-tenth of a millimeter. To enable this location to be made with accuracy and also to simulate the heat transfer of a radium needle, the platinum cores on which the two pairs of coils were wound, were turned to conical points, which protruded about a millimeter beyond the first turn of each coil at the end remote from the two current leads.

4. Results

TABLE 1. *Resistances of calibrating coils*

Coils	Distance from pointed end of coil to potential leads	R	r	$R-r$
	cm	*Ohms*	*Ohms*	*Ohms*
Manganin	2.40	2.269	0.839	1.421
Constantan	2.30	10.047	3.225	6.822
Do	1.50	9.103	2.264	6.839

The results obtained for $R-r$ for both the pair of manganin and the pair of constantan coils are shown in table 1.

The results for the thermoelectric power (dE/dT) from which the Peltier coefficient (TdE/dT) may be determined are shown in table 2. These can be compared with the value of 61.2 μV/deg obtained at 25° C by direct measurement of the thermoelectric power.

TABLE 2. *Mean thermoelectric power of Peltier junctions*

$R-r$	Current	Residual deflection, d_1-d_2	Thermoelectric power, dE/dT
Ohms	*ma*	*mm*	*μv/deg*
1.421	25.357	5.5_5	59.26×10^{-6}
1.421	25.629	11.2	58.84
1.421	26.425	19.6_5	59.17
1.421	28.060	43.6_5	59.15
6.831	4.473_5	−7.0	59.09
6.831	5.226	0.9_5	59.12

The average of the first four values, for the manganin coils, is 59.12×10^{-6} μv/deg at 25.4° C; and the average of the last two values, for the constantan coils, is $59.10_5\times10^{-6}$ μv/deg at 24.3° C. An average value of 59.11×10^{-6} μv/deg in the region of 25° C has therefore been assumed in calculating the results that follow.

Results for the scale sensitivity, s, for different currents and for different cup fillings are given in table 3.

After these preliminary calibrations, little remained to be done but to use the radio-balance, and it transpired that it was not necessary to limit its use to only the conventional method of balancing the energy dissipation of a radioactive source against the Peltier cooling. Experiments have been carried out chiefly with four radium preparations in platinum-iridium needles. These preparations have been compared with the National Primary Radium Standard

TABLE 3. *Galvanometer-scale sensitivity*

Cup fillings	Current	$2I^2C$	Galvanometer deflection	Scale sensitivity *
	ma	*μw*	*mm*	*mm/μw*
Silicone vacuum oil only.	3.097	109.4	36.1_5	0.330_0
	4.743	167.5	55.2_5	$.329_9$
	6.081	214.7	71.2_5	$.331_8$
	8.768	309.6	102.8_5	$.332_2$
1-mg dummy needles with silicone vacuum oil.	6.088	215.4	71.2_5	$.330_8$
	11.903	421.2	139.5	$.331_2$
5-mg dummy needles with silicone vacuum oil.	2.996	106.0	35.0	$.330_2$
	9.003	318.6	106.6	$.334_6$
	15.008	531.0	176.4_5	$.332_2$

* Average value of $s=0.331_5$ mm/μw.

and found, after correction for gamma-ray absorption in the platinum-iridium walls, to have the following values:

No. 35915	10.19 mg.
No. 35917	4.96 mg.
No. 35919	1.049 mg.
No. 35920	0.988 mg.

If one of these sources be placed in cup A and a dummy needle in cup B, there will be an increase in the temperature of cup A and a corresponding deflection of the thermopile galvanometer. However, the largest of these sources, preparation 35915, causes a rise in temperature of the cup above its surroundings of only approximately 0.25 deg. C. The loss of heat by radiation and gaseous conduction through the surrounding air will therefore be quite negligible, and the heat will be carried away mainly by conduction through the Peltier and thermopile leads. This quantity of heat will therefore be proportional to the temperature difference, or, conversely, the rise in temperature of the cup will be directly proportional to the quantity of energy dissipated within it. In other words, the galvanometer deflection should be directly proportional to the quantity of energy dissipated within it, and is therefore, in turn, directly proportional, in the case of radium, to the quantity of radium in the needle. It is necessary to qualify this statement in the case of preparations of radium that have been sealed at widely different dates and to take into account the small differences in energy dissipation caused by the growth of Po^{210}. With this qualification, however, the radio-balance has been found to provide an excellent method for quickly and accurately comparing the ratios of quantities of radium, simply by observing the ratios of the galvanometer deflections.

As an example of this method, the change in the galvanometer deflections on interchanging a radium source with a dummy between cup A and cup B is shown (fig. 5) plotted against milligrams of radium, for 3 of the 4 radium preparations used. Up to 5 mg of radium the scale deflection is a linear function of the mass of radium, but in order to preserve linearity up to 10 mg, it was necessary to convert scale deflections to angular deflections.

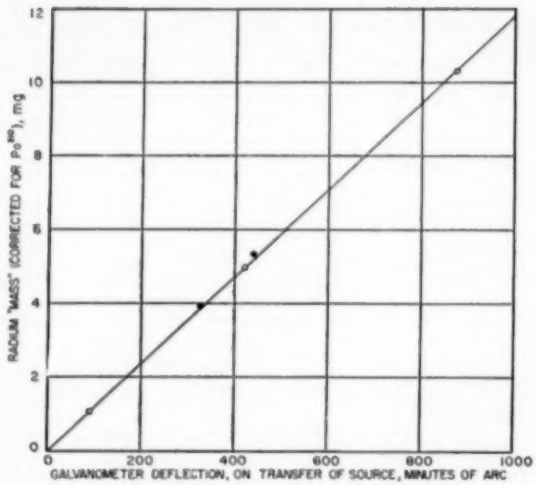

FIGURE 5. *Galvanometer deflection in minutes of arc as a function of milligrams of radium transferred from cup A to cup B.*

Open circles are for sources 35919, 35917, and 35915. Solid circles are difference readings for source 35919 and source 35917 (=3.91 mg of Ra) and for source 35917 and source 35915 (=5.23 mg of Ra). In order to reduce all readings to a comparable norm the milligram content has been increased by the ratio of column 4 to column 5 in table 5 to allow for the fact that the radium content, as determined by gamma-ray measurements, does not take into account the growth of polonium. The stated accuracy of the certification of the Radium Testing Laboratory is ±0.7 percent. This uncertainty in mass is approximately represented by the diameter of the open circles for the 10.19-mg source (=10.32±0.07 mg, corrected for polonium).

It should perhaps be emphasized at this juncture that the energy emitted in the form of gamma radiation is largely lost from the radio-balance. With radium in equilibrium with its short-lived daughters, alpha radiation accounts for about 87 percent of the energy emission, recoil nuclei for about 2 percent, primary beta radiation for about 4 percent, and gamma radiation and secondary beta radiation for about 7 percent. Polonium in equilibrium would contribute a further 20 percent.

The energies dissipated by sources 35915, 35917, 35919, and 35920 were now measured by the transfer method between cups A and B, using the Peltier cooling and heating to equalize source and dummy, respectively. It later transpired that these sources, although purchased at the same time, had been sealed at different dates and it therefore became necessary to correct for the growth of the 5.3-Mev alpha particle due to Po^{210}. This was done by using a relation derived by Curie and Yovanovitch [4], who neglected the effect of the short-lived intermediaries between radium and radium D and between radium D and polonium. This relation, the numerical constants of which were later revised by Sanielevici [5], Zlotowski [6], and then by Jordan [7], using more accurate half-life data, gives $Q_{\alpha_{Po}}$, the heat generated by the Po^{210} alpha particles, as a function of the time t in years as follows:

$$Q_{\alpha_{Po}}=27.26(1-1.0175e^{-0.05105t}+0.0173e^{-1.329t})\text{cal g}^{-1}\text{ hr}^{-1} \quad (6)$$

The results obtained are summarized in table 4. All sources are corrected for polonium growth to October 1953.

The ratios of these sources obtained by gamma-ray comparisons in the Bureau's Radium Testing Laboratory and by the radio-balance are summarized in table 5. The stated accuracy of the Radium Testing Laboratory results is ±0.7 percent.

Values obtained at other times for the energy emission of sources 35917 and 35919 are given in table 6.

Values for source 35917 were also determined by using cup A and cup B individually. For this purpose, it is necessary to determine the resistance R_A and R_B of the Peltier junctions to cups A and B. Using eq (2), these were found to be 46.30×10^{-3} and 46.07×10^{-3} ohm, respectively. As has been mentioned previously, however, it is difficult to remove completely the residual thermopile zero deflections for each cup individually. In this determination therefore these zero deflections were determined initially, and the values for the source energy emission were reduced to these afterward by extrapolation. However, this method is tedious compared with the transfer method. The results obtained by using eq (1) are shown in table 7.

One final point of note is that the radio-balance can be used to compare two nearly equal sources by the transfer method without using any Peltier current at all. From figure 5 the scale sensitivity for transfer of a mass of radium from cup A to cup B is 0.0193 mg/mm. On placing source 35919 in cup A and source 35920 in cup B, an out-of-balance deflection of +1.9 mm was observed. On interchanging the sources, an out-of-balance deflection of −1.4 mm was observed, giving a total change on transfer of 3.3 mm. In actual practice, twice this deflection is observed on reversing the current through the galvanometer, but for convenience in recognizing whether cup A is warmer or cooler than cup B, these are reduced to half the deflection to the right (+) or left (−) of zero.

A change of deflection on transfer corresponds therefore to a difference between sources 35919 and 35920 of 0.064 mg, with 35919 the greater (a positive deflection corresponds to cup A, being at a higher temperature than cup B).

Thus if we assume that source 35919 consists of 1.049 mg of radium, as certified by the Radium Testing Laboratory, then source 35920 comprises 0.985 mg (compared with 0.988 mg as certified by the Radium Testing Laboratory).

This application is also illustrated for widely differing sources in figure 5, where points derived by taking differences between sources 35915, 35917, and 35919 have been plotted.

A series of experiments was also carried out with the radio-balance, using individual cups in an evacuated bell jar at approximately 5×10^{-5} mm Hg pressure, with a view to determining whether the loss of heat from the cups by radiation and gaseous conduction was of significance. In general, it was found

TABLE 4. *Energy dissipation per milligram of radium*

Source	Date sealed	Value	Balancing current	Change of residual galvanometer deflection on transfer, (d_1-d_2)	Energy dissipation	Energy dissipation per milligram of radium	Energy dissipation of radium less the polonium contribution [a]
		mg Ra	ma	mm	μw	μw/mg Ra	μw/mg Ra
35915	April 6, 1951	10.19	42.674	11.8	1541.1	151.2	149.3
35917	November 6, 1952	4.96	21.587	−4.1$_5$	749.0	151.0	150.5
35919	December 22, 1949	1.049	3.850	8.0	159.9	152.4	149.4
35920	December 22, 1949	0.988	3.855	5.2	151.7	153.5	150.5

[a] Average energy dissipation per milligram of radium (less Po^{210} contribution) equals 149.9 μw/mg ±0.4 percent, which is equal to 128.9 cal g^{-1} hr^{-1} ±0.4 percent. (±0.4 percent represents a 95-perent confidence limit.)

TABLE 5. *Measured relative values of radium sources*

Source	NBS Radium Testing Laboratory		Radio-balance		
	Value	Ratios	Energy dissipation	Energy dissipation less polonium contribution	Ratios
	mg		μw	μw	
35915	10.19	1	1541.1	1521.8	1
35917	4.96	0.487	749.0	746.0	0.490
35919	1.049	.1029	159.9	156.8	.1030
35920	0.988	.0970	151.7	148.6	.0976

TABLE 6. *Energy dissipation of two radium sources*

Source	Energy dissipation less polonium contribution [a]	Date of measurement
	μw	
35917	743.3	September 1, 1953.
35917	744.3	Do.
35917	748.7	September 24, 1953.
35917	748.7	September 25, 1953.
35917	746.5	October 22, 1953.
35919	159.0	September 1, 1953.
35919	158.8	Do.
35919	[b] 156.6	Do.
35919	156.8	October 22, 1953.

[a] The mean value for source 35917 is 746.3 μw, with a standard deviation of 0.3 percent. The mean value for source 35919 is 157.8 μw, with a standard deviation of 0.8 percent.
[b] No dummy used in other cup.

TABLE 7. *Determination of the energy emission from a radium source, using the radio-balance cups individually*

Cup	Balancing current	Residual galvanometer deflection [a]	Temperature	Energy dissipation, [a] $PC-C^2R$
	ma	mm	°K	μw
A	47.767	+0.1$_5$	297.8	735.2
A	48.323	−1.1	297.8	742.1
B	48.651	0	297.7	747.1
B	49.033	−1.0	297.7	752.0

[a] The initial "zero" deflections for cups A and B, with a dummy 5-mg needle that had been left to come into thermal equilibrium in each, were −1.3 and −1.0 mm, respectively. Thus the value of source 35917 as determined in cup A is, by extrapolation, 743.2 μw. The value for cup B is 752.0 μw. The average value for cups A and B is 747.6 μw (or 745.3 μw after correcting for the growth of polonium) compared with 746.5 μw obtained by the transfer method (also corrected for polonium growth).[f]

that the radio-balance was much more unruly, the extraneous thermal effects being more difficult to track down and eliminate. This method of using the radio-balance was therefore abandoned in favor of the methods described. The use of silicone vacuum-pump oil originated, however, from the experiments with the apparatus in a vacuum, but its use was continued because of the obvious advantage of a low-vapor-pressure liquid from the point of view of avoiding decreases in temperature due to evaporation.

5. Comparison With the Mound Laboratory Calorimeters

As the total energy emission of two radium needles, the milligram content of which had been measured in terms of the National Primary Radium Standard, had recently been measured in the calorimeters of the Mound Laboratory, it has been possible to compare their results with those obtained with the radio-balance.

The total radium content of these two radium sources as measured by the Radium Testing Laboratory was 10.20 mg.

The Mound Laboratory obtained results both with their microcalorimeter and their macrocalorimeter. With the former they found the total energy output of the two needles to be 1.634 μw, with 0.1 cm equivalent lead absorption; with the latter, they found it to be 1.65 μw, with 1.1 cm equivalent of lead absorption.

Initially, it was assumed by the Mound Laboratory that these needles had been sealed recently. However, it has transpired that they had been first tested by the National Bureau of Standards in June 1939, and that considerable correction had to be made for the growth of Po^{210}.

By using a value of 4.185 j/cal and the value of 10.20 mg of radium, the Mound Laboratory results reduce to 137.8 cal g^{-1} hr^{-1} (microcalorimeter, 0.1 cm Pb equivalent) and 139.2 cal g^{-1} hr^{-1}(macrocalorimeter, 1.1 cm Pb equivalent), both uncorrected for Po^{210} growth and therefore including all energy contributions down to that due to the Po^{210} alpha particles.

The cups of the radio-balance are 0.04 cm thick; in each case the wall thickness of the platinum-iridium needle was 0.05 cm. As the mass-absorption coefficients of copper, platinum, and lead are, for the purpose of making a gamma-ray absorption correction in this energy range, sufficiently near to equality, and as the needles consist of 90 percent of platinum, it will be sufficiently accurate to reduce the absorption of the platinum-iridium needles and the copper cups for gamma radiation to their equiva-

lent total absorption in lead using the densities of copper, platinum, and lead. This gives a gamma-ray absorption of the needles and cups equivalent to that of 0.126 cm of lead.

Assuming that the radium needles had been sealed for 14 years prior to their measurement by the Mound Laboratory between December 1952 and February 1953, the contripution due to Po^{210} would have been 9.5 cal g^{-1} hr^{-1}, as calculated from eq (6). We have, therefore, the following results for the energy output of 1 g of radium and its products down to radium D:

128.3 cal g^{-1} hr^{-1}	Mound microcalorimeter with 0.1 cm Pb equivalent.
129.7 cal g^{-1} hr^{-1}	Mound macrocalorimeter with 1.1 cm Pb equivalent.
128.9 cal g^{-1} hr^{-1}	NBS radio-balance with 0.126 cm Pb equivalent.

These results have been reduced, for the purpose of comparison, to the same value of equivalent absorption, using the measurements of Zlotowski [6], who determined the energy emission of four radium sources calorimetrically by using different thicknesses of lead absorber around the sources. Zlotowski's results are shown in figure 6, where the heat absorbed in the calorimeter is plotted as a function of thickness of lead absorber. By using this curve the Mound Laboratory results may be reduced to an equivalent thickness of lead equal to 0.126 cm and compared directly with the NBS value. The results then obtained are

Mound microcalorimeter	128.5 cal g^{-1} hr^{-1}.
Mound macrocalorimeter	125.4 cal g^{-1} hr^{-1}.
NBS radio-balance	128.9 cal g^{-1} hr^{-1}.

The probable error of the mean value obtained from 10 readings with each of the Mound calorimeters is ± 0.5 percent. The probable error of the mean value obtained from 4 readings of the NBS radio-balance is ± 0.2 percent.

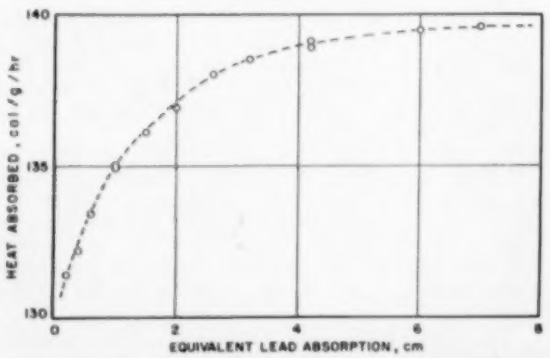

FIGURE 6. *Heat absorbed from 1 mg of radium per hour as a function of equivalent absorption in lead, after Zlotowski* [6].

The point at 7 cm of 139.6 cal g^{-1} hr^{-1} is the extrapolated value for the total heat emission of radium-226 and its daughters down to Ra C'.

6. Conclusion

It is proposed to apply the radio-balance described in this paper to the measurement of the average energy of beta emitters and also to a number of other appropriate problems. A new radio-balance is being constructed with a view to comparing the U. S. and Canadian National radium standards. Two such standards were compared with quite promising results in the radio-balance here described, but the cups of this radio-balance are somewhat too small for these sources. It is interesting to note, however, that the radio-balance is so responsive that a comparison agreeing well with the known data was carried out between the U. S. and Canadian National radium standards in as short a time as 1 hr.

From table 3 the average value of the scale sensitivity for transfer is 0.332 mm/μw. As deflections may be read to about 0.1 mm (i. e., 0.2 mm on reversal of the current through the galvanometer), it should be possible to determine an energy emission to about a third of a microwatt. Thus a 30-μw source should be susceptible of measurement with an accuracy of about 1 or 2 percent. Such a value, corresponding to about 0.2 mg of radium, probably represents the lower limit of usefulness of the radio-balance.

Grateful acknowledgment is made to D. L. Timma and to K. C. Jordan of the Mound Laboratory of the Monsanto Chemical Co., for their courtesy in carrying out the calorimetric measurements on the two radium needles that had been calibrated by the NBS Radium Testing Laboratory in terms of the National Primary Radium Standard. Thanks are also expressed to T. I. Davenport of the Radium Testing Laboratory for suggesting and arranging that these radium needles should be measured by the Mound Laboratory, and to him and his colleagues, C. C. McCraven and L. F. Paolella, for supplying a number of calibrated radium needles for frequent rechecks of their values, and also for valuable assistance in the construction of the radio-balance container. Also gratefully acknowledged is the kind assistance of Chester Peterson, of the NBS Resistance and Reactance Section, for his calibration of the standard resistances used and for the loan of a standard cell; Joseph A. Kelly, Jr., vice president of the Radium Chemical Co., for the loan of two 1-mg and two 5-mg empty platinum-iridium needles for use as dummy sources; and of S. Eugenia Thomas, of the Temperature Measurements Section, for measuring the thermoelectric power of a number of thermocouples constructed from the chromel and constantan wires used to make the Peltier junctions.

7. References

[1] H. L. Callendar, Proc. Phys. Soc. (London) **23,** 1 (1911).
[2] F. E. Hoare, Phil. Mag. **6,** 828 (1928).
[3] F. E. Hoare, Phil. Mag. **13,** 386 (1932).
[4] M. Curie and D.-K. Yovanovitch, J. phys. radium **6,** 33 (1925).
[5] A. Sanielevici, J. chim. phys. **30,** 513 (1933)
[6] I. Zlotowski, J. phys. radium **6,** 242 (1935).
[7] K. C. Jordan, private communication.

WASHINGTON, November 17, 1953.

Journal of Research of the National Bureau of Standards Vol. 52, No. 4, April 1954 Research Paper 2487

Some Factors Affecting the Dimensional Stability of the Silver-Tin-(Copper-Zinc) Amalgams*

J. A. Mitchell,[1] I. C. Schoonover, George Dickson, and H. C. Vacher

An investigation of the X-ray diffraction characteristics and of the dimensional changes of silver-tin-(copper-zinc) amalgams during and after their hardening period indicated that uncombined mercury was present in the amalgams after the initial solidification and that this uncombined mercury disappeared during the period when greatest dimensional changes occur. On the basis of the data obtained, it is postulated that the expansion during the hardening of amalgam results from diffusion of uncombined mercury throughout the material; the subsequent shrinkage then results from combination of this mercury with existing phases or with residual alloy.

1. Introduction

Although an enormous amount of experimental work has been done on the silver-tin-(copper-zinc)[2] amalgams [1,2,3,4,5,6],[3] no mechanism has been proposed that will satisfactorily explain the initial contraction, subsequent expansion, and final contraction that occur during the first 24 hr after amalgamation. Various investigators have attempted to explain these changes in terms of mercury content of the amalgam system. Their difficulty may have resulted from the failure to differentiate between total mercury and combined mercury in this system. It is probable that in the hardening of the heterogeneous mass not all the mercury is in the combined form. Chemical analysis of the amalgam would not distinguish between combined and uncombined mercury. Furthermore, photomicrographic evidence [7] indicates that the rate of attack on the alloy particles by mercury may vary widely, depending upon the conditions under which the specimen was prepared. The possible diffusion of this mercury, if it is present, and its subsequent reactions with the alloy may account for the dimensional changes observed in the hardened amalgam.

With this in mind, the investigation was undertaken to determine (1) whether uncombined mercury was present after the amalgam had hardened, (2) whether the uncombined mercury, if present, continued to take part in any reaction, and (3) whether the dimensional changes that occur in hardened amalgam could be correlated with this reaction.

2. Experimental Approach and Procedures

X-ray diffraction methods cannot be used to detect the presence of free or uncombined mercury in an amalgam at room temperature because the mercury, being a liquid at this temperature, does not have a crystalline structure and does not give an X-ray diffraction pattern. However, if the mercury is chilled below its solidification point, typical lines representing mercury are detected by diffraction methods. Therefore, if uncombined mercury is present in amalgam immediately after hardening, it should be possible to determine its presence by X-ray investigation of amalgam specimens held below the freezing temperature of mercury. Furthermore, it should be possible to study the rate of disappearance of the uncombined mercury with time by periodic examination of the specimen at temperatures below the freezing point of mercury.

X-ray diffraction patterns of the amalgams at low temperatures were obtained from specimens that were manually condensed, using standard dental procedures, in a stainless-steel mold and specimen-holder combination (fig. 1). Immediately after condensation, the amalgam specimens were frozen by introducing liquid nitrogen into the chamber beneath the specimen. An iron-constantan thermocouple was inserted in the specimen holder, near the specimen for temperature determination.

Three commercial amalgam alloys were used in the investigation. Amalgams were produced by triturating the alloys with mercury in a mechanical amalgamator, using the mercury-alloy ratio of 2 to 3 for alloys 1 and 2, and a ratio of 2 to 3.6 for alloy 3.

A high-angle spectrometer goniometer [8] was used to obtain chart records of the copper K-alpha diffraction. The diffraction unit was operated at 35 kv and a tube current of 20 ma. The angular speed of the scanning arm was 1 deg/min, and the chart speed was ½ in./min.

X-ray diffraction characteristics were obtained with the specimen and its holder maintained at the constant reduced temperature (−125° C) during the making of chart records in a 2θ range of 80 to 28 deg. The specimen was then warmed to mouth temperature (37° C) and aged at that temperature until the next low-temperature diffraction-chart recording was made.

The X-ray diffraction technics described above were used also to determine the effect of addition of

*A dissertation submitted to the faculty of the Graduate School, Georgetown University, in partial fulfillment of the requirements for the degree of Master of Science.

[1] Guest worker at the National Bureau of Standards, and member of Dental Corps, Department of the Navy.

[2] The chemical symbols Ag-Sn-(Cu-Zn) are used hereafter. Copper-zinc is placed in parentheses because these elements are not always present in the above-mentioned amalgams.

[3] Figures in brackets indicate the literature references at the end of this paper.

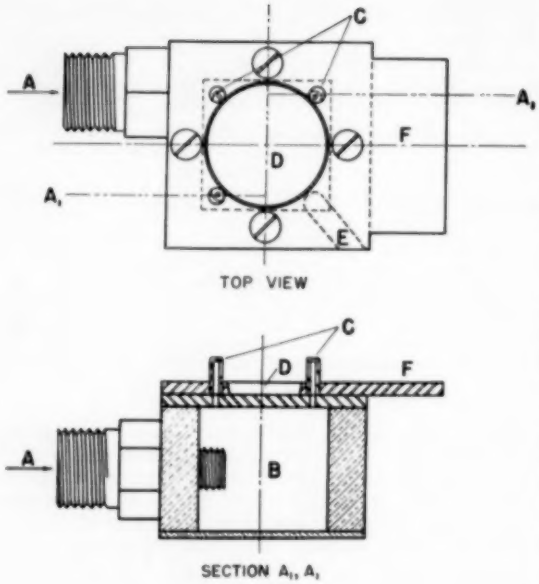

FIGURE 1. *Amalgam mold and specimen holder for low-temperature X-ray diffraction studies.*

Holder enclosed in a cylindrical box. Specimen retained in holder and alternately cooled to −125° C by liquid nitrogen and warmed to 37° C by a wire-wound resistor regulated with a variable autotransformer.
A, Liquid nitrogen intake; B, liquid-nitrogen chamber; C, jets; D, specimen; E, thermocouple rest; F, arm fastened to goniometer shaft.

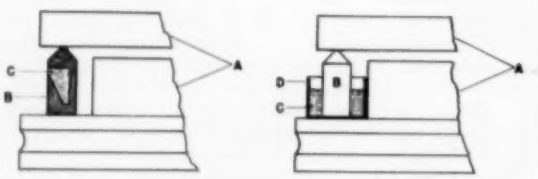

FIGURE 2. *Measurement of dimensional change of fully hardened amalgam specimens after addition of mercury.*

Mercury added internally and externally.
A, Dental interferometer; B, specimen; C, mercury; D, iron cup.

mercury to fully hardened amalgam specimens. Seven-day-old specimens were immersed in mercury for 12 hr, removed and cooled to −125° C, and examined by X-ray diffraction. The specimens were kept at 37° C during the next 24 hr, except for periodic cooling to −125° C while the diffraction charts were made.

To examine the effect of uncombined mercury on dimensional changes of hardened amalgam, mercury was added both externally and internally to hardened amalgam specimens, and their dimensional changes were measured by means of dental interferometers [9], (fig. 2). Hardened specimens of amalgam in iron cups were positioned in interferometers. Mercury was added to the cups, and the dimensional changes were observed over a period of 15 days on two series of specimens held at 21° and 37° C, respectively. In other experiments a small hole was drilled in the specimen and mercury injected into the hole in the amalgam by means of a hypodermic syringe after the specimens had been positioned in the interferometers. Dimensional changes were then observed over a period of 15 days. Temperatures were maintained by constant-temperature air baths.

In two of the above experiments the supply of mercury was removed from contact with the specimens after the period of 15 days, and dimensional changes were observed for an additional period of 26 days.

To obtain information on the effect of temperature on the reactions occurring during the hardening of the dental amalgams, dimensional changes of amalgams prepared and observed at various temperatures were also determined interferometrically.

3. Results

3.1. X-ray Diffraction Examination of the Ag-Sn-(Cu-Zn) Amalgams

As shown in table 1, one of the three commercial amalgam alloys used in the investigation was a silver-tin-zinc alloy, one a silver-tin-copper-zinc, and the other a silver-tin-copper alloy. Upon examining their X-ray diffraction patterns (fig. 3), it is evident that the variation in copper and zinc content has little effect on the diffraction patterns as the position of the principal peaks are identical in all three charts.

TABLE 1. *Chemical composition of alloys investigated*

Elements	Alloys		
	1	2	3
	%	%	%
Ag	74.5	70.2	70.1
Sn	25.0	25.6	26.5
Cu	0.0	2.4	3.4
Zn	0.5	1.8	0.0

X-ray diffraction charts of pure mercury at −125° C show a number of well-defined peaks (fig. 4, a). A specimen of amalgam containing the Ag-Sn-Cu-Zn alloy was made at room temperature (25° C), placed in position, and its X-ray pattern determined at −125° C 5 min after the start of mix (fig 4 (b). The characteristic peaks of the uncombined mercury can be seen as represented by the solid-black areas. As the specimen is aged through longer periods of time at 37° C, the characteristic peaks of the uncombined mercury tend to disappear, and after 6 hr they are scarcely detectable (fig. 4 (c), and fig. 5). This time period corresponds generally to the period during which significant expansion and contraction are commonly observed. Simultaneously with this reduction in uncombined mercury, there is a disap-

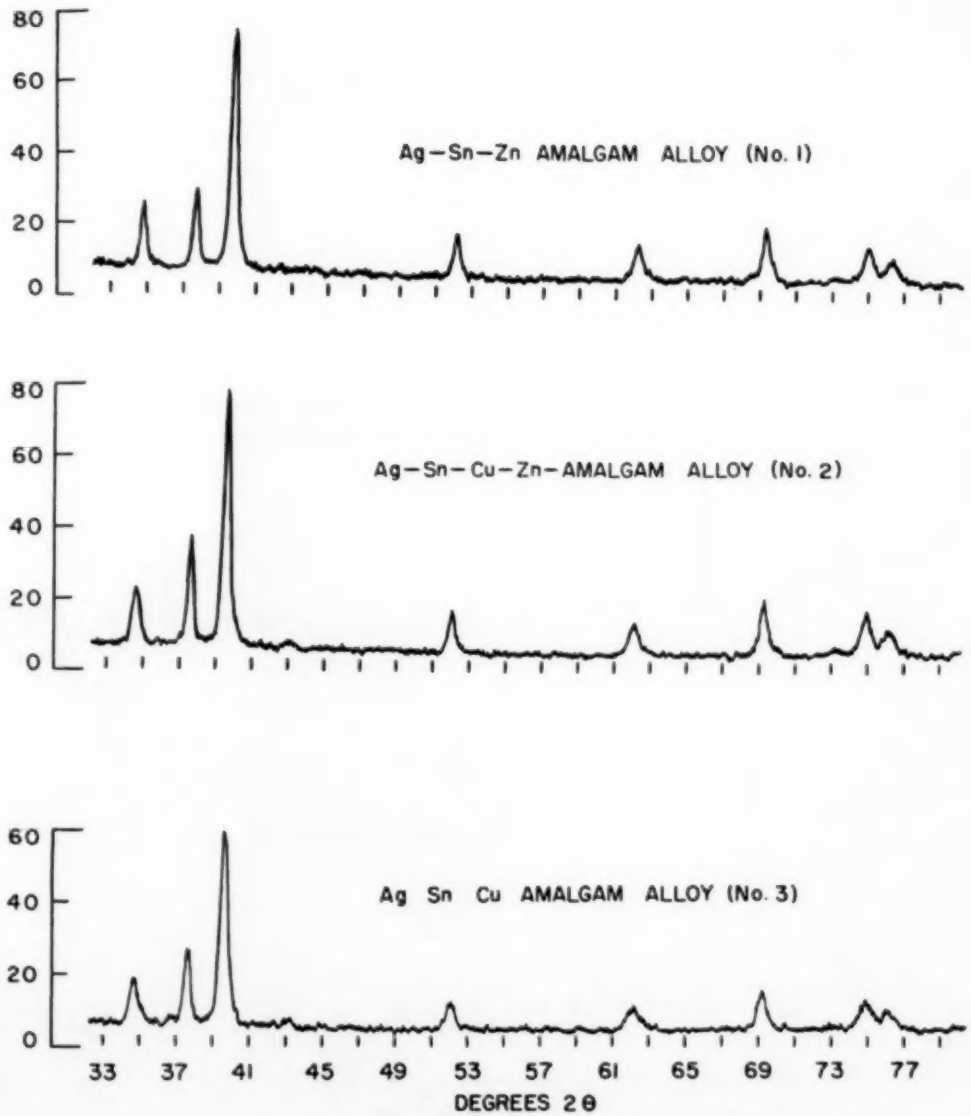

FIGURE 3. *X-ray diffraction charts (with a scale factor of 4) made at 25° C.*

The similarity of the charts for the three alloys indicates that none of the lines shown are dependent upon the copper or zinc content of the alloys.

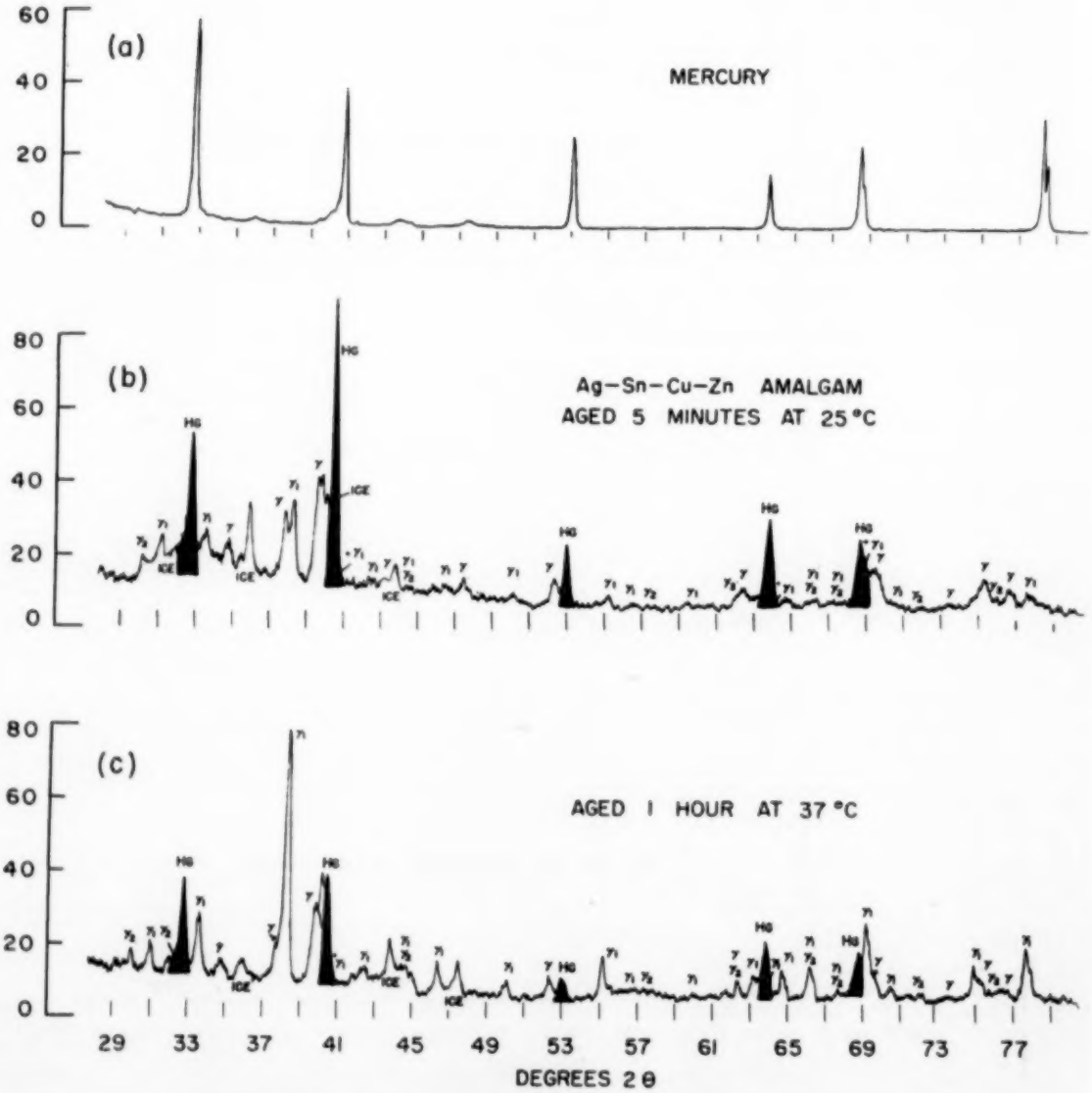

FIGURE 4. *X-ray diffraction charts made at −125° C.*

a, Scale factor of 32 used for obtaining the tracings of mercury. b and c, Scale factor of 4 used for the remainder of the procedures. Height of the peaks of γ_1 and γ_3 lines hidden by the mercury lines were determined by X-ray diffraction charts made at 37° C. Lines representing ice formation are labeled "ICE."

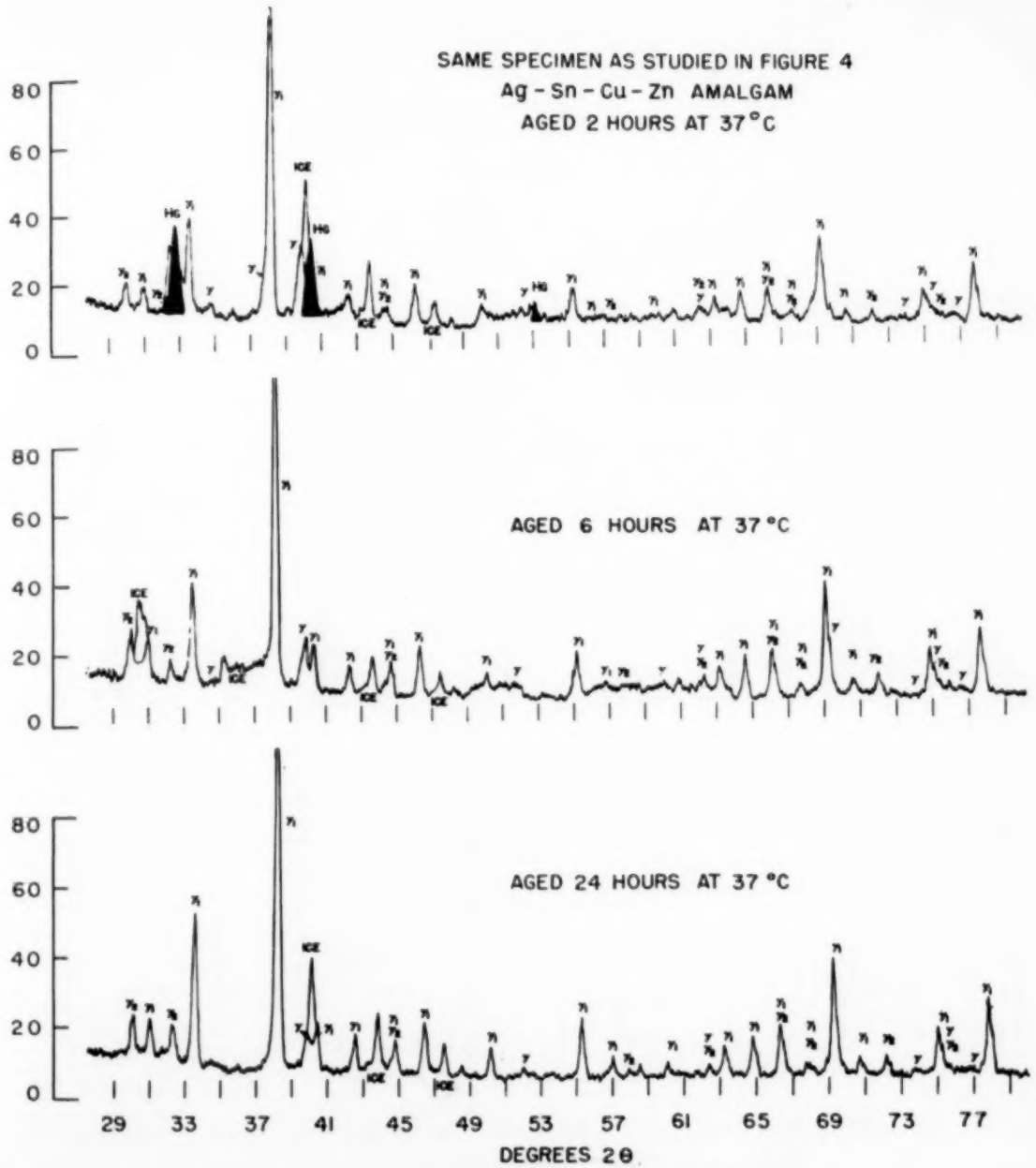

FIGURE 5. *X-ray diffraction charts made at −125° C.*

(See legend for fig. 4, b and c)

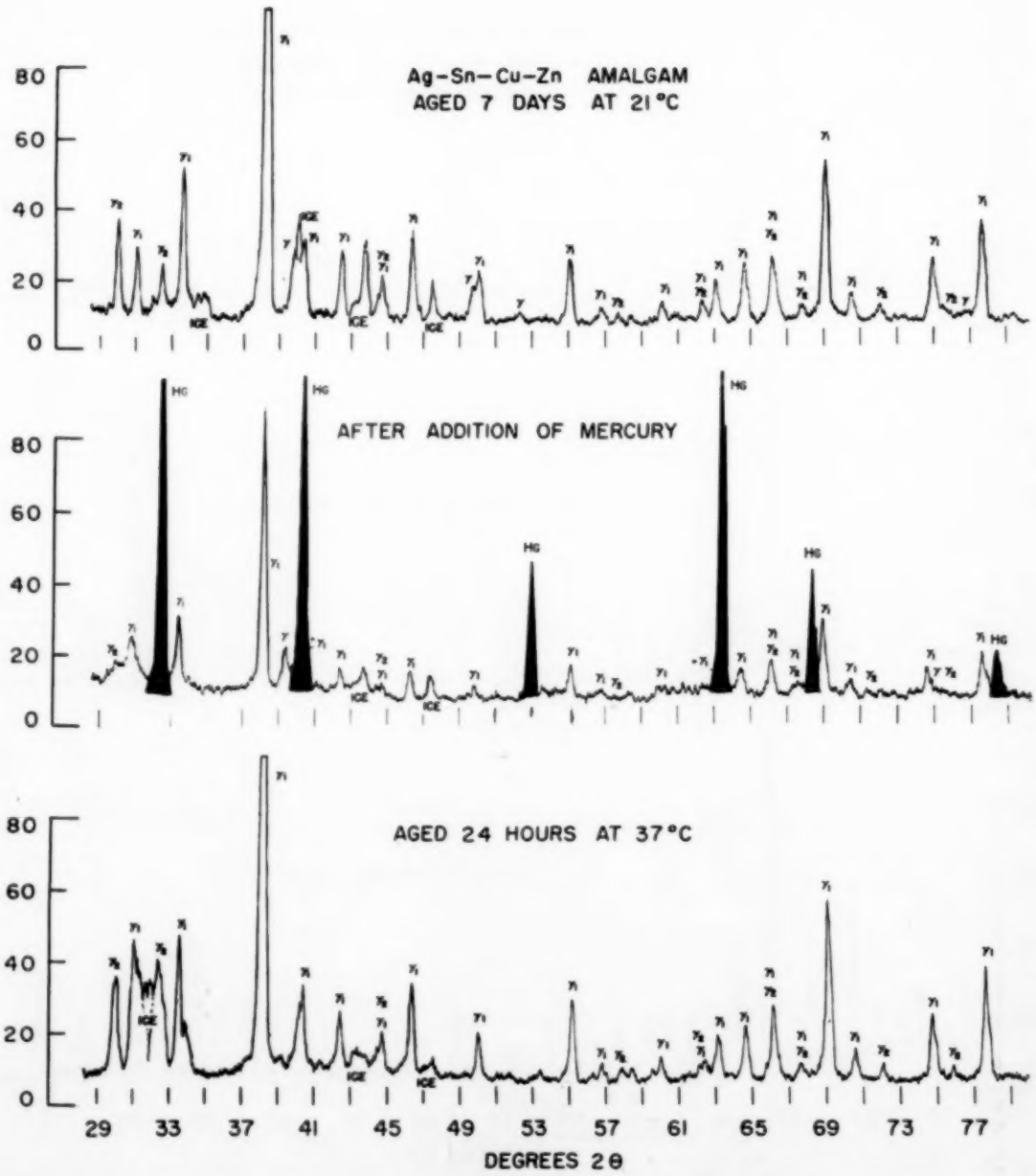

FIGURE 6. *X-ray diffraction charts made at −125° C.*

(See legend for fig. 4, b and c)

pearance of the lines representing the original alloy (γ)[4] and an increase in the γ_1 and γ_2 phases (fig. 4 (b) and (c), and fig. 5). This indicates that the disappearance of the free mercury lines was through combination of the mercury with the alloy to form mercury compounds.

X-ray diffraction charts made periodically at reduced temperatures after the addition of mercury to fully hardened amalgam showed intense mercury lines in the specimens observed immediately after removal from the mercury bath (fig. 6). These mercury lines were not detected after the specimens had been held at 37° C for 24 hr or at 21° C for 3 days. In figure 6 it can be seen that mercury on the surface of the specimens reduces the intensity of the lines representing the original alloy and γ_1 and γ_2 phases. After aging for 24 hr, the mercury has combined with the original alloy as indicated by the absence of γ and uncombined mercury lines.

Consideration was given to the possibility that the intermediate phases in the Ag-Sn-(Cu-Zn) amalgams might have a higher mercury solubility at room temperature than at temperatures below the freezing point of mercury. Under such conditions, crystalline mercury at low temperatures might be formed by rejection from a solid solution existing at room temperature. However, the disappearance of the lines representing uncombined mercury indicates that such a rejection does not occur to a significant extent if at all.

3.2. Dimensional Change Determinations of the Ag-Sn-(Cu-Zn) Amalgams

The addition of mercury to the hardened specimens produced large expansions, whether the mercury was added internally or externally (fig. 7). Specimens maintained at 37° C expanded much more than those maintained at 21° C. The great difference in expansion between the two specimens placed in mercury baths at 37° C may result from imperfections or other variations in the individual specimens that affect the rate of diffusion of mercury into the amalgam. Only very slight dimensional changes occurred after removal of the supply of excess mercury from hardened specimens (fig. 8).

Amalgam specimens prepared and maintained at either 21° or 37° C showed a rapid initial contraction, followed by some expansion during the first 24-hr period. Average values for dimensional changes are plotted against time in figure 9, 10, and 11. Ag-Sn-Zn amalgams prepared at 21° C and maintained at 37° C gave an over-all shrinkage, whereas those prepared and maintained at 21° C gave an over-all expansion (fig. 9 and table 2). Ag-Sn-Cu-Zn amalgams prepared and maintained at 37° C also had greater initial contraction, lower maximum expansion and greater over-all contraction than those prepared and maintained at 21 °C (fig. 10 and table 2). Ag-Sn-Cu-Zn amalgams initially observed at 21° C and then subjected to a temperature increase to 37° C shrank more than those maintained at 21° C

[4] γ: original alloy (Ag_3Sn+Cu, Zn), γ_1: Ag_2Hg_3, γ_2: Sn_7Hg [3, 5, 6].

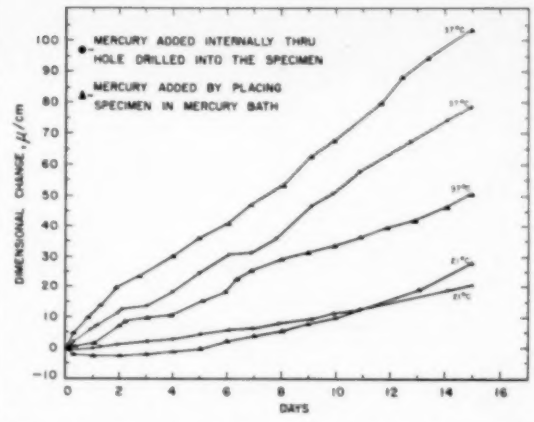
MERCURY ADDED INTERNALLY THRU HOLE DRILLED INTO THE SPECIMEN
MERCURY ADDED BY PLACING SPECIMEN IN MERCURY BATH
DIMENSIONAL CHANGE, μ/cm
DAYS

FIGURE 7. *Dimensional changes in* Ag-Sn-Cu-Zn *amalgam (alloy 2) resulting from addition of mercury.*

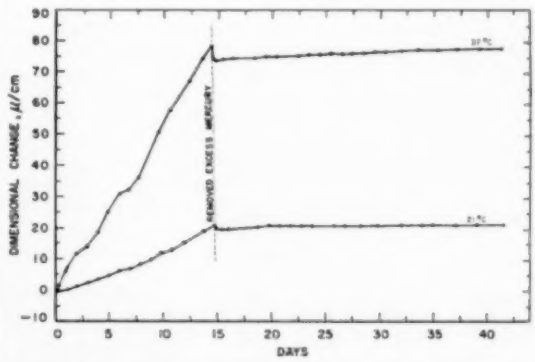

FIGURE 8. *Dimensional changes of* Ag-Sn-Cu-Zn *amalgam (alloy 2) resulting from addition and removal of mercury.*

0 days, mercury added internally through hole drilled into specimen; 15 days, excess mercury removed from hole drilled into specimen.

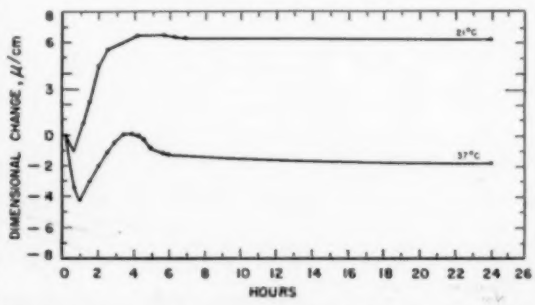

FIGURE 9. *Comparison of dimensional changes of* Ag-Sn-Zn *amalgam (alloy 1) at 21° C and at 37° C.*

Specimens prepared at 21° C.

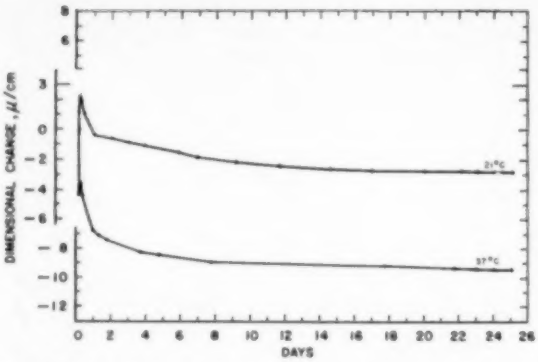

FIGURE 10. *Comparison of dimensional changes of* Ag-Sn-Cu-Zn *amalgam (alloy 2) at 21° C and at 37° C.*

Specimens prepared at 21° C and at 37° C, respectively.

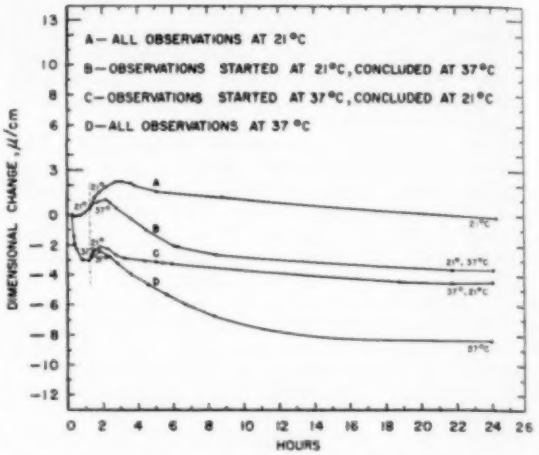
A— ALL OBSERVATIONS AT 21°C
B—OBSERVATIONS STARTED AT 21°C, CONCLUDED AT 37°C
C—OBSERVATIONS STARTED AT 37°C, CONCLUDED AT 21°C
D—ALL OBSERVATIONS AT 37°C
DIMENSIONAL CHANGE, μ/cm
HOURS

FIGURE 11. *Comparison of dimensional changes of* Ag-Sn-Cu-Zn *amalgam (alloy 2) at 21° C and at 37° C.*

Specimens prepared at 21° C.

TABLE 2. *Dimensional changes and their standard errors for* Ag-Sn-(Cu-Zn) *amalgams at 21° and 37° C*

Alloy	Temperature of observation [a]	Number of specimens observed	Fiducial observation 15 min after start of mix			Fiducial observation 10 min after start of mix (change 24 hr)	Typical curves
			Initial contraction	Maximum expansion	Change in 24 hr		
	°C		μ/cm	μ/cm	μ/cm	μ/cm	
1	21	7	−1.3 ±0.1	+7.0 ±0.3	+6.2 ±0.3	+4.3 ±0.5	Figure 9.
	37	8	−4.1 +0.4	+0.0 ±0.3	−2.1 ±0.3	−6.2 +0.4	
	Difference		2.8 ±0.5	7.0 ±0.4	8.3 ±0.5	10.5 ±0.6	
[b] 2	21	4	−0.3 ±0.05	+2.1 ±0.4	−0.9 ±0.5	.....	Figure 10.
	[c] 37	4	−4.2 ±0.6	−3.4 ±0.4	−7.0 ±0.5	.....	
	Difference		3.9 ±0.6	5.5 ±0.6	6.1 ±0.6	.....	
2	21	15	−0.3 ±0.05	+2.0 ±0.2	−1.0 ±0.2	−2.6 ±0.3	Figure 11, curves A and D.
	37	7	−2.6 ±0.3	−2.0 ±0.3	−8.6 ±0.3	−12.5 ±0.5	
	Difference		2.3 ±0.3	4.0 ±0.4	7.6 ±0.4	10.0 ±0.6	
2	21	15	−0.3 ±0.05	+2.0 ±0.2	−1.0 ±0.2	.....	Figure 11, curves A and B.
	21; changed to 37	4	(d)	+1.3 ±0.4	−3.4 ±0.4		
	Difference		.....	0.7 ±0.5	2.4 ±0.5	.....	
2	37	7	−2.6 ±0.3	−2.0 ±0.3	−8.6 ±0.3	.....	Figure 11, curves C and D.
	37; changed to 21	4	(d)	−1.7 ±0.4	−4.6 ±0.4		
	Difference		.....	0.3 ±0.5	4.0 ±0.6	.....	
[e] 3	21	10	−0.3 ±0.05	+3.6 ±0.3	+2.4 ±0.3	+1.2 ±0.4	
	37	7	−1.8 ±0.2	+1.4 ±0.3	−2.1 ±0.3	−5.2 ±0.5	
	Difference		1.5 ±0.2	2.2 ±0.4	4.5 ±0.4	6.4 ±0.6	

[a] Specimens prepared at 21°, unless otherwise noted.
[b] 24-day period, with fiducial observation 15 min after start of mix: 21° C gave an average of −3.0 ±0.3 μ/cm, 37° C gave an average of −9.9 ±0.3, giving a difference of 6.9 ±0.4.
[c] Specimens prepared at 37° C.
[d] Not comparable with alloys 1 and 2 because of differences in alloy-mercury ratio and mixing time.
[e] Not observed.

during the observation period (fig. 11 and table 2). Specimens held at 37° C and then subjected to a temperature decrease to 21° C shrank less than those maintained at 37° C (fig. 11 and table 2). Ag-Sn-Cu amalgams observed at 37° C also shrank more than those observed at 21° C (table 2).

Averages of the differences in dimensional changes of the Ag-Sn(Cu-Zn) amalgams at 21° and 37° C are given in table 2, together with their standard errors. The standard error in each case depends on the number of specimens and on the precision of a single measurement. The latter was evaluated separately for each period of hardening, by pooling the variances, obtained for all amalgams, of the measurements made at that setting time.

In table 2 it is also shown that the fiducial observation (zero reading) taken 10 min after start of mix yielded a significantly lower expansion or greater contraction value over a 24-hr period than the 15-min fiducial observation. This variation results from the fact that a larger portion of the initial shrinkage is observed when the 10-min fiducial reading is used.

4. Discussion of Results

The observations of dimensional changes, along with the X-ray diffraction evidence that uncombined mercury is present in the amalgam, tend to substantiate the theory that the mechanism of dimensional change is associated with the presence of the uncombined mercury.

The following mechanism is postulated to explain the physical phenomena observed. The initial shrinkage always observed results from the formation of compounds of mercury and alloy having a smaller volume than the sum of the original volumes of the alloy and mercury. The subsequent expansion that is observed results from the diffusion into new areas of uncombined mercury entrapped in spaces throughout the amalgam. The reaction of this uncombined mercury with existing phases or with residual alloy to form compounds of lesser volume would then account for the contraction that follows the expansion of the amalgam.

This mechanism would account for the dimensional changes that occurred on the addition of mercury to hardened amalgam. When mercury is added to hardened amalgam the diffusion of this mercury throughout the specimen would produce the large expansion observed. The slight shrinkage observed immediately after the removal of the supply of mercury could result from the combination of free mercury in the specimen with existing phases or with residual alloy.

The greater shrinkage of amalgam mixed and maintained at 37° C rather than at 21° C may result from a more rapid chemical combination and disappearance of the uncombined mercury at elevated temperatures.

The proposed mechanism would also account for the shrinkage of amalgam that occurs from overtrituration or excessive working during condensation, in that either of these treatments would tend to reduce the amount of uncombined mercury by either furnishing new surfaces for reaction with the mercury or by actual mechanical removal of the mercury. These treatments would also tend to distribute the uncombined mercury present more uniformly throughout the amalgam so that there would be fewer mercury-rich areas from which diffusion could take place. On the basis of this explanation, a reduction in size of the alloy particle or a heat treatment, which would make the particles more reactive, would tend to cause a reduced expansion or a shrinkage of the amalgam.

5. Summary

Residual, or uncombined, mercury has been demonstrated by X-ray diffraction studies to be present in amalgams after their initial solidification.

This uncombined mercury disappears during the period when greatest dimensional changes occur in the hardening of the amalgam system.

A possible mechanism for the dimensional changes, based on the presence and disappearance of the uncombined mercury, is presented.

6. References

[1] V. G. Black, Physical properties of silver-tin amalgams, Dental Cosmos **38,** 965 (December 1896).

[2] W. A. Gray, Volume changes in amalgams, J. Inst. Metals **29,** 139 (1923).

[3] Marie Gayler, The theory of the setting of dental amalgams, J. Brit. Dental Assoc. **60,** 11 (July 1936).

[4] M. L. Ward, F. A. Peyton, and E. O. Scott, New concepts of mercury content in amalgams, J. Dental Research **16,** 316 (August 1937).

[5] A. R. Troiana, An X-ray study of dental amalgams, J. Inst. Metals **58,** 247 (1938).

[6] G. Ryge, J. C. Moffett, and A. G. Barlow, Microstructural observations and X-ray diffraction studies of silver-tin amalgams, J. Dental Research **32,** 152 (1953).

[7] D. L. Smith, G. W. Ferguson, and I. C. Schoonover, The microstructure of dental amalgam, J. Am. Dental Assoc. **47,** 305 (September 1953).

[8] X-ray diffraction instrument and operating manual, North American Philips Corporation, Inc., Mt. Vernon, N. Y.

[9] Wilmer Souder and G. C. Paffenbarger, Physical properties of dental materials, NBS Circular 433 (1942).

Washington, October 30, 1953.

Journal of Research of the National Bureau of Standards Vol. 52, No. 4, April 1954 Research Paper 2488

A Colorimeter for Pyrotechnic Smokes*

Isadore Nimeroff and Samuel W. Wilson

A tristimulus photoelectric colorimeter has been designed to measure the chromaticities of pyrotechnic smokes having highly saturated colors. To minimize edge effects and rear-wall reflection, the smoke chamber was designed as a 36-inch cube. Three filters were designed to approximate the daylight CIE standard observer functions for the source-filter-phototube combinations of the instrument. As the CIE $\bar{y}$- and $\bar{z}$-functions are unimodal, little difficulty was encountered in designing filters to approximate these functions. The CIE x-function, which is bimodal, required a divided filter to approximate its two lobes. The filter constructed was composed of two sectors, one approximating the "blue lobe", the other approximating the "red lobe" of the $\bar{x}$-function. Satisfactory results have been obtained with this colorimeter, using Munsell papers as standards.

1. Introduction

In 1931 the International Commission on Illumination [1][1] (CIE) adopted a system for reducing spectrophotometric data to color coordinates in three-space. The reduction of such data for a single specimen entails a considerable amount of computation. To avoid this computation, Twyman and Perry [2] suggested in 1930 that three filters duplicating the then proposed standard-observer functions could be used in a photoelectric instrument. Several such instruments, now called photoelectric colorimeters [3], have been designed since then. The photosensitive elements in colorimeters have been barrier photocells [4, 5], vacuum phototubes [6], and multiplier phototubes [7, 8].

This paper describes a colorimeter, using multiplier phototubes, designed at the request of representatives of the Army Chemical Center to be used for evaluating the colors of pyrotechnic smokes. This instrument was needed to determine progress in the development of saturated smoke colors and to check on reproduction of specified smoke colors.

2. Filter Design

The colorimetric spectral functions approximated in this colorimeter by combined source-filter-phototube response are those established by the CIE. The theory of the design of filters is based on two propositions (1) that the three CIE observer functions represent the colorimetric system of the average normal observer, and (2) that each of these functions can be approximated by the proper selection of optical filters in combination with a light source and a phototube. As the instrument is intended to evaluate the color of nonfluorescent smokes as if they were viewed in daylight (6,500° K), even though in the colorimeter they are illuminated by incandescent-lamp light (2,780° K), the proper correction was incorporated in the filter design. Had the colorimeter been intended to evaluate the color of fluorescent, as well as nonfluorescent, smokes as viewed under daylight, the approximation of the CIE function would be accomplished by phototube and filter combination alone, but the illuminator would then be required to yield artificial daylight.

The CIE spectral-response functions, $\bar{x}$, $\bar{y}$, and $\bar{z}$, under daylight spectral conditions, E_v, are respectively, $\bar{x}E_v$, $\bar{y}E_v$, and $\bar{z}E_v$. If the illuminator yields spectral distribution, E_i, the spectral responses, S_x, S_y, and S_z, of the phototubes for each of these functions must be altered by filters having spectral transmittances T_x, T_y, and T_z, respectively, in order to refer to viewing by daylight. This condition may be stated mathematically:

$$\left.\begin{aligned} E_i T_x S_x K_x &= \bar{x} E_v \\ E_i T_y S_y K_y &= \bar{y} E_v \\ E_i T_z S_z K_z &= \bar{z} E_v \end{aligned}\right\}, \tag{1}$$

where K_x, K_y, and K_z are proportionality constants, independent of wavelength for their respective functions. The desired relative spectral transmittances then are determined by solving eq (1) for $K_x T_x$, $K_y T_y$, and $K_z T_z$.

The filter design is accomplished by determining the proper combination of colored glasses. Where the transmittance, T_0, of a glass of stock thickness d_0, is to be changed to a transmittance, T_1, the following equation must be solved for the new thickness, d_1:

$$T_1 = (T_0)^{d_1/d_0}(k^2)^{1-(d_1/d_0)}, \tag{2}$$

where k is unity minus the Fresnel reflectance of the glass. The approximate value of k for glass is 0.96. To minimize the work entailed in this computation a thickness-transmittance nomograph was used [9].

Figure 1 shows the spectral-response curves of several multiplier phototubes (RCA 5819) as calibrated by the NBS Radiometry Laboratory. The first phototube purchased had the response shown by curve A. Because of the relatively high response of this phototube in the region about 580 mμ the spectral transmittances of required filters for CIE functions must have absorption bands in this region.

*This project was done under contract with the Chemical Corps, Department of the Army.

[1] Figures in brackets indicate the literature references at the end of this paper.

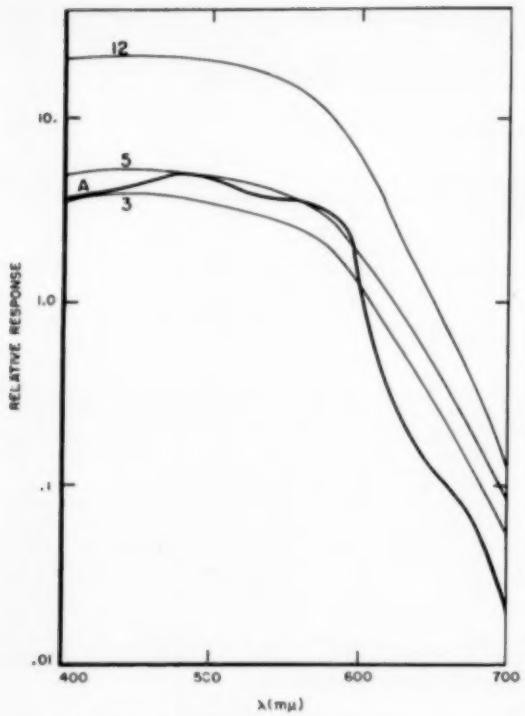

FIGURE 1. *Spectral-response curves of several multiplier phototubes*

To duplicate these complex transmittance curves the technique of divided-disk filters was devised. Fortunately, the phototubes purchased later had normal responses, as shown by curves 3, 5, and 12, of figure 1, thereby simplifying the filter-design problem. The phototubes having these curves are the ones used in the colorimeter for functions y, x, and z, respectively.

As no combination of glasses has ever achieved duplication of the bimodal $\bar{x}$-function in a single filter, the divided-disk technique devised for the complex transmittances required for phototube A was applied to the design of the bimodal $\bar{x}$-function. This division requires that one part of the single filter approximate the "blue lobe" and the other part approximate the "red lobe" of the $\bar{x}$-function. The transmittance of the ideal filter, T_x, for the $\bar{x}$-function may be divided into its two lobes, T_{xb} and T_{xr}, thus $T_x = T_{xb} + T_{xr}$. In terms of relative transmittance, this becomes

$$K_x T_x = K_x (T_{xb} + T_{xr}). \tag{3}$$

The actual approximation consists of a disk, area A, with one fraction, a/A, of the total area having spectral transmittance T'_{xb}, and the remaining fraction $1-(a/A)$, having spectral transmittance T'_{xr}. Then the transmittance, T'_x, of the actual filter is

$$T'_x = \frac{a}{A} T'_{xb} + \frac{A-a}{A} T'_{xr}. \tag{4}$$

The conditions that the spectral lobes of the approximate filter be properly proportional to those of the ideal filter are: The summation under each lobe of the approximation must equal the corresponding summation under the ideal filter, thus

$$\begin{aligned} \sum K_{xb} T'_{xb} &= \sum K_x T_{xb} \\ \sum K_{xr} T'_{xr} &= \sum K_x T_{xr}. \end{aligned} \tag{5}$$

The ratio of the summation under the two lobes in the approximate filter must equal the ratio of the summation under the two lobes of the ideal filter, thus

$$\frac{\sum \frac{a}{A} T'_{xb}}{\sum \frac{A-a}{A} T'_{xr}} = \frac{\sum T_{xb}}{\sum T_{xr}}. \tag{6}$$

But substituting the values of T'_{xb} and T'_{xr} from eq (5) into eq (6) gives

$$\frac{a}{A} = \frac{K_{xb}}{K_{xr} + K_{xb}}. \tag{7}$$

The area of the disk of radius r may be divided into either segments or sectors. Consider the segment division. The total area, A, is πr^2, and the area of the segment, a, is $(r^2/2)(\theta - \sin\theta)$, where θ, in radians, is the central angle subtended by the segment, as shown in figure 2,a. Then

$$\frac{a}{A} = \frac{1}{2\pi}(\theta - \sin\theta). \tag{8}$$

After the value of θ is computed, the segment is determined by computing, $x = r\cos(\theta/2)$.

Although relatively easy to construct, a filter with this type of division of the disk has two major difficulties. The disk, once constructed, is useful only with a circular opening of radius r. As the segment is displaced from the center of the disk, one must assume that the spectral response of the photosensitive surface of the phototube is completely uniform.

Consider now the sector division of a disk filter. The area of the sector (see fig. 2,b) is equal to $r^2\theta/2$, where θ, the sector angle, is in radians. Then $a/A = \theta/2\pi$. If the sector angle, expressed in degrees, is ρ, then

$$\frac{a}{A} = \frac{\rho}{360°}. \tag{9}$$

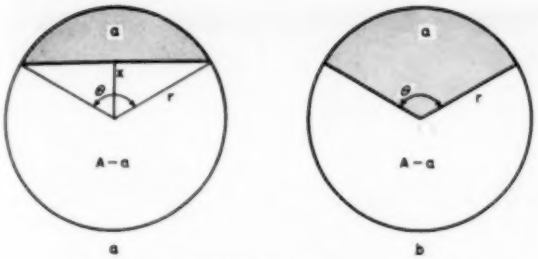

FIGURE 2. *Divided disks for $\bar{x}$-function filter*

a, Segment division; b, sector division.

This type of division, although more difficult to construct, does overcome the major difficulties of the segment division. The spectral character of the transmitted light is independent of the radius of the disk. One must assume only that the spectral response of the photosensitive surface of the phototube is radially symmetrical. This is a reasonable assumption for the head-on-type phototube used, as the photosensitive surface is evaporated onto the center of the cathode, thereby yielding a close approach to radially symmetrical sensitivity. This radial symmetry can readily be tested, furthermore, by rotating the sectored filter in its own plane and observing if the output of the phototube changes. For either type of division the center of the disk must be carefully positioned over the center of the photosensitive surface.

Because of the advantages outlined above, the sector division of the filter was used. On the basis of the application of eq (2) to the published spectral transmittance of stock glass, the combinations yielding the best expected approximation to the two lobes of the $\bar{x}$-function were chosen. The design data are

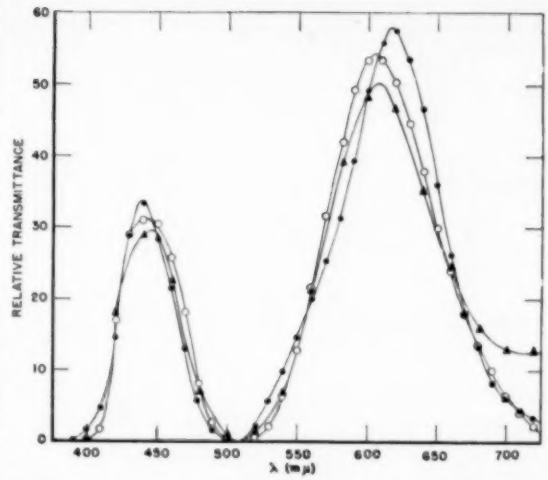

FIGURE 3. *Spectral transmittance of the desired (●), expected (▲), and actual (○) filters for CIE $\bar{x}$-function.*

shown in table 1. The sector angle was determined by substituting eq (7) into eq (9), giving

$$\rho = 360° K_{zb}/(K_{zr} + K_{zb}). \tag{10}$$

for the $\bar{x}$-function filter designed for this colorimeter, $K_{zb} = 0.915$, $K_{zr} = 5.483$, and $\rho = 51.5°$. The expected relative transmittance, $K''_x T''_x$, for this filter is shown in figure 3 compared with the desired relative transmittance, $K_x T_x$, and the achieved relative transmittance, $K'_x T'_x$, of the actual filter. The actual filter proved to be a better approximation to the desired filter than had been expected from the design data.

TABLE 1. *x-function filter design data*

λ	$K_x T_x$	$K_x T_{xb}$ (blue lobe)	$K_x T_{xr}$ (red lobe)	T''_{xb} 5433[a] (7.5 mm) 3389[a] (1 mm)	T''_{xr} 9788[a] (3 mm) 3304[a] (6 mm)	$T''_{xb} K_{xb}$ $K_{xb} = 0.915$	$T''_{xr} K_{xr}$ $K_{xr} = 5.483$	$K''_x T''_x$
				%	%			
380	0.1	0.1	.....	0	.....	0	.....	0
400	1.6	1.6	.....	0	.....	0	.....	0
20	14.7	14.7	.....	19.8	.....	18.1	.....	18.1
40	33.4	33.4	.....	31.8	.....	29.1	.....	29.1
60	21.5	21.5	.....	24.6	.....	22.5	.....	22.5
80	5.8	5.8	.....	7.5	0	6.9	0	6.9
500	0.2	0.1	0.1	0.7	0.09	0.6	0.5	1.1
20	2.2	.....	2.2	0	.29	0	1.6	1.6
40	9.9	.....	9.9	.....	1.23	.....	6.7	6.7
60	20.1	.....	20.1	.....	3.86	.....	21.2	21.2
80	31.5	.....	31.5	.....	7.17	.....	39.3	39.3
600	49.2	.....	49.2	.....	8.85	.....	48.5	48.5
20	57.5	.....	57.5	.....	8.49	.....	46.6	46.6
40	46.6	.....	46.6	.....	6.43	.....	35.3	35.3
60	26.1	.....	26.1	.....	4.43	.....	24.3	24.3
80	13.0	.....	13.0	.....	2.92	.....	16.0	16.0
700	6.1	.....	6.1	.....	2.36	.....	12.9	12.9
20	3.5	.....	3.5	.....	2.36	.....	12.9	12.9
	343.0	77.2	265.8	84.4	48.48	77.2	265.8	343.0

[a] Corning glass code numbers.

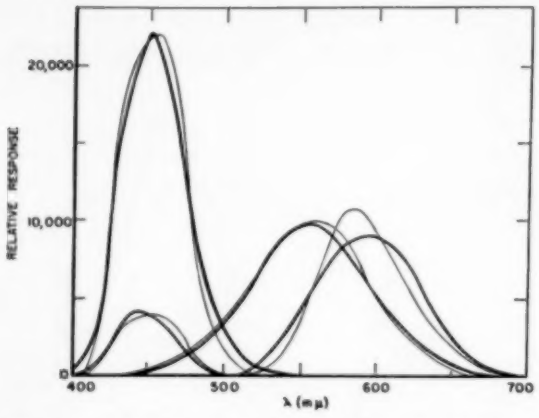

FIGURE 4. *CIE tristimulus functions (heavy lines) and the approximate functions of the colorimeter.*

As the CIE $\bar{y}$- and $\bar{z}$-functions are unimodel little difficulty was encountered in designing filters to approximate these functions. For the source-filter-phototube combinations of this colorimeter, the approximations (light lines) to the CIE tristimulus functions (heavy lines) are shown in figure 4.

3. Description of Apparatus

3.1. Chamber

Most of the colorimeters heretofore designed have been used for measurement of colors of opaque or transparent media. For these media, where edge effect is negligible, the size of the illuminated and viewed area of the medium was determined by the sensitivity of the instrument. The instrument here described is being used to measure the color of translucent media, pyrotechnic smokes. As the smokes are translucent, that is, light scattering as well as transmitting, and reflecting, a rather large chamber having a uniformly illuminated window is required to minimize edge effects.

Figure 5 shows a general view of the apparatus. The chamber is a 1-yd cube made of Dural. One side of the cube has a ¼-in. plate-glass window 32 in. sq. To determine if the window was sufficiently large, circular openings of increasing size were placed over the window. The aperture effect decreased to zero when the opening was still well within the window size. To determine if reflection from the chamber walls would affect the results obtained when the chamber is filled with smoke, measurements were made on a smoke by using alternately a black and a white rear wall. As the wall reflection and window size had little effect upon the measurements, the conclusion was reached that the chamber had been made sufficiently large.

A blower is installed either to stir the smoke in order to obtain uniform distribution in the chamber or to exhaust the smoke after colorimetric measurements are made. A door serves as access to the chamber for purposes of placing a smoke grenade in the chamber and firing it. To facilitate entering the chamber in order to clean the window, an additional door was constructed on the side of the chamber (not shown in fig. 5).

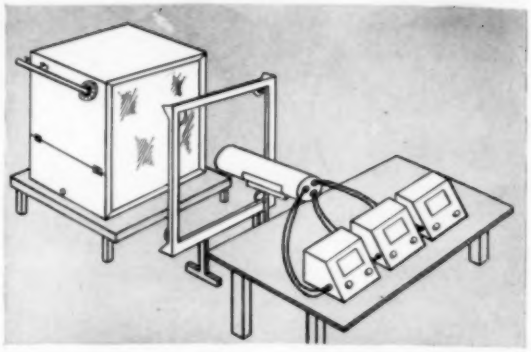

FIGURE 5. *General view of apparatus, showing smoke chamber, illuminators, optical-assembly tube, and photometers.*

3.2. Optical Arrangement

The smoke is illuminated by four 150-w incandescent floodlamps, mounted on a frame. The uniformity of illumination on the window was checked by means of a foot-candle meter.

The smoke is viewed perpendicularly through a lens that focuses upon a central region of the window. The lens is mounted at one end of a brass tube equipped with baffles to minimize stray light. The tristimulus filters are mounted in front of the phototubes. To achieve compactness of the viewing assembly, head-on-type phototubes were used.

3.3. Photometers

To measure accurately the chromaticity coordinates of saturated colors, a colorimeter is required to evaluate low reflectance in one spectral region and high reflectance in another spectral region with equal precision. As the colors of the pyrotechnic smokes are highly saturated and further development will improve their saturation, this colorimeter requires highly sensitive photometers and phototubes. To satisfy these requirements and for expediency, commercially available multiplier photometers and phototubes were used. The Photovolt Multiplier Photometer, model 520–M, known to be reasonably sensitive and stable, was chosen for use in the colorimeter. One minor adaptation of the photometers, required to permit the use of 5819 phototubes, instead of 1P21 phototubes for which the photometer was designed, was the replacement of the 10-prong socket with 9 dynode resistors by a 14-prong socket with 10 dynode resistors. To obtain direct readings of tristimulus values, X, Y, and Z, on the corresponding photometers, modification of the microammeter circuit of each photometer was anticipated. but

only the Z-scale photometer required an increase in meter sensitivity.

4. Results With Colorimeter

As the source-filter-phototube combination does not completely duplicate the CIE functions, best results are obtained by calibrating the colorimeter with standards having spectral selectivities similar to those of the smokes. But as no spectral data are available for any smokes, standards of Munsell charts having colors similar to those of the smokes investigated were chosen and gave satisfactory results. Table 2 shows the Munsell notations for three different smokes reduced from data obtained with the colorimeter at the time of firing (t_0) and within 10 min (t_{10}) of that time, compared with notations obtained simultaneously by visual estimates through a daylight filter. The instrumental colorimetric data were converted to Munsell book notation, so that comparisons could be made with the visual estimates obtained by comparison with the color scales in a Munsell book of color. The colorimeter yields hues and values in substantial agreement with visual estimates, but yields generally higher chromas than visually obtained estimates. The uncertainty in a visual estimate of hue and value is approximately one half-step. As the Munsell book does not contain chips with chromas as high as those of these smokes, the uncertainty in visual estimates of chroma is of the order of two steps. One possible reason for the discrepancy between the instrumentally and visually obtained chromas is that the approximation to the $\bar{z}$-function is deficient in the region between 500 and 550 mμ, thereby yielding relatively low Z-values for yellow and red smokes.

TABLE 2.

Smoke color	Munsell notations		Time
	Instrumental	Visual	
Red	3*R*3.5/15	5R4/10	t_0
	3.5*R* 3/13	4*R*4/10	t_{10}
Do	4.5*R*3.5/14	5*R*4/12	t_0
	5*R* 2/10	5*R*2/7	t_{10}
Yellow	5*Y*6.5/10	5*Y*6/8	t_0
	5*Y* 4/6	4.5*Y*5/6	t_{10}

Table 3 shows Munsell notations of three different smoke colors taken on smokes fired under outdoor daylight (clear, sunny day) compared with notations obtained by reduction of instrumental data for duplicate smokes. The satisfactory correspondence between the sets of data indicates that the smokes were not strongly fluorescent and that the CIE functions had been adequately approximated.

TABLE 3.

Smoke color	Munsell notations	
	Instrumental	Visual
Red	5*R*3/14	5*R*5/14
Yellow	7*Y*8/12	7.5*Y*7/10
Green	4*G*2/3	3*G*3/3

5. References

[1] Commission International de l'Éclairage, Proc. of the Eighth Session, Cambridge, England, p. 19 (Sept. 1931).
[2] F. Twyman and J. W. Perry, Improvements in or relating to colorimeters, British Patent Spec. No. 324351 (Jan. 20, 1930).
[3] K. S. Gibson, Photoelectric photometers and colorimeters, Instruments **9,** 309 (1936).
[4] B. T. Barnes, A four-filter photoelectric colorimeter, J. Opt. Soc. Am. **29,** 400 (1939).
[5] R. S. Hunter, Photoelectric tristimulus colorimetry with Three Filters, NBS Circular 429 (July 1942).
[6] L. G. Glasser and D. J. Troy, A new high sensitivity differential colorimeter, J. Opt. Soc. Am. **42,** 652 (1952).
[7] G. C. Sziklai, A tristimulus photometer, J. Opt. Soc. Am. **41,** 321 (1951).
[8] G. P. Bentley, An industrial tristimulus color matcher, Electronics **24,** 102 (1951).
[9] Glass color filters by Corning, Corning Glass Works (1948).

WASHINGTON, November 9, 1953.

Journal of Research of the National Bureau of Standards Vol. 52, No. 4, April 1954 Research Paper 2489

Simplification of Calculations in Routine Density and Volumetric Determinations

Charles T. Collett

In density and volumetric determinations, certain methods of weighing have encouraged the use of approximations. These can be avoided by minor changes in procedure that simplify calculations. The use of counterpoises is shown to eliminate some buoyancy corrections.

1. Introduction

In the course of performing numerous density and volumetric determinations several methods were compared with regard to the calculations associated with them.

Some methods involved equations that were found adequate and correct but too complicated to be desirable for routine work. For example, Gould and Stott [1] represent the density of a liquid in a glass picnometer by an equation of 26 terms and some 37 brackets, parentheses, shillings, etc.

Other systems were observed to lead the worker into dilemmas, from which he escaped by the use of approximations. These did not reduce the accuracy of his computed values, but were time-consuming and difficult to record in concise form. Often the steps of the calculations were worked out on scratch paper and then discarded, only the terminal values of the series being permanently recorded.

The methods and equations finally selected for everyday use were derived from inspection of the component forces acting on the arms of a balance in equilibrium, i. e., forces resulting from the masses pushing downward and the buoyant effects pushing upward. Because these equations are based on considerations that are elementary to the problem, it would seem highly probable that they have been used before, and perhaps published. A search of the literature has not revealed them, at least not in the forms shown here. Certainly, they have been neglected in modern practice, and their simplicity and usefulness suggest that they should be presented for consideration.

2. Hydrostatic Weighing

Consider that it is desired to find the mass, M_s, of a glass object of irregular shape by the conventional substitution weighing. Assume that at all times a constant load, c, remains on the right pan of the laboratory balance, a condition that will be unchanged during all weighings subsequently discussed, and the designation as right or left being an arbitrary identification without other significance.

[1] F. A. Gould and Verney Stott, Glazebrook's dictionary of applied physics, III, 127 (Peter Smith, New York, N. Y., 1950).

Equilibrium is established by placing on the left pan brass weights e and f, whose masses are M_e and M_f and which are subject to air-buoyancy effects, B_e and B_f. M_c is the mass of c, and B_c is the air buoyancy on c. Then

$$M_e-B_e+M_f-B_f=M_c-B_c. \tag{1}$$

If the glass specimen, s, is then placed on the left pan, and equilibrium restored by removing weight f,

$$M_e-B_e+M_s-B_s=M_c-B_c, \tag{2}$$

where M_s represents the mass of the specimen and B_s the air buoyancy acting upon it. The second weighing must be accomplished within a reasonably short time, so that the air density has not changed. Subtracting eq (2) from eq (1), and rearranging,

$$\begin{aligned} M_s &= M_f-B_f+B_s \\ &= M_f-\frac{M_f}{\rho_f}\rho_a+V_s\rho_a \\ &= M_f\left(1-\frac{\rho_a}{\rho_f}\right)+V_s\rho_a, \end{aligned} \tag{3}$$

where ρ_a is the density of the air, ρ_f is the density of the weights, and V_s is the volume of the specimen.

ρ_a can be obtained by well-known methods,[2] and ρ_f is usually known. However, V_s is unknown due to the shape of the specimen and is customarily found by means of hydrostatic weighing.

A suspension is fitted below the left pan to support a basket immersed in a liquid, usually distilled water, and equilibrium is secured by the addition of weights g and h on the pan. Let M_k equal the mass of the suspension system and B_k and B'_k the respective air and water buoyancy effects.

$$M_g-B_g+M_h-B_h+M_k-B_k-B'_k=M_c-B_c. \tag{4}$$

The next operation must be performed within a short period of time, that is, before the density of the air or the water has changed appreciably. The speci-

[2] N. Bauer, Technique of organic chemistry, vol. I, part 1, Physical Methods, p. 273 (Interscience Publishers, Inc., New York, N. Y., 1949). N. S. Osborne, E. C. McKelvey, and H. W. Bearce, Density and thermal expansion of ethyl alcohol and of its mixtures with water, Bul. BS 9, 327 (1913) 8197 (see p. 378).

men is immersed within the basket and is subject to buoyancy effect B'_s. Weight h is removed to restore equilibrium. Then

$$M_g - B_g + M_k - B_k - B'_k + M_s - B'_s = M_c - B_c. \quad (5)$$

Subtracting eq (5) from eq (4)

$$\begin{aligned} B'_s &= M_s - M_h + B_h \\ &= M_s - M_h + \frac{M_h}{\rho_h}\rho'_a \\ &= M_s - M_h\left(1 - \frac{\rho'_a}{\rho_h}\right). \end{aligned} \quad (6)$$

Again an unknown, M_s, appears on the right side of the equation, making it impossible to use directly the relationship

$$\begin{aligned} V_s &= \frac{B'_s}{\rho_w} \\ &= \frac{M_s - M_h\left(1 - \frac{\rho'_a}{\rho_h}\right)}{\rho_w}, \end{aligned} \quad (7)$$

where ρ_w is the density of the water.[3]

The unknown quantities may be eliminated from the right-hand sides of eq (3) and (7) by substitution. The resulting equations can be solved directly but contain more terms, thus:

$$M_s = \frac{M_f\left(1 - \frac{\rho_a}{\rho_f}\right) - M_h\left(\frac{\rho_a}{\rho_w}\right)\left(1 - \frac{\rho'_a}{\rho_f}\right)}{1 - \frac{\rho_a}{\rho_w}}. \quad (8)$$

$$V_s = \frac{M_f\left(1 - \frac{\rho_a}{\rho_f}\right) - M_h\left(1 - \frac{\rho'_a}{\rho_f}\right)}{\rho_w - \rho_a}. \quad (9)$$

However, if eq (9) is solved first, the value of V_s may be used in eq (3), which is much shorter.

Equations (3) and (7) may be solved by the use of approximations, a method that has been found in considerable use.[4] In a typical case it was found necessary to remove weights equal to 11.6954 g after the glass sample was placed on the pan. Air density was determined to be 0.001170 g/ml, and the weights were known to have a density of 8.4 g/cm³. From eq (3):

$$\begin{aligned} M_s &= 11.6954\left(1 - \frac{0.001170}{8.4}\right) + V_s(0.001170) \\ &= 11.6938 + V_s(0.001170), \text{ in grams.} \end{aligned} \quad (10)$$

For the hydrostatic weighing, equilibrium was maintained by removing 6.4711 g after the sample was placed in the immersed basket. Densities of the water and air were 0.996953 g/ml and 0.001176 g/ml. From eq (7)

$$\begin{aligned} V_s &= \frac{M_s - 6.4711\left(1 - \frac{0.001176}{8.4}\right)}{0.996953} \\ &= \frac{M_s - 6.4702}{0.996953} \text{ ml.} \end{aligned} \quad (11)$$

The first approximation is secured by using the apparent weight of the sample in place of M_s in eq (11), giving

$$\text{approx.}_1\ V_s = \frac{11.6954 - 6.4702}{0.996953} = 5.2412 \text{ cm}^3. \quad (12)$$

This approximate value for V_s is used in eq (10), and we have

$$\text{approx.}_1\ M_s = 11.6938 + 5.2412\ (0.001170) = 11.6999 \text{g}. \quad (13)$$

The second approximations are

$$\text{approx.}_2\ V_s = \frac{11.6999 - 6.4702}{0.996953} = 5.2457 \text{ cm}^3 \quad (14)$$

$$\text{approx.}_2\ M_s = 11.6938 + 5.2457(0.001170) = 11.6999 \text{ g}. \quad (15)$$

These last approximate values are accepted for the real values, as obviously no further change will occur.

A minor alteration in this procedure will simplify the equations and entirely eliminate the use of approximations. The suspended, immersed basket is retained, but the specimen rests on the left pan during the first weighing, and equilibrium is produced by the presence of weight g. Equation (4) then becomes

$$M_g - B_g + M_s - B_s + M_k - B_k - B'_k = M_c - B_c. \quad (16)$$

For the second weighing the specimen is transferred to the basket to be immersed as before, but to produce equilibrium it is necessary to add weight h on the pan.[5] Equation (5) then is changed to:

$$M_g - B_g + M_h - B_h + M_k - B_k - B'_k + M_s - B'_s = M_c - B_c. \quad (17)$$

Subtracting eq (17) from eq (16)

$$\begin{aligned} B'_s - B_s &= M_h - B_h \\ V_s(\rho_w - \rho_a) &= M_h - \frac{M_h}{\rho_h}\rho_a \\ V_s &= \frac{M_h\left(1 - \frac{\rho_a}{\rho_h}\right)}{\rho_w - \rho_a}. \end{aligned} \quad (18)$$

[3] A similar equation appears in Bul. BS **9**, 327 (1913) S197, see p. 384, where the density of a liquid is found by immersing a sinker of known mass and volume.
[4] NBS Circular 487, p. 2 (1950).
[5] The transfer of sample from pan to basket is described by W. Watson (A textbook of physics, p. 175, Longmans, Green & Co., London, 1902), but the calculations are not mentioned.

Because the densities of weight h, air, and water can be secured easily, it is apparent that eq (18) contains no unknowns on the right-hand side, and the exact value of V_s may be calculated at once. After its volume is thus determined, the object is weighed in air in the conventional manner, after which eq (3) can be solved.

The same glass piece previously considered was also weighed by this latter method. After the sample was moved from the pan to the immersed basket, it was necessary to place 5.2243 g on the pan. The densities of the air and water were respectively 0.001170 and 0.996953 g/ml, and of the weights, 8.4 g/cm.[3]

From eq (18)

$$V_s=\frac{5.2243\left(1-\frac{0.001170}{8.4}\right)}{0.996953-0.001170}=5.2457 \text{ cm}^3. \quad (19)$$

The sample was then weighed in air in the conventional substitution method, 11.6954 g being removed after the specimen was placed on the pan. Air density was 0.001170 g/ml.

From eq (3):

$$M_s=11.6954\left(1-\frac{0.001170}{8.4}\right)+5.2457(0.001170) \quad (20)$$

$$=11.6999 \text{ g}.$$

3. Weighing a Picnometer by the Counterpoise Method

Weighing a picnometer is a special case of determining the mass of a glass object having irregular shape and unknown volume, and is therefore subject to the same general principles. If an attempt is made to use conventional substitution weighing, the same dilemma will of course arise, that is, neither the mass nor the volume is known, and neither can be determined without knowledge of the other. The volume here referred to is the volume of material (glass) that will displace air during the weighing, and does not refer to the capacity of the container, or so-called "internal volume."

Furthermore, the interior of the picnometer for liquids is of necessity closed to the outside except for limited entrances, usually capillary tubes of small diameter. For this reason, filling, emptying, cleaning, and drying are not quickly accomplished, and the observer will wish to hold the number of such operations to a minimum. For example, a series of trials may be performed while the same liquid remains in the instrument, only minor adjustments of level being made between succeeding weighings.

Thus the weighing of the empty picnometer and the weighing of the filled picnometer are often separated by considerable periods of time, and the air density, and hence the air buoyancy effects, will vary.

However, the user of the picnometer is not primarily interested in the mass of the instrument; this value is never required except as a tare, and its consistent treatment as such throughout all operations will permit the use of simple calculations with no approximations. By the use of a counterpoise the picnometer's mass and its buoyancy in air may be entirely eliminated from all calculations, and in fact need never be known at any time.[6]

The counterpoise is a second picnometer similar in size and shape to the first, made of glass with the same density, and the two instruments must be approximately equal in mass. A small protuberance is provided on each, such as the handle on the cap, and by grinding and polishing it is not difficult to adjust the masses within a milligram. However, the two instruments may be allowed to differ by as much as 0.1 g because the difference in buoyant effects when they are suspended from opposite balance pans with equilibrium maintained by weights is $(\Delta/\rho_g-\Delta/\rho_f)\rho_a$, where Δ is the difference between the masses of the two picnometers, and ρ_g, ρ_f, and ρ_a are the densities of the glass, weights, and air. If Δ is 0.1 g and the respective densities are about 2.5, 8.4, and 0.0012 g/ml, the difference in buoyant effect will be negligible.

In conventional laboratory practice the mass, volume of glass, and internal volume of a picnometer are not usually determined each time the instrument is used, but only at the time it is calibrated. With occasional checking, these values are considered true as long as there is no reason to suspect a change. In the method to be considered, only the internal volume at various temperatures is determined.

The counterpoise is placed upon the right pan with a constant load composed of weights e and f, and the active picnometer is placed on the left pan with weights E and F sufficient to secure a state of balance, from which the equation may be written

$$M_P-B_P+M_E-B_E+M_F-B_F=$$

$$M_p-B_p+M_e-B_e+M_f-B_f, \quad (21)$$

where M is the mass, and B is the air buoyancy effect of the object indicated by the subscript letter; P and p being the active picnometer and the counterpoise picnometer.

The picnometer is next filled with a sample, S, which will be distilled water during the calibration and later the particular liquid being tested for density. Balance is restored by removing weight F. Then

$$M_P-B''_P+M_S-B''_S+M_E-B''_E=$$

$$M_p-B''_p+M_e-B''_e+M_f-B''_f. \quad (22)$$

It has been observed that the two weighings may be performed at different times, thus a change in air density is to be expected. The buoyant effects in eq (22) will not be equal to those in eq (21) except by coincidence and are thus designated as B''.

[6] N. Bauer, Technique of organic chemistry, I, part 1, Physical methods, p. 272 (Interscience Publishers, Inc., New York, N. Y., 1949).

Subtracting eq (22) from eq (21), we have

$$M_F - B_F - B_P - B_E + B_P'' + B_E'' - M_S + B_S'' =$$

$$B_p'' + B_e'' + B_f'' - B_p - B_e - B_f. \quad (23)$$

Assume that the small difference in mass between P and p in eq (21) and (22) has been compensated by a corresponding difference in E and e, so that

$$M_P + M_E = M_p + M_e. \quad (24)$$

It has been shown that the buoyancy effects may be considered equal, that is,

$$B_P + B_E = B_p + B_e. \quad (25)$$

Also

$$B_P'' + B_E'' = B_p'' + B_e''. \quad (26)$$

It follows that M_F must be equal to M_f, and as the weights have the same density, B_F and B_f are equal.

We then have

$$M_S - B_S'' = M_F - B_f'', \quad (27)$$

which is essentially the same as eq (3).

$$M_S - \frac{M_S}{\rho_S}\rho_a'' = M_F - \frac{M_F}{\rho_F}\rho_a'', \quad (28)$$

where ρ_a'' is the air density corresponding to eq (22).

$$M_S = M_F \frac{1 - \frac{\rho_a''}{\rho_F}}{1 - \frac{\rho_a''}{\rho_S}}. \quad (29)$$

As the sample in the picnometer during calibration is water at a known temperature, the density ρ_S is read from standard tables, and the volume then is M_S divided by that density. This process is repeated at different temperatures until a calibration curve has been developed for the picnometer over the desired range.

When a liquid of unknown density is to be tested the weighing procedure is exactly the same. However, eq (27), as shown in eq (3), can be rewritten to obtain

$$M_S = M_F\left(1 - \frac{\rho_a''}{\rho_F}\right) + V_S\rho_a''. \quad (30)$$

The picnometer having been previously calibrated, V_S is readily determined and

$$\rho_S = \frac{M_S}{V_S} = \frac{M_F\left(1 - \frac{\rho_a''}{\rho_F}\right) + V_S\rho_a''}{V_S}. \quad (31)$$

For example, when a picnometer was calibrated according to the method described, a weight of 120.9878 g was on the left pan with the empty instrument, and 21.1467 g when it was filled with distilled water at a temperature of 24.288° C. The densities of the weights, air, and water were determined to be 8.4; 0.001170, and 0.997257 g/ml, respectively. From eq (29) the mass of the water was

$$M_S = 99.8411\,\frac{1 - \frac{0.001170}{8.4}}{1 - \frac{0.001170}{0.997257}} = 99.9445 \text{ g}. \quad (32)$$

The volume of the instrument was

$$V_S = \frac{99.9445}{0.997257} = 100.2194 \text{ ml}. \quad (33)$$

This was used as one point on a calibration curve.

When the instrument was used to test a sample of heptane a weight of 116.5413 g was required on the left pan with the empty picnometer. It was then filled with the sample at a temperature of 24.992° C, and balance was restored by reducing the weight on the pan to 48.5356 g. The densities of the weights and the air were 8.4 and 0.001173 g/ml, respectively. From the previously drawn calibration curve the volume of the instrument at that temperature was known to be 100.2201 ml.

Using eq (31), the density of the heptane was

$$\rho_S = \frac{68.0057\left(1 - \frac{0.001173}{8.4}\right) + (100.2201)(0.001173)}{100.2201}$$

$$= 0.67964 \text{ g/ml}. \quad (34)$$

Washington, October 19, 1953.

Journal of Research of the National Bureau of Standards Vol. 52, No. 4, April 1954 Research Paper 2490

Infrared Spectrum of Hydrogen Sulfide in the 6,290-cm^{-1} Region[1]

Harry C. Allen, Jr.[2] and Earle K. Plyler

The absorption of hydrogen sulfide in the region 6,100 to 6,500 cm^{-1} has been measured under high resolution. The rotational fine structure has been analyzed through the use of published energy tables for the rigid rotor. A classical centrifugal-distortion correction was applied to the rigid energy levels. It is found that there are two overlapping bands in this region, a normally strong, A-type band, the $(n_1, n_2, n_3) = (1,1,1)$, and a normally weak, B-type band, which becomes strong enough to be observed by borrowing intensity from the A-type band through a Coriolis interaction. The B-type band is the lower component of the resonating pair (2,1,0) and (0,1,2). The excited state inertial parameters giving the best fits are (1,1,1) band, $A = 10.398$, $B = 8.935$, $C = 4.548$, $\mu_0 = 6289.26$ cm^{-1}; (0,1,2) band, $A = 10.394$, $B = 8.918$, $C = 4.547$, $\mu_0 = 6288.28$ cm^{-1}.

1. Introduction

The absorption of hydrogen sulfide in the 1.6 μ region has been measured previously under low resolution and the rotational fine structure of the band envelope analyzed [1].[3] As it is now possible to increase the resolution 10 times, it was thought advisable to remeasure this region. The analysis of the new data confirms the main conclusions of the previous analysis, i. e., the absorption is due largely to the A-type band (1,1,1). However, the improved data show a second and weaker band overlapping the (1,1,1) band. This second band is a B-type band and is assigned as the lower component of the resonating pair (0,1,2) and (2,1,0).

2. Experimental Procedure

The measurements of the 1.6-μ band of hydrogen sulfide were made on an infrared grating spectrometer constructed in the Bureau's Radiometry Section. The grating has 15,000 lines/in., and the rulings extend over 7½ in. A lead-sulfide cell is used as the detecting element. Other details of the instrument are given in a previous paper [2]. In the measurement of the hydrogen-sulfide spectra at 1.6$^-\mu$ it is possible to use narrow slits (0.03 mm), and sharp lines separated by 0.15 cm^{-1} could be resolved. Two cells were used in the measurements, one 60 cm and the other 600 cm in length. The long cell was so constructed that there was no loss in aperture. This cell transmits about 85 percent of incident energy. A detailed description of this cell is given in another publication [3]. Various pressures were used in the absorption cells so that both weak and strong lines could be observed. Figure 1 shows a recorder tracing obtained on unruled paper for the 600-cm

[1] The work reported herein was supported in part by the Office of Naval Research (under ONR Contract N5ori-76, Task Order V).
[2] Atomic Energy Commission Postdoctoral Fellow, Department of Chemistry, Harvard University, Cambridge, Mass.
[3] Figures in brackets indicate literature references at the end of this paper.

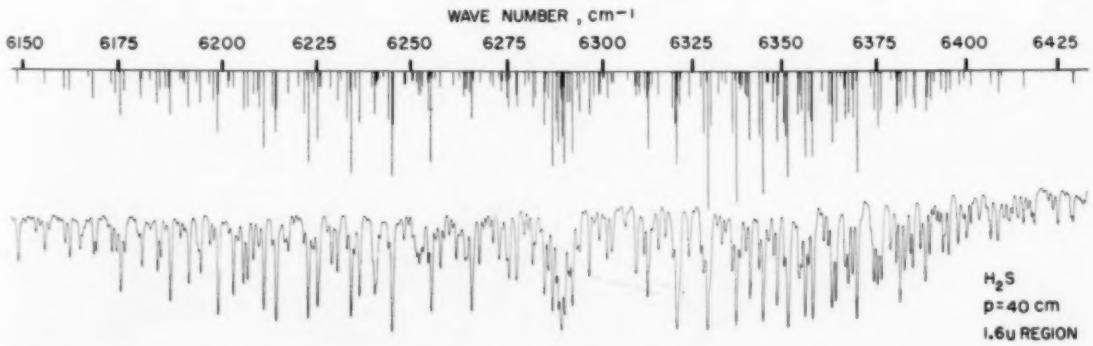

FIGURE 1. *Absorption bands (1, 1, 1) and (2, 0, 1) for hydrogen sulfide in the region 6,100 to 6,500 cm^{-1}.*

The calculated positions of the lines are shown above the spectra.

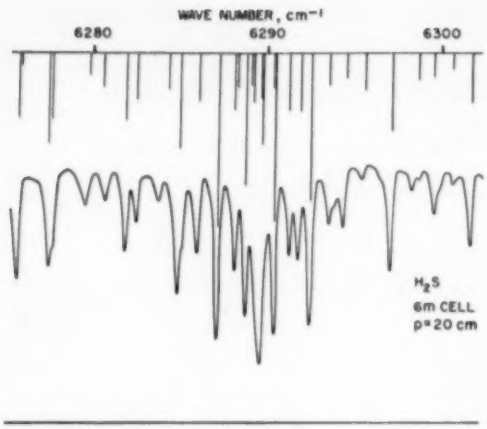

FIGURE 2. *Center of (1,1,1) band at slow scanning speed.*
The calculated positions and their intensities are placed above the spectra.

cell, with hydrogen sulfide at a pressure of 40 cm Hg. Figure 2 represents the center of the same region obtained by using a slower scanning speed.

The frequencies of the absorption peaks were obtained by using a comparison spectrum. Higher orders of the atomic lines of mercury, krypton, argon, and neon were superimposed on the absorption band. An arrangement of shutters was used so that either the absorption lines or the emission line could be recorded on the chart, and thus the shifting of position of the atomic line by the overlapping of the absorption line was avoided. Several tracings were measured, and the frequency given for each line is a result of the average of several determinations. In these measurements the precision of most lines is 0.1 cm^{-1} or better. The experimental determinations of the frequencies are listed in table 1.

TABLE 1. *Comparison of observed and calculated spectra in 1.6 μ region*

Line No.	Intensity	Observed wave number	Transition	Calculated wave number (111)	Calculated wave number (012)	Intensity
		cm^{-1}		cm^{-1}		
31	3.8	6148.77	$11_{-10}-12_{-11}$	6148.86	.....	0.6
			$11_{-11}-12_{-12}$	.....	.....	.2
32	.5	6149.51				
33	.2	6150.19				
34	.7	6150.65				
35	.3	6151.99				
36	1.7	6153.21				
37	.1	6154.45				
38	3.2	6155.60	$10_{-7}-11_{-8}$	6155.52	.....	.2
			$10_{-8}-11_{-9}$	.....	.....	.6
39	1.3	6156.67				
40	.1	6157.63				
41	.6	6158.79	7_5-8_4	6158.72	.....	.1
			5_1-6_0	6158.82	.....	.1
42	.6	6159.55				
43	2.5	6160.71	$9_{-4}-10_{-5}$	6160.71	.....	.8
			$9_{-5}-10_{-6}$	.....	.....	.3
			$10_{-9}-11_{-11}$	.....	6160.93	.5
			$10_{-10}-11_{-12}$	.....	.....	.2
44	3.7	6162.05	$10_{-10}-11_{-11}$	6162.20	.....	1.1
			$10_{-9}-11_{-10}$	.....	.....	.4
45	.2	6163.05				
46	.3	6163.58	7_1-8_0	6163.41	.....	.2
47	3.0	6164.63	$8_{-2}-8_{-3}$	6164.41	.....	.6
			$8_{-1}-8_{-2}$	6164.45	.....	.2
48	1.8	6165.23	7_4-8_3	6165.18	.....	.4
49	1.0	6165.83	7_6-8_5	6165.63	.....	.2
50	.1	6166.80	$9_{-7}-10_{-7}$	.....	6166.70	1.0
			$9_{-6}-10_{-6}$	.....	.....	.3
51	3.5	6168.13	5_5-6_6	.....	6167.82	.9
			$9_{-5}-10_{-7}$	6168.01	.....	1.0
			$9_{-7}-10_{-8}$	.....	.....	.3
52	2.9	6168.73				
53	.2	6168.87				
54	.1	6170.87				
55	1.0	6171.79				
56	3.4	6172.63	$8_{-4}-9_{-5}$	6172.59	.....	.9
			$8_{-3}-9_{-4}$	.....	.....	.3
57	3.2	6173.83	4_2-5_3	6173.75	.....	.2
			$9_{-6}-10_{-9}$	.....	6173.81	.8
			$9_{-8}-10_{-10}$	.....	.....	.3
			6_4-7_3	6174.00	.....	.9
58	6.7	6174.94	6_2-7_1	6174.64	.....	1.2
			$9_{-9}-10_{-10}$	6174.90	.....	.6
			$9_{-9}-10_{-9}$	.....	.....	1.7
59	3.3	6175.87	7_0-8_{-1}	6175.78	.....	0.9
			5_3-6_3	.....	6176.09	.6
60	.4					
61	.4	6178.15				
62	1.5	6178.95	$8_{-3}-9_{-7}$	.....	6178.92	.6
			$8_{-5}-9_{-8}$	.....	.....	.2
63	1.9	6179.43	6_6-7_5	6179.08	.....	.4
64	4.6	6180.19	$7_{-1}-8_{-2}$	6180.07	.....	.3
			$8_{-3}-9_{-6}$	6180.18	.....	.5
			$8_{-6}-9_{-7}$	.....	.....	1.5
65	1.2	6180.71	4_0-5_0	6180.79	.....	.6
66	.6	6181.49				
67	1.3	6182.19	6_0-7_0	6182.13	.....	.3
68	.1	6182.83	$7_{-2}-8_{-3}$	.....	6182.60	.6
			$7_{-3}-8_{-4}$	.....	.....	.2
69	4.9	6184.17	4_1-5_0	.....	6183.66	.6
			$7_{-2}-8_{-3}$	6183.97	.....	1.4
			$7_{-3}-8_{-4}$	.....	.....	.5
70	3.7	6184.95	6_6-7_{-1}	.....	6185.02	1.4
71	1.3	6186.21	$8_{-7}-9_{-9}$	.....	6186.37	1.2
			$8_{-8}-9_{-8}$	.....	.....	.4
			4_2-5_3	.....	6186.82	
72	7.3	6187.48	$8_{-9}-9_{-9}$	6187.48	.....	2.5
			$8_{-7}-9_{-8}$	.....	.....	.8
73	.1	6189.09				
74	1.9	6189.98	5_3-6_2	6190.05	.....	.6
75	1.3	6190.86	$7_{-5}-8_{-5}$	.....	6190.81	1.9
			$7_{-4}-8_{-6}$	.....	.....	.6
76	1.0	6191.37	$9_{-8}-9_{-7}$	6191.24	.....	.3
			$10_{-9}-10_{-8}$	6191.11	.....	.1
77	5.7	6192.09	$7_{-4}-8_{-5}$	6192.00	.....	2.1
			$7_{-5}-8_{-6}$	.....	.....	.7
78	.1	6193.37				
79	2.2	6194.23	$6_{-1}-7_{-2}$	.....	6193.95	.8
			$6_{-2}-7_{-3}$	.....	.....	.3
80	2.9	6194.69				
81	.5	6195.26	$6_{-2}-7_{-2}$	6195.00	.....	1.9
			$6_{-3}-7_{-3}$	.....	.....	.6
82	2.6	6197.53	5_4-6_3	6197.54	.....	.9
83	2.2	6198.76	$7_{-7}-8_{-7}$	.....	6198.55	1.7
			$7_{-6}-8_{-7}$	.....	.....	.6
84	8.3	6199.62	$7_{-6}-8_{-7}$	6199.63	.....	3.4
			$7_{-7}-8_{-8}$	.....	.....	1.1
			5_5-6_3	6199.83	.....	1.7
85	.3	6201.15				

TABLE 1. *Comparison of observed and calculated spectra in 1.6-μ region*—Continued

Line No.	Intensity	Observed wave number	Transition	Calculated wave number (111)	Calculated wave number (012)	Intensity
		cm^{-1}		cm^{-1}		
86	1.5	6202.45	$6_{-3}-7_{-3}$		6202.42	1.2
			$6_{-4}-7_{-4}$			.4
			5_0-6_0		6202.49	.7
87	6.8	6203.57	$6_{-4}-7_{-3}$	6202.42		2.8
			$6_{-3}-7_{-3}$			.9
88	1.0	6204.17	$5_{-1}-6_1$		6203.92	
89	2.2	6205.01				
90	5.9	6206.29	5_0-6_{-1}	6205.28		2.4
			3_2-4_4		6206.51	
91	5.6	6207.30	4_2-5_3	6207.32		2.8
92	3.8	6208.70	4_1-5_3	6208.80		
93	2.5	6210.11	3_1-4_3		6209.72	1.6
			$6_{-3}-7_{-2}$		6210.43	2.1
			$6_{-6}-7_{-6}$			.7
94	7.9	6211.46	$6_{-4}-7_{-2}$	6211.46		4.4
			$6_{-3}-7_{-2}$			1.5
95	2.5	6213.67	$5_{-1}-6_{-1}$		6213.49	
			$5_{-3}-6_{-3}$		6213.50	
			4_1-5_2	6213.89		.5
96	9.0	6214.69	$5_{-2}-6_{-2}$	6214.63		3.5
			$5_{-3}-6_{-4}$			1.2
			4_0-5_{-1}	6214.82		3.0
97	.1	6215.79				
98	2.1	6216.90	$8_{-4}-8_{-3}$	6216.53		.3
			$8_{-3}-8_{-4}$	6216.53		.1
			$7_{-2}-7_{-4}$	6216.64		.1
			$7_{-6}-7_{-3}$	6216.66		.4
99	3.2	6217.93	4_1-5_0	6217.80		.9
			4_1-5_{-1}		6217.68	.8
100	.7	6219.11				
101	.5	6220.37				
102	.3	6221.06	3_1-4_2		6220.86	
103	2.5	6221.89	5_3-6_3		6221.90	2.5
			$5_{-4}-6_{-4}$			.9
104	8.7	6222.98	2_0-3_0	6222.46		.7
			$5_{-4}-6_{-3}$	6222.94		5.3
			$5_{-5}-6_{-5}$			1.8
105	2.8	6224.03	3_1-4_2	6224.10		.8
			$4_{-2}-5_{-2}$		6224.11	.5
106	2.9	6224.46	$4_{-1}-5_{-2}$	6224.44		1.7
107	8.1	6225.49	$4^{-1}-5_{-2}$	6225.22		4.0
			$4_{-1}-5_{-2}$			
			2_1-3_2		6225.40	1.3
			3_1-4_2	6225.67		1.2
108	1.5	6227.97				
109	4.3	6229.07	$7_{-3}-7_{-2}$	6228.79		
			$6_{-6}-6_{-3}$	6228.82		.6
			$6_{-3}-6_{-4}$	6228.85		.2
			$7_{-4}-7_{-3}$	6228.81		.5
110	.2	6229.80				
111	5.0	6230.40	3_2-4_1	6230.62		2.3
112	1.3	6231.08	2_2-3_2		6231.13	.6
113	3.1	6232.85	$4_{-3}-5_{-3}$		6232.86	2.8
			$4_{-4}-5_{-4}$			.9
114	8.9	6233.93	3_0-4_{-2}		6233.60	.5
			$3_{-1}-4_{-1}$		6233.83	1.6
			$4_{-4}-5_{-5}$	6234.06		6.0
			$4_{-3}-5_{-4}$			2.0
115	3.5	6234.81	$3_{-1}-4_{-2}$	6235.15		1.4
116	7.0	6236.35	3_0-4_{-1}	6236.35		4.0
117	.4	6238.18				
118	3.8	6239.73	$6_{-3}-6_{-1}$		6239.55	.6
			$5_{-4}-5_{-2}$		6239.63	.6
119	6.8	6240.28	2_0-3_1	6240.32		3.3
120	5.8	6240.66	$5_{-4}-5_{-3}$	6240.62		.3
			$5_{-4}-5_{-2}$	6240.67		.8
			$6_{-4}-6_{-1}$	6240.81		.8
121	2.1	6241.57	$7_{-2}-7_{-1}$	6241.29		.6
122	.7	6242.67	2_0-3_0		6242.57	.5
123	3.0	6243.76	$3_{-2}-4_{-2}$		6243.79	2.8
			$3_{-2}-4_{-4}$		6243.84	1.0
124	10.0	6244.71	$3_{-2}-4_{-3}$	6244.83		6.1
			$3_{-3}-4_{-4}$			2.0
			2_0-3_{-1}	6244.94		4.2
125	.7					
126	.6	6246.48				
127	2.5	6247.97	2_1-3_0		6247.96	1.0
					6248.34	.9
128	1.0	6249.13				
129	1.7	6250.12	4_1-4_{-1}		6250.02	.8
			$6_{-1}-6_1$		6250.26	.7
130	2.8	6250.90				
131	3.7	6251.35	$6_{-2}-6_1$	6251.29		.9
132	4.4	6251.98	$5_{-3}-5_{-1}$		6251.69	.8
			$4_{-4}-4_{-1}$	6252.01		1.1
133	3.1	6252.33	1_1-2_1		6252.41	1.7
134	3.3	6252.95	$5_{-2}-5_{-1}$	6252.85		1.2
135	4.6	6254.32	$2_{-2}-3_{-2}$		6254.03	.8
			$7_{-4}-7_1$		6254.35	.5
			$2_{-1}-3_{-1}$		6254.40	2.5
136	8.5	6255.17	$2_{-2}-3_{-3}$	6254.97		5.4
			$2_{-1}-3_{-2}$			1.8
			6_0-6_1	6255.29		.5
137	2.1	6256.40	7_0-7_1	6256.60		.6
138	4.9	6257.56	1_1-2_0	6257.54		1.2
139	2.0	6258.37				
140	1.9	6259.80				
141	1.4	6260.73	$4_{-1}-4_1$		6260.74	1.1
142	4.0	6261.66				
143	1.7	6262.70	4_0-4_1	6262.36		.5
			$3_{-3}-3_{-1}$		6262.97	.9
144	1.7	6263.60	$1_{-1}-2_{-1}$		6263.50	1.8
			7_3-7_5		6263.54	.5
145	4.1	6264.01	3_3-3_{-1}	6264.01		1.4
146	3.9	6264.65	$1_{-1}-2_{-2}$	6264.75		1.4
147	8.5	6265.85	4_1-4_2		6265.23	.9
			1_0-2_{-2}		6265.25	.5
			$4_{-1}-4_0$	6265.51		.6
			$5_{-1}-5_1$		6265.60	.6
			1_0-2_{-1}	6265.91		3.7
			7_1-7_3		6266.04	.7
148	4.5	6267.68	5_0-5_2		6267.20	.7
149	1.4	6268.71	$2_{-1}-2_2$	6268.42		.4
150	.9	6269.48				
151	1.5	6270.57	$2_{-1}-2_1$		6270.62	.9
152	2.7	6271.38	$2_{-2}-3_1$	6271.29		1.2
153	4.0	6272.94	0_0-1_0		6273.23	.5
154	1.3	6273.73	7_2-7_1	6270.40		.8
			5_1-5_3		6237.57	1.6
155	4.0	6274.96	4_0-4_2		6274.55	.7
			$3_{-1}-3_1$		6275.00	2.1
156	5.7	6275.47	0_0-1_{-1}	6275.54		2.8
			$2_{-1}-2_0$	6275.71		0.6
157	6.3	6277.39	3_1-3_2		6277.36	2.0
			3_0-3_1	6277.52		2.8
158	2.3	6279.53	4_1-4_2	6279.71		1.0
159	1.5	6280.70	2_0-2_2		6280.56	.8
160	4.7	6281.81	5_2-5_3	6281.99		2.9
161	2.7	6282.43	$1_{-1}-1_1$		6282.43	2.0
162	1.7	6283.72				
163	7.1	6284.89	1_0-1_1	6284.88		4.1
			7_4-7_3	6285.15		1.6
164	5.0	6285.93	2_1-2_2	6285.98		2.1
165	8.4	6287.17	3_2-3_3	6287.12		7.5
166	6.1	6288.15	4_3-4_4	6288.10		2.4
167	8.2	6288.80	5_4-5_3	6288.71		5.7
168	9.8	6289.62	6_5-6_6	6289.11		1.3
			7_4-7_7	6289.07		2.2
			5_5-5_4	6289.67		1.9
			6_6-6_5	6289.82		3.9

TABLE 1. *Comparison of observed and calculated spectra in 1.6-μ region*—Continued

Line No.	Intensity	Observed wave number	Transition	Calculated wave number (111)	Calculated wave number (012)	Intensity
		cm^{-1}		cm^{-1}		
169	8.6	6290.44	4_4-4_2	6290.36	.....	7.3
			8_8-8_7	6290.49	.....	1.2
170	5.3	6291.33	3_3-3_2	6291.22	.....	2.5
171	5.4	6291.80	6_6-6_5	6292.09	.....	2.4
172	8.4	6292.48	2_2-2_2	6292.37	.....	6.4
173	4.0	6293.64	1_1-1_0	6293.49	.....	1.4
			1_1-1_{-1}	.....	6293.91	2.1
174	3.8	6294.31	5_5-5_5	6294.44	.....	1.0
175	.7	6295.50	2_2-2_0	6295.53	.....	.8
176	5.8	6297.14	4_2-4_1	6297.07	.....	3.3
177	1.0	6298.45	3_3-3_1	.....	6298.37	2.0
178	.7	6298.79	.....	.....	.....	.....
179	3.2	6299.69	4_2-4_0	.....	6299.59	.8
			3_1-3_0	6299.60	.....	1.0
			3_3-3_{-1}	.....	6299.84	2.2
180	.7	6300.85	1_0-0_0	.....	6300.26	.5
			5_5-5_5	.....	6300.81	1.7
			2_2-2_{-2}	.....	6300.93	.5
181	4.8	6301.81	2_2-2_{-1}	6301.65	.....	2.1
182	4.1	6303.17	1_1-0_0	6302.75	.....	.9
			6_2-6_1	6303.28	.....	.9
183	.2	6304.72	.....	.....	.....	.....
184	1.5	6306.42	5_5-5_{-1}	.....	6306.58	1.4
185	1.9	6306.94	5_1-5_0	.....	6306.91	.6
186	.6	6307.65	.....	.....	.....	.....
187	5.4	6309.77	3_3-3_{-1}	6309.62	.....	1.1
			4_0-4_{-1}	6309.77	.....	1.9
188	.7	6310.44	4_3-4_1	.....	6310.12	1.0
			$2_{-2}-1_0$	.....	6310.38	.6
			$3_{-1}-3_{-1}$	.....	6310.82	1.1
189	4.3	6311.73	$2_{-1}-1_0$	6311.67	.....	1.4
			$3_{-1}-3_{-2}$	6311.83	.....	.5
190	8.0	6312.83	$2_{-1}-1_{-1}$	.....	6312.10	2.1
			4_1-4_{-1}	.....	6312.74	1.3
			$2_{-2}-1_{-1}$	6312.77	.....	4.7
191	4.7	6313.25	3_0-3_{-2}	6313.34	.....	1.5
192	2.3	6314.07	7_1-7_{-1}	.....	6313.94	.6
			4_1-4_{-2}	6314.12	.....	.5
193	1.2	6314.43	.....	.....	.....	.....
194	4.0	6315.73	6_3-6_1	.....	6315.57	.7
			5_2-5_{-1}	6316.01	.....	1.1
195	3.1	6317.62	6_0-6_{-1}	6318.29	.....	1.1
196	4.8	6319.66	$5_{-1}-5_{-3}$	.....	6319.07	1.0
			$3_{-3}-2_{-1}$	.....	6319.68	2.9
			6_1-6_{-1}	.....	6319.98	.8
			$3_{-2}-2_0$	.....	6320.01	1.0
197	10.0	6320.75	$4_{-1}-4_{-3}$	.....	6320.52	.9
			2_0-1_1	6320.57	.....	4.1
			$3_{-2}-2_{-1}$	6320.71	.....	6.4
			$3_{-2}-2_{-2}$	6320.55	.....	2.1
198	6.7	6321.47	$4_{-2}-4_{-3}$	6321.30	.....	1.3
			5_0-5_{-3}	6321.39	.....	1.4
199	.1	6322.70	7_2-7_1	6322.28	.....	.6
200	4.7	6324.00	2_1-1_1	.....	6323.99	2.0
201	2.2	6324.37	.....	.....	.....	.....
202	.7	6325.39	.....	.....	.....	.....
203	4.2	6327.23	$3_{-1}-2_1$	.....	6327.04	1.2
204	6.0	6327.98	$4_{-4}-3_{-2}$	.....	6327.97	1.2
			$4_{-3}-3_{-3}$	.....	6328.01	3.5
205	1.00	6329.01	$5_{-3}-5_{-5}$	.....	6328.79	.8
			7_0-7_{-2}	6328.92	.....	.7
			$4_{-4}-3_{-4}$	6329.01	.....	7.5
			$4_{-3}-3_{-2}$	.....	.....	2.5
206	7.0	6329.51	$6_{-2}-6_{-3}$	6329.25	.....	1.3
			3_0-2_1	6329.56	.....	3.8
207	1.9	6331.46	.....	.....	.....	.....
208	1.4	6332.00	$3_{-1}-2_0$	6332.23	.....	1.7
209	3.7	6332.85	3_0-2_0	.....	6332.68	.6
210	2.7	6333.89	2_2-1_{-1}	6333.85	.....	.9
211	0.2	6334.50	.....	.....	.....	.....
212	5.7	6335.65	$5_{-5}-4_{-3}$	.....	6335.71	3.7
			$5_{-4}-4_{-4}$	.....	.....	1.2
213	10.0	6336.75	$8_{-2}-8_{-3}$	6336.59	.....	.5
			$5_{-4}-4_{-3}$	6336.75	.....	7.8
			$5_{-5}-4_{-4}$	.....	.....	2.6
			$6_{-3}-5_{-5}$	.....	6336.95	.5
214	4.3	6337.78	$7_{-2}-7_{-5}$	6337.47	.....	.7
			3_1-2_2	6337.57	.....	1.4
			$4_{-2}-3_0$	.....	6338.05	.7
			$6_{-4}-6_{-5}$	6338.22	.....	1.1
215	1.0	6338.85	$7_{-3}-7_{-4}$	6338.59	.....	
216	3.3	6339.37	$4_{-1}-3_0$	6339.41	.....	1.7
			$4_{-1}-3_{-1}$	.....	6339.71	2.1
217	7.6	6340.65	$4_{-2}-2_{-1}$	6340.48	.....	5.4
218	.2	6341.53	.....	.....	.....	.....
219	.4	6341.97	.....	.....	.....	.....
220	4.8	6342.93	$6_{-3}-5_{-5}$	.....	6343.10	3.5
			$6_{-6}-5_{-4}$	.....	.....	1.2
221	9.3	6344.12	$6_{-6}-5_{-5}$	6344.17	.....	7.3
			$6_{-5}-5_{-4}$	.....	.....	2.4
222	2.5	6345.57	3_2-2_2	.....	6345.22	.8
			$8_{-4}-8_{-5}$	6345.15	.....	.5
			$7_{-4}-7_{-7}$	6345.71	.....	.5
223	3.9	6346.86	5_0-4_{-1}	.....	6346.75	2.4
			$5_{-2}-4_{-2}$	.....	6347.06	.8
224	8.0	6347.98	$5_{-2}-4_{-1}$	6347.92	.....	5.5
			$5_{-3}-4_{-2}$	6348.15	.....	1.8
225	4.5	6350.01	$7_{-1}-6_{-3}$	.....	6350.09	3.1
			$7_{-6}-6_{-6}$	.....	.....	1.0
			3_3-2_1	6350.42	.....	1.9
226	9.4	6351.32	4_0-3_1	6351.04	.....	5.1
			$7_{-6}-6_{-5}$	6351.19	.....	6.3
			$7_{-7}-6_{-6}$	.....	.....	2.1
227	.2	6352.53	.....	.....	.....	.3
228	.7	6353.04	$8_{-5}-8_{-6}$	.....	.....	.1
			$8_{-6}-8_{-7}$	6353.03	.....	.4
229	5.6	6353.79	4_2-3_1	6353.57	.....	3.4
230	5.7	6354.21	4_1-3_1	.....	6353.91	1.7
231	4.7	6354.48	$6_{-4}-5_{-2}$	.....	6354.64	.8
			$6_{-3}-5_{-3}$	.....	6354.68	.23
232	8.8	6355.69	$5_{-3}-4_1$	.....	6355.35	1.2
			$6_{-4}-5_{-3}$	.....	6355.94	5.1
			$6_{-3}-5_{-2}$	.....	.....	1.7
233	5.0	6356.45	$8_{-7}-7_{-7}$	.....	6356.71	2.4
			$8_{-8}-7_{-8}$	.....	.....	.8
234	9.3	6357.79	5_0-4_1	6357.65	.....	3.9
			$8_{-8}-7_{-7}$	6357.91	.....	5.1
			$8_{-7}-7_{-8}$	.....	.....	1.7
235	2.0	.....	.....	.....	.....	.....
236	1.0	6359.73	.....	.....	.....	.....
237	2.7	6360.63	$5_{-1}-4_0$	6360.29	.....	1.5
			5_0-4_0	.....	6360.18	.5
238	2.9	6361.88	$7_{-5}-6_{-3}$	.....	6361.85	2.0
			$7_{-4}-6_{-4}$	.....	6361.96	.7
239	7.9	6363.07	$9_{-9}-8_{-7}$	.....	6362.96	1.9
			$9_{-8}-8_{-8}$	.....	.....	.6
			$7_{-4}-6_{-3}$	6363.07	.....	4.2
			$7_{-5}-6_{-4}$	.....	.....	1.4
240	7.2	6364.14	$9_{-8}-8_{-7}$	6364.08	.....	3.8
			$9_{-9}-8_{-8}$	.....	.....	1.3
241	2.1	6364.52	.....	.....	.....	.....
242	1.0	6365.31	$6_{-2}-5_0$	.....	6365.20	.5
243	5.0	6366.60	$6_{-1}-5_{-1}$	.....	6366.44	1.4
			$6_{-1}-5_0$	6366.69	.....	1.2
244	5.1	6366.80	.....	.....	.....	.....
245	7.2	6367.44	$6_{-2}-5_{-1}$	6367.48	.....	3.3

TABLE 1. *Comparison of observed and calculated spectra in 1.6-μ region*—Continued

Line No.	Intensity	Observed wave number	Transition	Calculated wave number (111)	Calculated wave number (012)	Intensity	Line No.	Intensity	Observed wave number	Transition	Calculated wave number (111)	Calculated wave number (012)	Intensity
		cm^{-1}		cm^{-1}					cm^{-1}		cm^{-1}		
246	6.0	6368.65	$8_{-8}-7_{-1}$	.....	6368.75	0.5	264	4.0	6387.15				
			$8_{-8}-7_{-8}$	.....	.....	1.5				5_4-4_4	.....	6387.79	0.9
			5_5-4_3	6368.83	.....	1.4	265	2.5	6388.03				
			$10_{-9}-9_{-9}$	6368.85			266	6.7	6388.44	$9_{-4}-8_{-3}$	6388.79	.....	1.6
			$10_{-9}-9_{-8}$							$9_{-5}-8_{-4}$	.....	.....	.5
247	9.5	6370.00	$10_{-9}-9_{-9}$	6370.00	.....	2.7				$11_{-8}-10_{-7}$	6388.79	.....	1.1
			$10_{-10}-9_{-9}$	.....	.....	.9				$11_{-9}-10_{-8}$	.....	.....	.4
			$8_{-8}-7_{-8}$	6370.02	.....	3.3	267	4.7	6389.55	5_3-4_3	.....	6389.52	2.2
			$8_{-8}-7_{-9}$	.....	.....	1.1	268	1.3	6390.47	5_2-4_2	.....	6390.49	.9
248	1.5	6371.06					269	2.0	6391.65				
249	.2	6372.34					270	2.0	6392.46	7_2-6_2	6392.41	.....	1.5
250	2.0	6373.39	$7_{-3}-6_{-3}$	.....	6373.24	1.2	271	5.0	6393.33				
			$7_{-2}-6_{-2}$	.....	.....	.4	272	3.3	6393.98	$8_{-2}-7_{-1}$	6393.82	.....	1.7
251	3.0	6373.96					273	5.0	6394.97	$10_{-8}-9_{-8}$	6395.07	.....	1.0
252	6.7	6374.54	$11_{-11}-10_{-9}$	.....	6374.33	.9				$10_{-9}-9_{-8}$	.....	.....	.3
			$11_{-10}-10_{-10}$	.....	.....	.3	274	4.4	6397.55	6_2-5_2	.....	6397.73	1.1
			$7_{-2}-6_{-1}$	6374.61	.....	3.0	275	.1	6398.78	7_1-6_2	6398.59	.....	.7
			$7_{-3}-6_{-2}$	.....	.....	1.0	276	1.3	6399.06				
253	6.8	6375.49	$9_{-7}-8_{-8}$	.....	6375.31	.7	277	3.9	6399.88	$9_{-2}-8_{-1}$	6400.36	.....	1.1
			$9_{-6}-8_{-6}$	.....	.....	.2	278	2.7	6401.20				
			6_1-5_2	6375.39	.....	.9	279	.7	6401.80				
			$11_{-10}-10_{-9}$	6375.52	.....	1.8	280	2.2	6403.45				
			$11_{-11}-10_{-10}$	.....	.....	.6	281	1.3	6403.69				
254	4.2	6376.17					282	1.2	6405.35				
255	6.7	6376.65	$9_{-4}-8_{-5}$	6376.62	.....	2.4	283	2.0	6406.07				
			$9_{-7}-8_{-6}$	.....	.....	.8	284	3.5	6406.67	8_0-7_1	6406.95	.....	1.4
255A	3.7	6378.86					285	1.3	6407.67				
256	3.6	6379.07	4_4-3_3	6379.03	.....	.7	286	3.0	6408.34				
			$12_{-11}-11_{-11}$	.....	6379.46	.6	287	4.1	6408.77	6_0-5_0	.....	6408.61	1.6
			$12_{-12}-11_{-10}$	.....	.....	.3	288	1.0	6409.49	6_0-5_1	.....	6409.50	.5
257	5.0	6380.51	6_0-5_0	6379.87	.....	.5	289	2.0	6410.26				
			6_0-5_1	6380.23	.....	3.3	290	2.0	6410.60				
			$12_{-11}-11_{-10}$	6380.69	.....	.4	291	2.2	6411.53				
			$12_{-12}-11_{-11}$	.....	.....	1.2	292	2.3	6412.08				
			$8_{-8}-7_{-3}$	.....	6380.54	.8	293	1.8	6412.82				
			$8_{-8}-7_{-4}$	.....	.....	.3	294	1.8	6414.21				
258	8.0	6381.72	6_1-5_1	.....	6381.64	.9	295	2.0	6414.48				
			$8_{-8}-7_{-3}$	6381.96	.....	2.3	296	2.8	6415.89	8_0-7_2	6415.76	.....	1.3
			$8_{-3}-7_{-3}$	.....	.....	.8	297	1.3	6417.14				
259	5.6	6382.85	$10_{-8}-9_{-7}$	6382.87	.....	1.6	298	2.1	6418.26				
			$10_{-7}-9_{-6}$	.....	.....	.5	299	2.7	6419.15				
			$7_{-1}-6_1$	.....	6382.99	.8	300	.3	6421.94				
260							301	.7	6423.05				
261	----	.....	6_0-5_2	6383.30	.....	1.1	302	1.5	6424.33				
262	4.3	6384.43					303	2.7	6425.52				
263	6.0	6385.16	7_0-6_1	6385.23	.....	2.2	304	.4	6427.40				
			6_2-5_2	.....	6385.47	2.9	305	2.0	6428.99				
							306	2.4	6429.50	7_1-6_2	.....	6249.57	1.0

3. Analysis of Experimental Results

The previous analysis of the low-resolution data showed that the absorption in this region could be accounted for by an A-type band, i. e., the dipole moment change along the least inertial axis. The previously calculated spectrum was compared to the new data, and the strong transitions were brought into agreement with the observed absorption peaks through the use of derivatives of the energy with respect to the inertial parameters [4]. Then all transitions of intensity sufficient to be observed were calculated. The fit between the observed and calculated spectra was very good, except that quite a few of the weaker peaks were not accounted for. Through the use of known ground-state energies [4] it was possible to determine that many of these unaccounted for peaks resulted from a B-type band centered about 1 cm^{-1} lower than the main band. The excited state inertial parameters for this band were determined as described previously [1]. A classical centrifugal distortion correction was applied to the excited-state energy levels of both bands [4].

The excited vibrational state of the A-type band is undoubtedly the (1,1,1) [1]. The excited vibrational state involved in the B-type band is probably the lower component of the resonating pair (0,1,2) and (2,1,0). A calculation based on the quadratic expression for the vibrational-band system of

hydrogen sulfide [5] predicts this band to be at 6,285 cm^{-1}, compared to the observed 6288.30 cm^{-1}.

The parameters giving the best fit of the observed data are (1,1,1) $A=10.398$, $B=8.935$, $C=4.548$, $\nu_0=6289.26$ cm^{-1}; (0,1,2) $A=10.394$, $B=8.918$, $C=4.547$, $\nu_0=6288.28$ cm^{-1}.

Many of the listed peak positions cannot be attributed to single transitions. The overlapping of two or more transitions will give an observed peak position that will not be the true frequency of any one transition. In many instances, however, definite assignments can be made. This is generally true for the extremely strong transitions because the observed frequency will not be greatly affected by weaker satellites. In the (1,1,1) band the mean deviation of 76 such assignments is 0.10 cm^{-1}. In the (0,1,2) band some 36 peaks were assigned that do not have a dual assignment in the (1,1,1) band. The mean deviation in this case was 0.09 cm^{-1}. That so many of the individual deviations are greater than the mean must be attributed to the effect of finite slit on overlapping transitions. This is especially true of the (0,1,2) band, which is very weak compared to the main band in this region. The classical centrifugal-distortion correction may also be responsible for some of the large deviations. However, it should be pointed out that for low J the corrections are small in any event, and for high J the correction should become classical. Another advantage of this method is that this correction can be evaluated level for level and applied to the rigid levels calculated from published energy tables. The agreement between the observed and calculated spectra may be seen in figure 1 and in table 1. The relative intensity scale within a given band is the same as that used in the previous analysis. In reporting the intensities, the line strengths in the (1,0,2) band were divided by two to give a better picture of the relative importance of the two bands. The P branch of the (1,1,1) band is roughly three times as strong as the P branch of the (0,1,2) band, and the R branch of the (1,1,1) band is approximately twice as strong as the R branch of the (0,1,2) band. Some transitions of the two bands appear to be different from the intensities that one would predict from simple theory. These intensity discrepancies no doubt arise from the effect of Coriolis interaction between the two bands.

The new values of the inertial parameters of the (1, 1, 1) band agree with those determined previously within the estimated error. As the (0, 1, 2) band is somewhat weaker, and the transitions somewhat harder to identify, it is felt that the inertial parameters for this band are not as well determined as those for the main band.

4. Discussion

In figure 1 it will be noted that the calculated spectrum does not account for all the observed absorption lines at the high and low limits of the band. The calculated spectrum in these regions is incomplete as calculations were not extended above $J=12$, the upper limit of published energy tables [6]. Likewise, the other half of the resonating pair, (0, 1, 2) and (2, 1, 0), is predicted to fall in the high-frequency region of this absorption. It has not been possible to locate any transitions that can be definitely assigned to a band having this upper state; however, it would in all probability be lost in the other two overlapped bands.

In the infrared spectra of water-type molecules, it has been observed that A-type bands are normally very much stronger than B-type bands. In the hydrogen-sulfide spectrum only two B-type bands, (0, 1, 0) and (0, 2, 0), have been observed. It may be possible that other B-type bands are present in the spectrum of hydrogen sulfide that are completely overlapped by strong A-type bands [5, 7, 8, 9]. In each case observed so far the overlapping bands have fitted the criterion for Coriolis-type interaction [10]. In the analysis of the rotational fine structure of all these bands, it has been possible to account for the observed absorption by calculating a theoretical spectrum with effective moments of inertia. There has been no drastic perturbation of individual energy levels. This is in line with what might be expected. As the inertial parameters of the two excited states are nearly the same, the initial separation of the unperturbed energy levels is very nearly constant. Both the interaction and the energy vary nearly as K^2; hence it is possible to fit the observed spectra through the use of effective moments of inertia [5], the effect of the Coriolis interaction being absorbed in the inertial constants. The extent of this effect cannot be ascertained until the vibrational system of hydrogen sulfide is better understood. The fact that these B-type bands are observed only when overlapped by a normally strong A-type band seems to indicate that the intensity is interchanged quite readily.

As has been observed in other B-type bands [11], R branch transitions between high τ levels of adjacent J values are apparently stronger than would be predicted by the simple rigid theory. There is still no adequate explanation for this.

The value of $\Delta=I_c-I_a-I_b$ lends additional support to the vibrational assignments proposed here. In both bands its value is large indicating that n_2 equals at least 1 in each of the excited states. The exact value of Δ is of little significance because of the presence of the Coriolis interaction.

5. References

[1] H. C. Allen, P. C. Cross, and M. K. Wilson, J. Chem. Phys. **18,** 691 (1950).
[2] Earle K. Plyler and Norman Gailar, J. Research NBS **47,** 248 (1951) RP2249.
[3] Norman Gailar and Earle K. Plyler, J. Research NBS **48,** 392 (1952) RP2327.
[4] P. C. Cross, Phys. Rev. **47,** 7 (1935).
[5] H. C. Allen, Thesis (University of Washington, 1951).
[6] G. W. King, R. M. Hainer, and P. C. Cross, J. Chem. Phys. **11,** 27 (1943).
[7] K. K. Innes, Thesis (University of Washington, 1951).
[8] G. L. Ordway, Thesis (University of Washington, 1952).
[9] H. R. Grady, P. C. Cross, and G. W. King, Phys. Rev **75,** 1450 (1949).
[10] E. B. Wilson, Jr., J. Chem. Phys. **4,** 313 (1936).
[11] H. C. Allen and P. C. Cross, J. Chem. Phys. **19,** 140 (1951).

WASHINGTON, August 20, 1953.

Journal of Research of the National Bureau of Standards Vol. 52, No. 4, April 1954 Research Paper 2491

New Formulas for Facilitating Osculatory Interpolation

Herbert E. Salzer

Hermite's n-point osculatory interpolation formula for equally spaced arguments at intervals of h, employing the function and its derivative is very much more accurate than the corresponding n-point Lagrangian formula and considerably more accurate than even the $2n$-point Lagrangian formula at intervals of h. Also it is specially suited for interpolation in many functions (e. g., Bessel, probability) that are tabulated with their derivative. To avoid the tremendous amount of labor in calculating the coefficients of f_i and f_i' in the forms that they are usually given, Hermite's formula is expressed as

$$f(x_0+ph)=\sum_i(\alpha_i f_i+\beta_i h f_i')/\sum_i \alpha_i + R_{2n}(p),$$

where

$$\alpha_i \equiv a_i/(p-i)^2+b_i/(p-i),\ \beta_i \equiv a_i/(p-i),$$

and where

$$a_i=k(n)/\left\{\prod_{j=-[(n-1)/2]}^{[n/2]}{}'(i-j)\right\}^2,\ b_i=-2L_i^{(n)\prime}(i)a_i,\ L_i^{(n)}(p)$$

being

$$\prod_{j=-[(n-1)/2]}^{[n/2]}{}'(p-j)/\prod_{j=-[(n-1)/2]}^{[n/2]}{}'(i-j).$$

The constant $k(n)$, which may be picked arbitrarily, is here chosen to make a_i and b_i integers. The exact values of a_i and b_i are given for $n=2(1)11$, $i=-[(n-1)/2]$ to $[n/2]$ so that this formula can be applied exactly for any polynomial up to the 21st degree. A schedule gives approximate upper bounds for the coefficients of $f^{(2n)}(\xi)h^{2n}\sim\Delta^{2n}f(x)$ in $R_{2n}(p)$.

When a function $f(x)$ and its first derivative are known at n points x_i, $i=1, 2, \ldots, n$, a highly accurate interpolation formula due to Hermite is given by

$$f(x)=\sum_{i=1}^{n}\{L_i^{(n)}(x)\}^2\{1-2L_i^{(n)\prime}(x_i)(x-x_i)\}f(x_i)+\sum_{i=1}^{n}\{L_i^{(n)}(x)\}^2(x-x_i)f'(x_i)+R_{2n}(x), \tag{1}$$

where

$$L_i^{(n)}(x)=\prod_{j=1}^{n}{}'(x-x_j)/\prod_{j=1}^{n}{}'(x_i-x_j),\quad j=i \text{ is absent from } \Pi', \tag{2}$$

and

$$R_{2n}(x)=f^{(2n)}(\xi)\left\{\prod_{j=1}^{n}(x-x_j)\right\}^2/(2n)!,\quad \text{least } x_i\le\xi\le \text{greatest } x_i. \tag{3}$$

Thus (1) is exact whenever $f(x)$ is a polynomial of degree less than or equal to $2n-1$.

When the points x_i are equally spaced at intervals of h, it is customary to alter the notation in x_i, letting i run from $-[(n-1)/2]$ to $[n/2]$ instead of 1 to n, where $[m]$ denotes the largest integer not exceeding m. Then it is convenient to choose a variable p given by $x=x_0+ph$ and to let $x_i=x_0+ih$. Also, $f(x)=f(x_0+ph)\equiv fp\equiv f$, $f(x_i)\equiv f_i$, and $f'(x_i)\equiv f_i'$. Then (1), for $f(x)$ considered as a function of p, is expressible as

$$f(x_0+ph)=\sum_{i=-[(n-1)/2]}^{[n/2]}\{L_i^{(n)}(p)\}^2\{1-2L_i^{(n)\prime}(i)(p-i)\}f_i+\sum_{i=-[(n-1)/2]}^{[n/2]}\{L_i^{(n)}(p)\}^2(p-i)hf_i'+R_{2n}(p), \tag{4}$$

where now

$$L_i^{(n)}(p)=\prod_{j=-[(n-1)/2]}^{[n/2]}{}'(p-j)/\prod_{j=-[(n-1)/2]}^{[n/2]}{}'(i-j), \tag{5}$$

and

$$R_{2n}(p)=f^{(2n)}(\xi)h^{2n}\left\{\prod_{j=-[(n-1)/2]}^{[n/2]}(p-j)\right\}^2/(2n)!,\quad x_{-[(n-1)/2]}\le\xi\le x_{[n/2]}. \tag{6}$$

There are many advantages in the use of (1) or (4) over the ordinary Lagrangian interpolation formula given (for equal spacing) by

$$f(x_0+ph)=\sum_{i=-[(n-1)/2]}^{[n/2]} L_i^{(n)}(p)f_i+R_n(p), \tag{7}$$

where

$$R_n(p)=f^{(n)}(\xi)h^n \prod_{j=-[(n-1)/2]}^{[n/2]}(p-j)/n!, \quad x_{-[(n-1)/2]}\leq\xi\leq x_{[n/2]}. \tag{8}$$

Thus letting $\prod_{j=-[(n-1)/2]}^{[n/2]}(p-j)$ be denoted by $L^{(n)}(p)$, and recalling that for reasonably small h we have approximately

$$f^{(n)}(\xi)h^n\sim\Delta^n f, \tag{9}$$

where $\Delta^n f$ is the approximate nth difference of the tabulated $f(x)$, the remainder term for (7) is of the order of $\Delta^n f L^{(n)}(p)/n!$, whereas that for (4) is of the order of $\Delta^{2n}f\{L^{(n)}(p)\}^2/(2n)!$. Apart from the fact that $\Delta^{2n}f$ is usually very much smaller than $\Delta^n f$, the factor $\{L^{(n)}(p)\}^2/(2n)!$ is equal to the square of $L^{(n)}(p)/n!$ (where the latter is usually very small and less than unity so that its square is ever so much smaller) multiplied by the very small quantity $n!/(n+1)\ldots(2n)$. The user can appreciate the improvement by comparing the approximate upper bounds for the multiplier of $f^{(2n)}(\xi)h^{2n}$ in $R_{2n}(p)$ of (4) which are tabulated in the schedule at the end, with the approximate upper bounds for the multiplier of $f^{(n)}(\xi)h^n$ in $R_n(p)$ of (7), which are tabulated in [3, p. xvi][1] and from which this present schedule was calculated. Thus it will be apparent that (4) is a very much more accurate formula than (7). Of course, we are comparing (4), a confluent form of a $2n$-point formula, with (7), which is only an n-point formula.

But it is important to note than even if (4) is compared with formula (7) taken for $2n$ points at intervals of h, instead of n points, the remainder term would differ from that in (4) (apart from a different ξ in $f^{(2n)}(\xi)$) by the presence of the factor $L^{(2n)}(p)$ instead of the factor $\{L^{(n)}(p)\}^2$, which has a very much smaller upper bound than the $L^{(2n)}(p)$, showing that wherever it is possible to be used, the n-point Hermite osculating interpolation formula is much to be preferred, regarding accuracy, to a $2n$-point Lagrangian interpolation formula at the same interval h. This last statement becomes intuitively plausible when the osculating interpolation formula for n points at intervals of h is regarded as a confluent form of a $2n$-point Lagrangian formula whose $2n$ points lie within a range of nh so that the "average interval" between those $2n$ points is only half the interval of h for the usual $2n$-point Lagrangian formula. Thus the upper bound for the remainder term of the n-point osculating formula would be expected to be of the order of $(1/2^{2n})$th of the upper bound for the remainder term of the $2n$-point Lagrangian formula; actual estimates show it to be even considerably smaller. For example, the 2-, 3-, 4-, and 5-point osculating formulas have error terms whose upper bounds are around 1/16th, 1/110, 1/640, and 1/3000 of the respective upper bounds of the error terms in the 4-, 6-, 8-, and 10-point Lagrangian formulas.

A second important advantage in (4) is that it is suited for use with very many tables where the derivative of the function is tabulated alongside of the function itself. For example, it is useful in tables of Bessel functions of the first and second kind [4, 5, 6] which give $J_1(x)=-J_0'(x)$, $Y_1(x)=-Y_0'(x)$, and probability functions [7], and in numerous tables of more elementary functions and their integrals, such as tables of sine, cosine, or exponential integrals [8, 9], where the derivative is very easy to obtain.

However, the use of (1) or (4) in the form usually presented [1, 2] requires a considerable amount of computational labor which mounts considerably as the number of points x_i increases. It is the purpose of this present article to provide a means of using (4) with a small fraction of the labor involved in the direct calculation of the coefficients of f_i and f_i'. The idea

[1] Figures in brackets indicate the literature references at the end of this paper.

behind this method goes back to a scheme first used by W. J. Taylor for calculating Lagrangian interpolation coefficients for functions tabulated at real equidistant arguments [10], and which was generalized by the present writer for functions tabulated at nonequidistant arguments [11], and also for complex arguments whether in Cartesian [12] or polar form [13, 14], and finally even for functions that are interpolable by expressions that are not transformable into polynomials [15]. Recently, the writer in looking for some way to reduce the amount of work in using (4), observed that Taylor's idea could be extended also to the calculation of osculating interpolation coefficients. In place of extensive tables of the $(2n-1)$th degree polynomial coefficients of f_i and f_i' in (4), one requires for each separate n only some fixed quantities a_i and b_i, which are exact integers and are tabulated below. To see this, one merely expresses (4) as

$$f(x_0+ph)=\{L^{(n)}(p)\}^2 \sum_{i=-[(n-1)/2]}^{[n/2]} \left\{\left(\frac{A_i^2}{(p-i)^2}-\frac{2L_i^{(n)\prime}(i)A_i^2}{(p-i)}\right)f_i+\frac{A_i^2}{(p-i)}\,h f_i'\right\}+R_{2n}(p), \tag{10}$$

where [2]

$$A_i=1\Big/\prod_{j=-[(n-1)/2]}^{[n/2]\prime}(i-j). \tag{11}$$

Now the right member of (4) or (10) without the $R_{2n}(p)$ gives the expression for a $(2n-1)$th degree polynomial, which, with its derivative, assumes preassigned values of f_i and f_i' at $x=x_i$, and moreover that polynomial is *uniquely determined by the f_i and f_i'*. For proof of uniqueness see [1, p. 85–86], where T. Fort gives a demonstration of the unique existence of a more general osculating formula. His proof is practically complete save for the explicit indication that the mode of representation of any $(mn-1)$th degree polynomial which is given at the bottom of page 85 is always possible (which is fairly obvious). Now we make use of this uniqueness of representation by putting $f(x)\equiv 1$ into (10), so that both f_i' and $R_{2n}(p)$ are zero, $f_i=1$, and we get

$$\{L^n(p)\}^2=\frac{1}{\sum_{i=-[(n-1)/2]}^{[n/2]}\left(\frac{A_i^2}{(p-i)^2}-\frac{2L_i^{(n)\prime}(i)A_i^2}{p-i}\right)}. \tag{12}$$

Thus from (10) and (12),

$$f(x_0+ph)=\frac{\sum_{i=-[(n-1)/2]}^{[n/2]}\left\{\left(\frac{a_i}{(p-i)^2}+\frac{b_i}{(p-i)}\right)f_i+\frac{a_i h}{(p-i)}\,f_i'\right\}}{\sum_{i=-[(n-1)/2]}^{[n/2]}\left(\frac{a_i}{(p-i)^2}+\frac{b_i}{(p-i)}\right)}+R_{2n}(p), \tag{13}$$

where a_i and b_i are given by

$$a_i=k(n)A_i^2, \tag{14}$$

$$b_i=k(n)\{-2L_i^{(n)\prime}(i)A_i^2\}, \tag{15}$$

and where $k(n)$ is any suitably chosen constant of proportionality that depends only upon n; In the present case the $k(n)$ was chosen as to give exact integral values for a_i and b_i instead of rational fractional values.

It is simplest to think of the approximation to $f(x)$ in the concise form

$$f\sim\frac{\Sigma(\alpha f_i+\beta_i h f_i')}{\Sigma\alpha_i}, \tag{16}$$

where

$$\alpha_i\equiv a_i/(p-i)^2+b_i/(p-i), \tag{17}$$

and

$$\beta_i\equiv a_i/(p-i). \tag{18}$$

[2] The dependence upon n of A_i, as well as of a_i and b_i given below, is not indicated, so as to avoid cumbersome notation.

In using (16), (17), and (18) with a desk calculator, it is easiest to first divide a_i by $p-i$ to get β_i, which is next both multiplied by hf_i' and increased by b_i. The latter, or β_i+b_i, is again divided by $(p-i)$ to give α_i, from which one obtains both $\alpha_i f_i$ and $\Sigma\alpha_i$ and finally $\Sigma(\alpha_i f_i+\beta_i h f_i')/\Sigma\alpha_i$.

The computation of the quantities a_i and b_i was quite straightforward. Since $A_i=(-1)^{[n/2]-i}\binom{n-1}{i+[(n-1)/2]}\Big/(n-1)!$, instead of A_i^2, the proportional quantities $\binom{n-1}{i+[(n-1)/2]}^2$ were calculated. Then they were multiplied by the $-2L_i^{(n)\prime}(i)$, which were calculated by differentiating the explicit polynomial expressions $L_i^{(n)}(p)$ and then setting $p=i$. All fractions in $-2\binom{n-1}{i+[(n-1)/2]}^2 L_i^{(n)\prime}(i)$ were cleared by multiplication of these quantities, as well as the $\binom{n-1}{i+[(n-1)/2]}^2$, by some suitable integer, for each n, to yield the exact integral values for a_i and b_i, which are tabulated below. The a_i and b_i were checked by both recomputation and by use in an example for every n where the answer was known exactly and where the computation by (13) (or the equivalent (16), (17), and (18)) doing the work in decimal form to avoid too much labor, gave agreement to 10 significant figures.

The schedule giving the approximate upper bounds for the coefficients of $f^{(2n)}(\xi)h^{2n}\sim\Delta^{2n}f$ in the error term $R_{2n}(p)$, (see (4) with (6), or (13)), namely, the quantities $\{L^{(n)}(p)\}^2/(2n)!$, was calculated from the approximate upper bounds for $L^{(n)}(p)/n!$ given in a schedule in [3, p. xvi], by squaring the entries in the latter and multiplying by $n!/(n+1)\ \ldots\ (2n)$. Thus, since the $L^{(n)}(p)/n!$ was tabulated only approximately, in some cases to only one significant figure, some of the upper bounds given here for $\{L^{(n)}(p)\}^2/(2n)!$ are not at all precise. For example, if we take a rounded 0.01 and square it to obtain 0.0001, the true value of that square may be only one-fourth as large or over twice as large, depending upon whether the 0.01 was rounded from 0.0051 or 0.0149. Hence in the schedule below, in some cases for the larger number of points, only the order of magnitude of an upper bound for the $\{L^{(n)}(p)\}^2/(2n)!$ is indicated. But more precise determination will hardly be needed there due to the extreme accuracy that is surely indicated even within the range of the uncertainty.

---

[1] T. Fort, Finite differences, p. 85–88 (Clarendon Press, Oxford, England, 1948).
[2] J. F. Steffensen, Interpolation, p. 33–34 (Williams & Wilkins, Baltimore, Md., 1927).
[3] National Bureau of Standards, Tables of Lagrangian interpolation coefficients (Columbia University Press, New York, N. Y., 1944; 2d ed. 1948).
[4] National Bureau of Standards, Table of the Bessel functions $J_0(z)$ and $J_1(z)$ for complex arguments (Columbia University Press, New York, N. Y., 1943; 2d ed. 1947).
[5] National Bureau of Standards, Table of the Bessel functions $Y_0(z)$ and $Y_1(z)$ for complex arguments (Columbia University Press, New York, N. Y., 1950).
[6] Harvard Computation Laboratory, The annals of the computation laboratory of Harvard University **III**, Tables of the Bessel functions of the first kind of orders zero and one (Harvard University Press, Cambridge, Mass., 1947).
[7] Tables of probability functions, NBS MT8, **I** (1941); NBS MT14, **II** (1942), 2d ed. (1948).
[8] Tables of sine, cosine, and exponential integrals, NBS MT5; NBS MT6 (1940).
[9] Table of sine and cosine integrals for arguments from 10 to 100, NBS MT12 (1942).
[10] W. J. Taylor, Method of Lagrangian curvilinear interpolation, J. Research NBS **35,** 151–155 (1945) RP1667.
[11] H. E. Salzer, Checking and interpolation of functions tabulated at certain irregular logarithmic intervals, J. Research NBS **46,** 74–77 (1951) RP2177.
[12] H. E. Salzer, Formulas for complex Cartesian interpolation of higher degree, J. Math. Phys. **28,** 200–203 (1949).
[13] H. E. Salzer, Alternative formulas for direct interpolation of a complex function tabulated along equidistant circular arcs, J. Math. Phys. **26,** 56–61 (1947).
[14] H. E. Salzer, Coefficients for polar complex interpolation, J. Math. Phys. **29,** 96–104 (1950).
[15] H. E. Salzer, Coefficients for facilitating trigonometric interpolation, J. Math. Phys. **27,** 274–278 (1949).

Table of a_i and b_i

Two-point

a_0	1	b_0	2
a_1	1	b_1	−2

Three-point

a_{-1}	1	b_{-1}	3
a_0	4	b_0	0
a_1	1	b_1	−3

Four-point

a_{-1}	3	b_{-1}	11
a_0	27	b_0	27
a_1	27	b_1	−27
a_2	3	b_2	−11

Five-point

a_{-2}	6	b_{-2}	25
a_{-1}	96	b_{-1}	160
a_0	216	b_0	0
a_1	96	b_1	−160
a_2	6	b_2	−25

Six-point

a_{-2}	30	b_{-2}	137
a_{-1}	750	b_{-1}	1625
a_0	3000	b_0	2000
a_1	3000	b_1	−2000
a_2	750	b_2	−1625
a_3	30	b_3	−137

Seven-point

a_{-3}	10	b_{-3}	49
a_{-2}	360	b_{-2}	924
a_{-1}	2250	b_{-1}	2625
a_0	4000	b_0	0
a_1	2250	b_1	−2625
a_2	360	b_2	−924
a_3	10	b_3	−49

Eight-point

a_{-3}	70	b_{-3}	363
a_{-2}	3430	b_{-2}	9947
a_{-1}	30870	b_{-1}	48363
a_0	85750	b_0	42875
a_1	85750	b_1	−42875
a_2	30870	b_2	−48363
a_3	3430	b_3	−9947
a_4	70	b_4	−363

Nine-point

a_{-4}	140	b_{-4}	761
a_{-3}	8960	b_{-3}	28544
a_{-2}	1 09760	b_{-2}	2 08544
a_{-1}	4 39040	b_{-1}	3 95136
a_0	6 86000	b_0	0
a_1	4 39040	b_1	−3 95136
a_2	1 09760	b_2	−2 08544
a_3	8960	b_3	− 28544
a_4	140	b_4	−761

Ten-point

a_{-4}	1260	b_{-4}	7129
a_{-3}	1 02060	b_{-3}	3 50649
a_{-2}	16 32960	b_{-2}	35 69184
a_{-1}	88 90560	b_{-1}	109 65024
a_0	200 03760	b_0	80 01504
a_1	200 03760	b_1	−80 01504
a_2	88 90560	b_2	−109 65024
a_3	16 32960	b_3	−35 69184
a_4	1 02060	b_4	−3 50649
a_5	1260	b_5	−7129

Eleven-point

a_{-5}	1260	b_{-5}	7381
a_{-4}	1 26000	b_{-4}	4 60900
a_{-3}	25 51500	b_{-3}	62 14725
a_{-2}	181 44000	b_{-2}	275 61600
a_{-1}	555 66000	b_{-1}	407 48400
a_0	800 15040	b_0	0
a_1	555 66000	b_1	−407 48400
a_2	181 44000	b_2	−275 61600
a_3	25 51500	b_3	−62 14725
a_4	1 26000	b_4	−4 60900
a_5	1260	b_5	−7381

Schedule of approximate upper bounds for $|L^{(\alpha)}(p)|^2/(2n)!$

(Figures in parentheses indicate the number of zeros between the decimal point and the first significant digit.)

Range of p	$\begin{cases} \\ 0<p<1 \end{cases}$	$\begin{matrix} -1\leq p\leq 0 \\ 1\leq p\leq 2 \end{matrix}$	$\begin{matrix} -2\leq p\leq -1 \\ 2\leq p\leq 3 \end{matrix}$	$\begin{matrix} -3\leq p\leq -2 \\ 3\leq p\leq 4 \end{matrix}$	$\begin{matrix} -4\leq p\leq -3 \\ 4\leq p\leq 5 \end{matrix}$
Two-point	.0026				
Four-point	.(5)82	.(4)25			
Six-point	.(7)26	.(7)55	.(6)62		
Eight-point	.(10)94	.(9)15	.(9)85	.(7)20	
Ten-point	.(12)34	.(12)49	.(11)18	.(10)18	.(9)78
Range of p	$0<\|p\|<1$	$1<\|p\|<2$	$2<\|p\|<3$	$3<\|p\|<4$	$4<\|p\|<5$
Three-point	.00021				
Five-point	.(6)57	.(5)38			
Seven-point	.(8)18	.(8)62	.(6)11		
Nine-point	.(11)60	.(10)15	.(9)12	.(8)40	
Eleven-point	.(13)6	.(13)6	.(12)2	.(11)6	.(9)1

WASHINGTON, May 12, 1953.

Journal of Research of the National Bureau of Standards Vol. 52, No. 4, April 1954 Research Paper 2492

Apparent Specific Volume of Polystyrene in Benzene, Toluene, Ethylbenzene, and 2-Butanone*

Maurice Griffel,[1] Ralph S. Jessup, Joseph A. Cogliano,[2] and Rita P. Park

Measurements have been made at temperatures near 27° and 30° C of the densities of purified benzene, toluene, ethylbenzene, and 2-butanone (methylethylketone), and of solutions of a purified sample of polystyrene in these solvents. Within the precision of the measurements (about 1 or 2 in 10^5 density) the apparent specific volume of the polystyrene is a constant independent of the concentration in any one solvent, but depends to some extent upon the solvent. The lowest values, which were obtained with 2-butanone, are about 1 percent lower than the highest values, which were obtained with ethylbenzene. The values are all lower than those of the virtual liquid polymer, obtained by extrapolation of data on specific volume above the glass transition temperature, although the data of other observers indicate that this is not true for all solvents. In all four solvents the change of the apparent specific volume with temperature is less than for the liquid polymer.

The changes in volume upon mixing of polystyrene with the solvents are shown to have a significant effect on such thermodynamic properties as heat, free energy, and entropy of mixing.

1. Introduction

Theoretical treatments of the thermodynamics of polymer solutions are usually based on assumptions that imply that there is no volume change on mixing of polymers and solvents. Experimentally, however, it is found that there is a small but measurable change in volme when mixing takes place at constant pressure [1, 2, 3, 4, 11, 12, 15].[3] Because a change in volume will affect the experimentally determined values of such thermodynamic quantities as heat, free energy, and entropy of mixing at constant pressure [5], a knowledge of the magnitude of the change in volume is of importance in comparing experimental results with theoretical predictions. The work described in this paper was undertaken to provide data to aid in interpreting the results of measurements of heats of mixing of polymers and solvents.

2. Materials

The polystyrene used was obtained from the Dow Chemical Co. through the courtesy of R. F. Boyer. It had been prepared by thermal polymerization without catalyst at 180° C. After receipt of the material it was purified as follows: 150 g of polystyrene was dissolved in about 750 ml of benzene, and was then precipitated by pouring the solution slowly into about 3 liters of well-stirred methanol. After allowing the precipitate to settle, the liquid was decanted. This procedure was repeated twice. The polystyrene was then dissolved in 2 liters of benzene, the mixture was frozen at −30° C. and most of the benzene was removed by evacuation at temperatures not exceeding 3° C. Evacuation was continued at a temperature of 70° C for about 10 days. The temperature was then gradually increased to 120° C over a period of about a week, and the pressure over the material was maintained at less than 10^{-4} mm of mercury. As a result of this treatment, the polystyrene was fused into a solid mass. To facilitate subsequent handling, it was ground in a cutting mill, so that the final product consisted of particles about 3 mm or less in diameter.

From observations of light scattering the values $M=190{,}000$ and $B=5.2\times10^{-4}$ cgs unit were obtained for weight average molecular weight and second virial coefficient, respectively, for the purified polymer.[4]

The volatile constituents of the purified polymer were determined[5] by heating a crushed sample to 150° to 160° C for 2 hr in a previously evacuated space of known volume, measuring the resulting increase in pressure, and making a mass spectrometric analysis of the gas evolved. The amounts of volatile constituents found in this way, expressed in percentage of the total weight of polymer, are as follows:

Constituent	Percentage by weight
Water	0.101
Carbon dioxide	.021
Benzene	.014
Total volatile impurities	0.136

The fact that appreciable amounts of volatile impurities remained after prolonged heating and evacuation, as described above, is in accord with the findings of Grassie [10] in regard to the difficulty of removing volatile impurities from polymers.

*This work was supported in part by the Reconstruction Finance Corporation, Office of Synthetic Rubber, in connection with the Government Synthetic Rubber Program.

[1] Present address, The Johns Hopkins University, Baltimore, Md.

[2] Present address, George Washington University, Washington, D. C.

[3] Figures in brackets indicate the literature references at the end of this paper.

[4] These values were obtained by M. Wales of the Polymer Structure Section of the Bureau.

[5] In the Mass Spectrometry Section of the Bureau.

The benzene used was purified [6] by fractional freezing. The other solvents were purified by distillation. Freezing-curve measurements [7] indicated a purity of 99.65 and 99.80 mole percent for the toluene and 2-butanone, respectively. The other solvents are believed to be of comparable purity, although no actual determinations of their purity were made. Although impurities in the solvents would affect the densities of both solvents and solutions, it seems very improbable that they would affect the apparent specific volume of the solute to an appreciable extent in view of the small differences between the values for apparent specific volume in different solvents. In table 1 the observed densities of the three hydrocarbon solvents are compared with "best" values of these properties derived from data reported in the literature [6].

TABLE 1. *Densities of hydrocarbon solvents*

Solvent	Density, g/cm³, at—			
	26.890° C		29.971° C	
	Literature values	Observed values	Literature values	Observed values
Benzene	0.87167	0.87165	0.86840	0.86834
Toluene	.86952	.86935	.85766	.85747
Ethylbenzene	.86096	.86123	.85826	.85851

3. Apparatus and Method

Densities of solvents and solutions of known composition were measured by means of picnometers, and values of apparent specific volume of polystyrene were calculated from the data.

The Pyrex picnometers used (A, fig. 1) are of the bicapillary type described by Heller and Thompson [1]. The capillaries were of "precision-bore" quality, and before sealing to the picnometers they were calibrated by measuring at ¼-in. intervals the length of a weighed mercury thread. They were found to have a uniform radius of 0.494 mm.

The completed picnometers had volumes of about 22 cm³ and were calibrated by weighing when empty and when filled with double-distilled water [14] at temperatures near 27° and 30° C. The values for the density of water were calculated from an equation derived by Tilton and Taylor [7] to represent the data of Chappuis [8]. Weighings were made to 0.1 mg or better on an Ainsworth semimicrobalance, using newly calibrated weights. Final weighings were made after allowing ample time for the attainment of temperature equilibrium in the balance. Two picnometers were used in the measurements, and a third was used as a tare in weighing. All weights were corrected for air buoyancy on the basis of observations of barometric pressure, temperature in the balance case, and relative humidity.

[6] By T. M. Mears of the Engine Fuels Section of the Bureau.
[7] By G. T. Furukawa of the Thermodynamics Section of the Bureau.

The positions of the two menisci relative to reference marks on the capillaries were read to 0.01 mm by means of a Gaertner traveling microscope. During these readings the picnometers were immersed in a water bath whose temperature during an experiment was maintained constant within about 0.002 deg C. The wall of the bath through which the menisci were observed was of plate glass. The temperature of the bath was measured by means of a strain-free platinum resistance thermometer and a special Mueller bridge.

The solutions were made up in 60 ml bottles with ground-glass stoppers as follows: A clean bottle containing a Pyrex-glass sealed stirring rod for use with a magnetic stirrer was weighed with its stopper, using a similar bottle for a tare. A sample of polystyrene of approximately known weight was then introduced into the bottle through a funnel in such a manner as to avoid getting any polystyrene on the ground-glass joint, and the bottle was again weighed. A measured amount (usually 50 ml) of solvent was introduced into the bottle, which was then closed with the ground-glass stopper. In handling the bottle great care was taken to avoid getting any solution on the ground-glass joint. The bottle was then placed on the magnetic stirrer, and stirring was continued until a uniform solution was obtained. When mixing was complete some solvent had condensed in the upper part of the bottle, in the ground-glass joint, and the inside of the stopper. This condensed solvent was removed by drawing clean dry air over these areas, and the stopper was replaced. The two empty picnometers were then weighed; following this, the bottle containing the solution was weighed, and the solution was transferred to the picnometers as described in the following paragraph.

The apparatus shown in figure 1 was used for transferring the solution to the picnometers with a minimum loss of solvent by evaporation. This apparatus consisted of the "wash-bottle" connections with a male standard-taper joint that replaced the stopper in the bottle containing the solution, and with a 22-gage hypodermic needle attached as shown. The solution was forced through the hypodermic needle into the picnometer by introducing helium into the wash bottle through the dryer (C, fig. 1) under a pressure of 2 to 10 lb/in². Rubber bands were used to hold the joints together. When the picnometer was almost filled the valve controlling the helium supply was closed, and the pressure was released by opening a pinchcock (not shown in fig. 1). The hypodermic needle was then disconnected from the filling apparatus and removed from the picnometer.

The ground-glass caps (D, fig. 1) were then put on and the picnometers were inverted and rotated so as to entrap a large bubble in the bulb and thereby remove small bubbles adhering to the wall. The removal of bubbles was found to be more difficult with solutions of high polystyrene content because of the high viscosity of such solutions, and for this reason, the mass fraction of polystyrene in the solutions was not carried above 0.1.

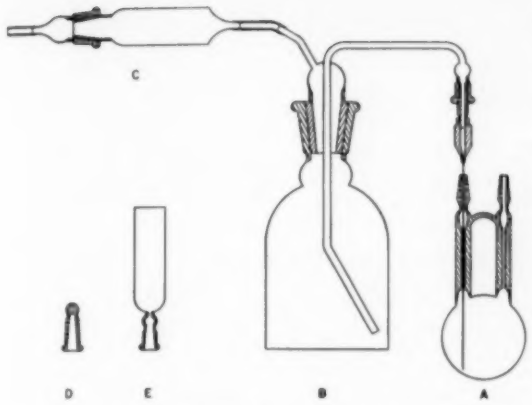

FIGURE 1. *Apparatus used in filling picnometers.*

A, Picnometer; B, bottle in which solutions were made up, with "wash-bottle" connections; C, tube containing drying agent to remove water from helium gas used to force solution from bottle, B, to picnometer; D, ground-glass cap for picnometer when being weighed; E, cap containing drying agent and cotton wet with solvent for use when picnometer was in water bath.

After the removal of air bubbles from the solution, the picnometers were placed in an upright position, any liquid entrapped in the capillaries was removed with a hypodermic syringe with a 27-gage needle, and the menisci were adjusted approximately to the proper height by means of the syringe. The picnometers were then placed in a holder and immersed in the thermostated bath to a point a little below the ground-glass joints, and final adjustment of the height of the menisci was made. Any solution adhering to the capillaries above the menisci was removed with a linen thread. While in the bath the drying tubes (E, fig. 1) containing calcium chloride were attached to the capillaries. A wad of cotton in the bottom of each drying tube was wet with a small amount of solvent to inhibit evaporation from the solution in the picnometer.

After sufficient time had elapsed for the attainment of thermal equilibrium the heights of the menisci relative to the reference marks on the capillary were observed by means of the traveling microscope. The picnometers were then removed from the bath, the drying tubes were replaced with the caps (D, fig. 1), and the picnometers were weighed after allowing sufficient time for the attainment of thermal equilibrium in the balance case.

4. Results

Observed values of density of solvents and solutions are given in table 2, together with values of apparent specific volume of polystyrene calculated

TABLE 2. *Experimental values of density and apparent specific volume, and values of density calculated from empirical equations of the form (1)*

Mass fraction polystyrene	Density, g/cm³, at—						Observed, apparent specific volume of polystyrene at—	
	26.860° C			29.971° C				
	Observed	Calculated	Observed−calculated	Observed	Calculated	Observed−calculated	26.860° C	29.971° C
BENZENE								
0	0.871653	0.871653	0×10^{-6}	0.868342	0.868350	-8×10^{-6}	.....	.....
0	.871655	.871653	+2	.868346	.868359	−4	.....	.....
0.019988	.875122	.875126	−4	.871852	.871850	+2	0.9197_5	0.9198
.050127	.880418	.880415	+3	.877204	.877183	+21	.9194	.9196
.100008	.889310	.889311	−1	.886143	.886153	−10	.9195	.9203
TOLUENE								
0	0.860345	0.860351_5	-7×10^{-6}	0.857467	0.857474	-7×10^{-6}	.....	.....
0	.860350	$.860351_5$	−2	.857471	.857474	−3	.....	.....
0.005016	.861253	.861255	−2	$.858383_5$	.858381	+2	0.9187	0.9185
.009973	$.862152_5$	.862149	+3	.859281	.859280	+1	.9183	.9186
.015046	$.863066_5$	.863067	0	.860202	.860201	+1	$.9186_5$	.9200
.020057	.863980	.863975	+5	$.861117_5$	.861113	+4	.9187	.9199
.040027	.867617	.867613	+4	$.864771_5$	.864767	+4	.9190	.9202
.100195	.878758	.878761	−3	.875963	.875963	−3	.9193	.9205
ETHYLBENZENE								
0	0.861225	0.861230	-5×10^{-6}	0.858512	0.858521	-9×10^{-6}	.....	.....
0	.861226	.861230	−4	.858515	.858521	−6	.....	.....
0.020076	.864816	.864812	+4	.862136	.862117	+19	0.9210	0.9210
.050028	.870222	.870211	+11	.867538	.867538	0	.9212	.9226
.100118	.879386	.879392	−6	.876753	.876757	−4	.9216	.9228
2-BUTANONE								
0	0.798850	0.798851	-1×10^{-6}	0.795575	0.795587	-12×10^{-6}	.....	.....
0	.798843	.798851	−8	.795584	.795587	−3	.....	.....
0.020128	.803243	.803257	−14	.800022	.800019	+3	0.9114	0.9102
.050108	.809949	.809911	+38	.806738	.806711	+27	.9093	.9100
.100312	.821288	.821304	−16	.818160	.818173	−13	.9108	.9111

TABLE 3. *Values of the constants ρ_1 and φ_2 in equation (1)*

Solvent	26.890° C		27.000° C		29.971° C		30.000° C	
	ρ_1	φ_2	ρ_1	φ_2	ρ_1	φ_2	ρ_1	φ_2
	g/cm³	*cm³/g*	*g/cm³*	*cm³/g*	*g/cm³*	*cm³/g*	*g/cm³*	*cm³/g*
Benzene	0.871653	0.91947	0.871535	0.91950	0.869350	0.92026	0.869319	0.92027
Toluene	.869351	.91929	.869249	.91933	.857474	.92050	.857447	.92051
Ethylbenzene	.861230	.92160	.861133	.92164	.858521	.92281	.858496	.92282
2-Butanone	.798851	.91065	.798734	.91066	.795587	.91103	.795556	.91103

therefrom, and with values of density calculated from empirical equations of the form

$$\rho = \frac{\rho_1}{1 - w_2(1 - \rho_1\varphi_2)}, \tag{1}$$

where w_2 is the mass fraction of polystyrene in the solution, ρ is the density of the solution, and ρ_1 and φ_2 are constants at a given temperature. This equation was derived from the definition of apparent specific volume on the assumption that this quantity is independent of composition of the solution and is equal to φ_2. Values of the constants ρ_1 and φ_2 were determined by the method of least squares from the experimental values of ρ and w_2 and are given in table 3. The values of φ_2 may be compared with the experimental values of apparent specific volume given in table 2.

It may be noted that eq (1) implies that density can also be represented by an equation of the form

$$\rho = \rho_1 + Ac_2, \tag{2}$$

where c_2 is the concentration of polymer in grams of polymer per cubic centimeter of solution, and where

$$A = (1 - \rho_1\varphi_2).$$

Table 2 shows that the agreement between the observed and calculated densities is within 1 or 2×10^{-5}, except in the case of solutions in 2-butanone, where the maximum difference is 4×10^{-5}. The results on 2-butanone solutions are less reliable than the others because of the difficulty of avoiding some absorption of water in handling. It is believed that the agreement between experimental and calculated densities is within the accuracy of the measurements. This substantiates the assumption made in deriving eq (1) that within the accuracy of the data the apparent specific volume of polystyrene is independent of the composition of the solutions over the composition range covered. This means, of course, that in this range the partial specific volume of the solute is constant and equal to the apparent specific volume, and that the partial specific volume of the solvent is constant and equal to the specific volume of the pure solvent.

5. Comparison With Previous Measurements

Values of apparent specific volume of polystyrene obtained in the present work are compared in figure 2 with values for the apparent specific volume in chlorobenzene and bromobenzene by Heller and Thompson [1], in benzene by Danes [11], in toluene by Boyer and Spencer [4], and in various solvents by Streeter and Boyer [15]. The values attributed to Boyer and Spencer were calculated from the density data given in reference [4]. They are somewhat higher than the values of partial specific volume attributed to Boyer and Spencer by Spencer and Gilmore [12]. Streeter and Boyer reported densities of solutions of various concentrations, expressed in grams of polymer per unit volume of solution, and values of partial specific volume calculated from these data. The value of partial specific volume in each solvent was calculated from two experimental points that lie exactly on a straight line drawn to represent density as a function of concentration. The two points used for this purpose were taken in the low-concentration range, except where there were seeming discrepancies in the data.

As stated previously, a linear relation between density and concentration (eq 2) implies that the partial specific volume is constant and equal to the apparent specific volume, which is related to the constants A and ρ_1 in eq (2) by $\varphi_2 = (1 - A)/\rho_1$. The use of points in the low-concentration range to determine the slope A is undesirable because, if the slope is constant, it can be determined more accurately by making use of the data over the entire concentration range. The present writers have found that, except for solutions in one solvent as noted later, the density data of Streeter and Boyer can be represented within 1 or 2×10^{-4} by equations of the form (2), with the constants ρ_1 and A determined by the method of least squares. There is no indication of a systematic trend in the deviations of experimental densities from such equations, so that within the accuracy of the measurements, the data of Streeter and Boyer indicate that φ_2 is a constant independent of concentration for each of the solvents (with the exception of the one referred to previously). For this reason, it seems preferable to calculate the values of φ_2 from the values of ρ_1 and A determined from all the data on each solvent by the method of least squares, and the values shown in figure 2 were obtained in this way.

The density data of Streeter and Boyer on solutions in *o*-dichlorobenzene depart from a straight line (eq 2) in a systematic manner by amounts that appear to be considerably in excess of the uncertainty of the data. Values of φ_2 calculated from experimental values of density by means of eq (1) can be represented graphically with a precision corre-

sponding to about 1×10^{-4} in density by a curve that is horizontal for values of concentration from 6 to 12 g/100 ml of solution, but which rises at lower concentrations and approaches a value of about $\varphi_2=1.0$ at zero concentration. The value for *o*-dichlorobenzene attributed to Streeter and Boyer in figure 2 was taken from the horizontal part of this curve.

Data not shown in figure 2 include a value $\varphi_2=0.877$ at 25° C derived from the data of Streeter and Boyer on solutions in chloroform; values of φ_2 in various solvents ranging from 0.88 to 0.93 at 20° C with uncertainties of ±0.01 to ±0.04 reported by Signer and Gross [2]; and the values, all at 20° C, $\varphi_2=0.939$ in benzene, 0.945 in 2-butanone, 0.953 in cyclohexane, and 0.889 in chloroform derived from data reported by Breitenbach and Frank [3] on the change in volume accompanying swelling of a cross-linked polystyrene containing 0.12 percent of divinylbenzene. It is possible, of course, that these latter values are not comparable with values of φ_2 derived from densities of solutions of polystyrene.

The straight line near the top of figure 2 represents an extrapolation of the linear equation given by Fox and Flory [9] for the specific volume of polystyrene of infinite molecular weight above the glass transition temperature, and may be regarded as representing the specific volume to be expected of bulk polystyrene if it could be obtained as a liquid at room temperature [1]. It is seen that most of the values of apparent specific volume in solution lie below this line, and that all the data indicate that the coefficient of expansion of dissolved polystyrene is somewhat smaller than that of the virtual bulk liquid. This is true also if we include the data of Danes over the temperature range from 15° to 65° C, and the data of Boyer and Spencer from 0° to 40° C.

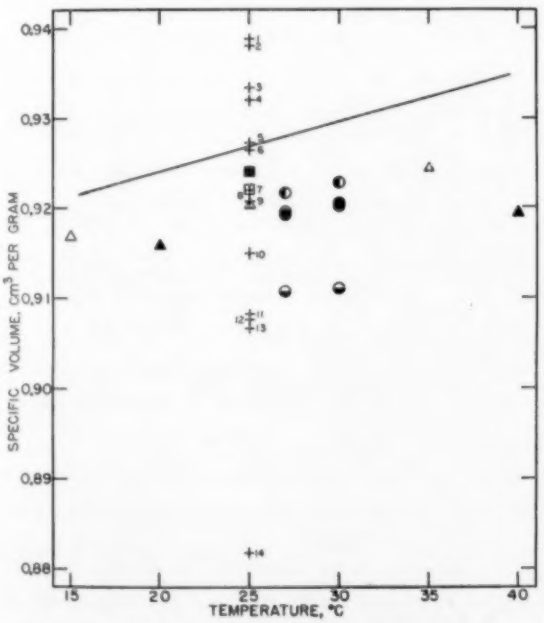

FIGURE 2. *Apparent specific volume of polystyrene in various solvents.*

■, Heller and Thompson, bromobenzene; □, Heller and Thompson, chlorobenzene; △, Danes, benzene; ▲, Boyer and Spencer, toluene; +, Streeter and Boyer, various solvents as follows: (1) Decalin; (2) *s*-chlorotriethylbenzene; (3) dioxane; (4) *o*-dichlorobenzene; (5) *s*-dichlorodiethylbenzene; (6) ethyl laurate; (7) benzene; (8) ethylbenzene; (9) toluene; (10) ethylacetate; (11) chloroform; (12) 2-butanone; (13) 2-heptanone; (14) tetralin.

The circles represent results of present work as follows; ○, Benzene; ●, toluene; ◐, ethylbenzene; ◒, 2-butanone.

The straight line near the top of the figure is an extrapolation of Fox and Flory's equation for the specific volume of polystyrene of infinite molecular weight above the glass-transition temperature.

6. Effect of Changes in Volume Upon Thermodynamic Properties

If we take the value 0.949_8 cm³/g calculated from the equation given by Fox and Flory [9] for the specific volume of solid polystyrene at 27° C, it will be seen that, according to the data given in table 3, the change in volume, $(\Delta V=\varphi_2-0.949_8)$, when 1 g of solid polystyrene is dissolved at 27° will have the following values for the various solvents:

Solvent	ΔV(27° C)
	cm³/g polystyrene
Benzene	-0.030_3
Toluene	$-.030_5$
Ethylbenzene	$-.028_2$
2-Butanone	$-.039_1$

It is of interest to consider the effect of such changes in volume upon thermodynamic properties of polystyrene solutions.[8] If polymer and solvent are initially at atmospheric pressure and if mixing is supposed to take place at constant volume, and then a change in volume, ΔV, is allowed to take place to bring the pressure back to atmospheric, the change in any thermodynamic quantity, G, due to the change in volume will be given by

$$\Delta G=\left(\frac{\partial G}{\partial V}\right)_T\Delta V.$$

For example, we obtain from well-known thermodynamic relations

$$\Delta H=\frac{T\alpha-1}{\beta}\Delta V,$$

$$\Delta U\simeq\frac{T\alpha}{\beta}\Delta V,$$

$$\Delta S=\frac{\alpha}{\beta}\Delta V,$$

$$\Delta F=-\frac{1}{\beta}\Delta V,$$

[8] Similar calculations have been made for various liquid mixtures by Scatchard, Wood, and Mochel [16] and by Wood and Gray [17].

where α and β are coefficients of expansion and compressibility, respectively. For an infinitely dilute solution in benzene at 27° C we obtain $\alpha = 1.232 \times 10^{-3}$ (° C)$^{-1}$ from the data of table 2, and from International Critical Tables [13], $\beta = 1.00 \times 10^{-4}$ bar^{-1}, so that at 27° C (=300° K)

$$\left(\frac{\partial H}{\partial V}\right)_T = -630 \ j/\text{cm}^3,$$

and for the change in volume of -0.0303 cm^3 upon solution of 1 g of solid polystyrene in benzene $\Delta H = 19.1$ $j = 4.6$ cal. Similarly, we obtain for the effect of volume change due to solution of 1 g of polystyrene in benzene at 27° C $\Delta U = -2.7$ cal, $\Delta S = -0.0089$ cal/° C, $\Delta F = 7.2$ cal. The values for ΔU and ΔH resulting from volume change upon mixing may be compared with a preliminary experimental value of approximately -6 cal for the heat of mixing of 1 g of polystyrene with toluene.

In a similar manner, taking the volume of the liquid polymer at 27° C as 0.927_9 [9], the changes in the thermodynamic functions due to change in volume on mixing 1 g of liquid polystyrene with benzene to form an infinitely dilute solution are calculated to be $\Delta H = +1.3$ cal, $\Delta U = -0.7_5$ cal, $\Delta S = -0.0025$ cal/°C, $\Delta F = +2.0_5$ cal.

According to Heller and Thompson [1] only the change in volume upon solution of liquid polystyrene, and therefore only the changes in the functions H, U, etc., calculated from this change in volume have thermodynamic significance, because of the fact that the solid polymer is not in a state of thermodynamic equilibrium. It will be seen that even in the case of the liquid polystyrene there is a significant change in the thermodynamic functions as a result of change in volume upon mixing with solvent.

As stated previously constancy of the apparent specific volume implies that the partial specific volume of the solvent is equal to the actual specific volume of the pure solvent. There is then no change in volume due to dilution and no effect of change in volume upon partial thermodynamic quantities, such as $\Delta\overline{H}_1$, $\Delta\overline{S}_1$, $\Delta\overline{F}_1$, etc., within the composition range covered.

It should be emphasized that the results reported in this paper are for unfractionated polystyrene of unknown molecular-weight distribution, which contained the amounts of impurities given previously. There appears to be no satisfactory method of reducing the results to the basis of pure polystyrene. The results may depend to some extent upon the molecular-weight distribution in the polymer. This problem has been discussed by Heller and Thompson [1] on the basis of certain assumptions regarding the relation between the specific volume of the virtual liquid polymer (which is known to depend upon molecular weight [9]) and the apparent specific volume in solution. If it is assumed that the number-average molecular weight of the polystyrene used in the present measurements is one-half of the weight-average and that the molecular weight distribution functions is that given by Lansing and Kraemer [18], then the treatment of Heller and Thompson [1] indicates that the measured apparent specific volume does not differ appreciably from that of a polystyrene having a uniform molecular weight of about 100,000.

7. Summary and Conclusions

Values are reported for the densities of purified benzene, toluene, ethylbenzene, and 2-butanone, and of solutions of polystyrene in these solvents at temperatures near 27° and 30° C. Within the accuracy of the measurements, values of apparent specific volume of polystyrene derived from the data are independent of composition of the solutions in the range 0.5 to 10 percent of polystyrene by weight.

The results confirm the conclusion of Heller and Thompson [1] that the apparent specific volume of polystyrene depends upon the solvent. This is also shown very strikingly by the results of Streeter and Boyer [15].

The changes in volume upon mixing of polystyrene with solvent are shown to have a significant effect on the thermodynamic properties of the solution.

8. References

[1] W. Heller and A. C. Thompson, J. Colloid Sci. **6,** 57 (1951).
[2] R. Signer and R. Gross, Helv. Chim. Acta **17,** 59 (1934).
[3] J. W. Breitenbach and H. P. Frank, Monatsh. **79,** 531 (1948).
[4] R. F. Boyer and R. S. Spencer, J. Polymer Sci. **3,** 97 (1948).
[5] J. H. Hildebrand and R. L. Scott, Solubility of nonelectrolytes (Reinhold Publishing Corporation, New York, N. Y., 1950).
[6] Selected values of the properties of hydrocarbons, American Petroleum Institute Research Project 44, at the Carnegie Institute of Technology, table 5a (Oct. 31, 1950).
[7] L. W. Tilton and J. K. Taylor, J. Research NBS **18,** 205 (1937) RP971.
[8] P. Chappuis, Bureau international des Poids et Mesures, Travaux et Memoires **13** (1907).
[9] T. G. Fox Jr. and P. J. Flory, J. Appl. Phys. **21,** 581 (1950).
[10] N. Grassie, J. Polymer Sci. **6,** 643 (1951).
[11] V. Z. Danes, Kolloid-Z. **68,** 110 (1934).
[12] R. S. Spencer and G. D. Gilmore, J. Appl. Phys. **20,** 502 (1949).
[13] International Critical Tables, **3,** 29 and 39 (McGraw-Hill Book Co., Inc., New York, N. Y., 1928).
[14] N. Bauer, Weissberger's Physical methods in organic chemistry, **1,** 69 (Interscience Publishers, Inc., New York, N. Y. 1945).
[15] D. J. Streeter and R. F. Boyer, Ind. Eng. Chem. **43,** 1790 (1951).
[16] G. Scatchard, S. E. Wood, and J. M. Mochel, J. Phys. Chem. **43,** 119 (1939); J. Am. Chem. Soc. **61,** 3206 (1939); and J. Am. Chem. Soc. **62,** 712 (1940).
[17] S. E. Wood and J. A. Gray, III, J. Am. Chem. Soc. **74,** 3729 (1952).
[18] W. D. Lansing and E. O. Kraemer, J. Am. Chem. Soc. **57,** 1369 (1935).

WASHINGTON, November 6, 1953